# Lawrence Berkeley National Laboratory
## Recent Work

**Title**

REACTION KINETICS OF THE PHOTOLYSIS OF N02, AND THE SPECTRA AND REACTION KINETICS OF THE FREE RADICALS IN THE PHOTOLYSIS OF THE Cl2-O2-CO SYSTEM

**Permalink**

**Author**

Barker, Alan Butler.

**Publication Date**

1972-09-01

# REACTION KINETICS OF THE PHOTOLYSIS OF $NO_2$, AND THE SPECTRA AND REACTION KINETICS OF THE FREE RADICALS IN THE PHOTOLYSIS OF THE $Cl_2$-$O_2$-CO SYSTEM

Alan Butler Harker
(Ph. D. Thesis)

September 1972

## DISCLAIMER

REACTION KINETICS OF THE PHOTOLYSIS OF $NO_2$,
AND THE SPECTRA AND REACTION KINETICS OF THE FREE RADICALS
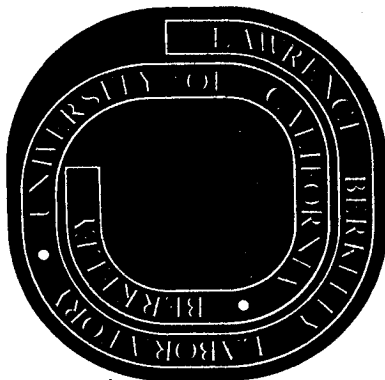IN THE PHOTOLYSIS OF THE $Cl_2-O_2-CO$ SYSTEM

## CONTENTS

REACTION KINETICS OF THE PHOTOLYSIS OF $NO_2$,
AND THE SPECTRA AND REACTION KINETICS OF THE FREE RADICALS
IN THE PHOTOLYSIS OF THE $Cl_2-O_2-CO$ SYSTEM

Alan Butler Harker

Inorganic Materials Research Division, Lawrence Berkeley Laboratory
and Department of Chemistry; University of California,
Berkeley, California

## ABSTRACT

### PART I

This investigation contains descriptions of two separate photo-chemical systems. The first is a study of the photolysis of $NO_2$ in $N_2$ by radiation in the wavelength region 300-400 nm. The kinetics of the $NO_2$ photolysis system were studied by monitoring the reacting species by infrared spectroscopic techniques. These techniques included initial slope measurements, steady-state concentration determinations, and molecular modulation studies on the $NO_2$ concentration during inter-mittent photolytic illumination of the system. From these spectroscopic measurements it was possible to determine rate constant ratios for the major reaction steps.

The photolytic decay of $NO_2$ was found to be consistent with the accepted mechanism:

$$NO_2 + h\nu \xrightarrow{\alpha I} NO + O(^3P)$$

$$NO + O + M \xrightarrow{k_1} NO_2 + M$$

$$NO_2 + O \xrightarrow{k_2} NO + O_2$$

$$NO_2 + O + M \xrightarrow{k_3} NO_3 + M$$

$$NO + NO_3 \xrightarrow{k_4} 2NO_2$$

$$NO_2 + NO_3 \underset{k_{6M}}{\overset{k_{5M}}{\rightleftharpoons}} N_2O_5 \quad K_{eq} = k_{5M}/k_{6M}$$
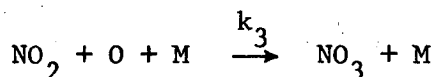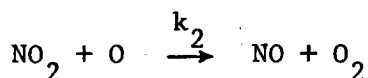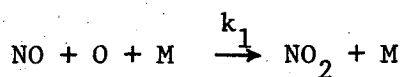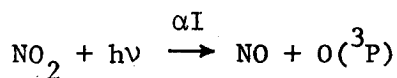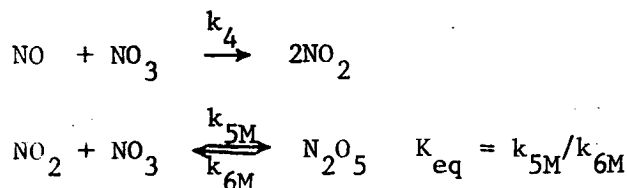
The kinetic measurements led to the following values for the rate constant ratios at 24°C with one atmosphere total pressure and nitrogen as the M gas.

$$k_1[M]/k_2 = 0.18 \pm .01$$

$$k_3[M]/k_2 = 0.221 \pm .005$$

$$k_4/K_{eq} = 0.71 \pm .014 \ (sec^{-1})$$

These measured values are in good accord with the literature results reported by Schuck, Stephens and Schrock[25] and Hisatsune, Crawford, and Ogg,[21] but they disagree substantially with the work done by Ford and Endow in 1957.[22]

The rate constant ratios determined in this work can be combined with literature values for $k_1$ and $K_{eq}$ to predict absolute values for the individual rate constants. Using an averaged literature value of $k_1 = 0.69 \times 10^{-32}$ ($cm^6/particle^2$-sec) and the value of $K_{eq} = 1.24 \times 10^{-11}$ ($cm^3/particle$) found by Schott and Davidson,[20] the following values are predicted for the rate constants in the $NO_2$ photolysis in $N_2$ at 24°C.

$$k_1 = 0.69 \times 10^{-32}$$

$$k_2 = 9.2 \times 10^{-12}$$

$$k_3 = 0.82 \times 10^{-31}$$

$$k_4 = 0.87 \times 10^{-11}$$

$$K_{eq} = 1.24 \times 10^{-11}$$

All units are $(cm^{3x}/particles^x$-sec) with the appropriate value for x. As a test for the accuracy of these rate constants a computer simulation of the photolysis was carried out and the results compared to the experimental data. The calculated results matched the experimental data within the limits of the experimental error.

## PART II.

The second part of this investigation deals with the spectra and reaction kinetics of the free radicals present in the chlorine catalyzed production of $CO_2$ from CO and $O_2$. Molecular modulation infrared and ultraviolet absorption bands belonging to an unknown radical species were observed in this system at 220 nm, 937 $cm^{-1}$, 1835 $cm^{-1}$ and 1905 $cm^{-1}$. From a comparison of the kinetic behavior of these absorptions with that of the ClO free radical absorption at 265 nm. the new radical species is shown to be a precursor to ClO. The kinetic behavior of the new free radical also indicates that it decomposes to give $CO_2$. From this information and a study of the overall rate law for the reaction the new free radical is identified as $ClCO_3$.

Another absorption was detected in the infrared at 970 $cm^{-1}$. From a comparison of its kinetic behavior to that of the 265 nm. ClO absorption, this band is identified as the fundamental vibrational absorption of ClO. By comparing the observed spectra with the calculated band envelope the Q branch of ClO is predicted to be at 950 $\pm$ 15 $cm^{-1}$.

In the kinetic study of this system the rate law for $CO_2$ formation is shown to be:

$$\frac{d\ CO_2}{dt} = k(\alpha I[Cl_2])^{1/2}\ [CO],$$

for the conditions of $[O_2] \approx 1$ atm.; $[Cl_2] \approx 2. \times 10^{15}$ molecules/$cm^3$ and $[CO] \approx 5. \times 10^{17}$ molecules/$cm^3$. This rate law is shown to be consistent with the following mechanism.

$$Cl_2 + h\nu \rightarrow 2Cl$$

$$Cl + O_2 + M \rightleftharpoons ClOO + M$$

$$Cl + CO + M \rightleftharpoons ClCO + M$$

$$ClOO + Cl \rightleftharpoons 2ClO$$

$$ClOO + Cl \rightarrow Cl_2 + O_2$$

$$ClCO + Cl_2 \rightarrow Cl_2CO + Cl$$

$$ClCO + Cl \rightarrow CO + Cl_2$$

$$ClO + ClO + M \rightleftharpoons Cl_2O_2 + M \rightarrow Cl_2 + O_2 + M$$

$$ClCO + O_2 + M \rightleftharpoons ClCO_3 + M$$

$$ClCO_3 + M \xrightarrow{k_{10'}} ClO + CO_2 + M$$

$$ClO + CO \xrightarrow{k_{11'}} Cl + CO_2$$

$$Cl + Cl + M \rightarrow Cl_2 + M$$
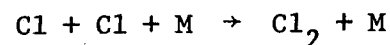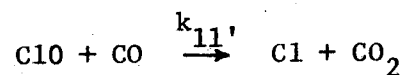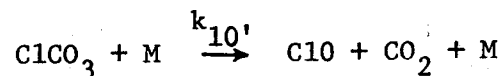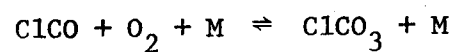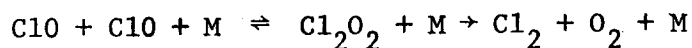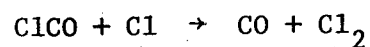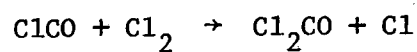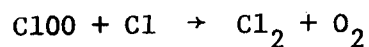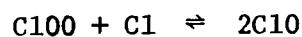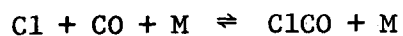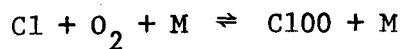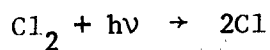
Using this mechanism and the chemical modulation method the rate constants $k_{10'}$ and $k_{11'}$ where found to be

$$k_{10'} = 1.9 \pm .2 \times 10^{-18} \ cm^3/particle\text{-}sec$$

and

$$k_{11'} = 1.4 \pm .14 \times 10^{-15} \ cm^3/particle\text{-}sec$$

From these values and the spectroscopic measurements the absorption coefficients of the free radical absorptions were determined at 1 atm with $O_2$ as the M gas. These values to the base e are:

$$\sigma_{ClCO_3}(220 \text{ nm}) = 1. \pm .25 \times 10^{-18} \text{cm}^2/\text{particle}$$

$$\sigma_{ClCO_3}(937 \text{ cm}^{-1}) \doteq 3.8 \pm 1. \times 10^{-19} \text{cm}^2/\text{particle}$$

$$\sigma_{ClO}(970 \text{ cm}^{-1}) = 3. \pm 2.5 \times 10^{-19} \text{cm}^2/\text{particle}.$$

PART I.   PHOTOLYSIS OF NITROGEN DIOXIDE

## I.   INTRODUCTION

The photolysis of nitrogen dioxide by the absorption of sunlight in the 300 to 400 nanometer range is one of the two primary sources of $^3P$ oxygen atoms in the lower atmosphere, the other being the photolysis of ozone.  Due to the large amount of $NO_2$ being introduced into the atmosphere by combustion, this reaction sequence becomes of great importance in the formation of photochemical smog.[1]

The photolysis of $NO_2$ and the reactions following from its dissociation into nitric oxide and $^3P$ oxygen atoms have been studied in the past, but there are conflicting reports in the literature as to the values of the reaction rate constants.

The postulated mechanism for the reaction sequence is given by:

$$NO_2 + h\nu \xrightarrow{\alpha I} NO + O\ (^3P) \tag{a}$$

$$NO + O + M \xrightarrow{k_1} NO_2 + M \tag{1}$$

$$NO_2 + O \xrightarrow{k_2} NO + O_2 \tag{2}$$

$$NO_2 + O + M \xrightarrow{k_3} NO_3 + M \tag{3}$$

$$NO_3 + NO \xrightarrow{k_4} 2NO_2 \tag{4}$$

$$NO_3 + NO_2 \underset{k_{6m}}{\overset{k_{5m}}{\rightleftharpoons}} N_2O_5 \qquad K_{eq} = k_{5m}/k_{6m} \tag{5,6}$$

$$O_2 + O + M \xrightarrow{k_7} O_3 + M \tag{7}$$

$$NO + O_3 \xrightarrow{k_8} NO_2 + O_2 \tag{8}$$
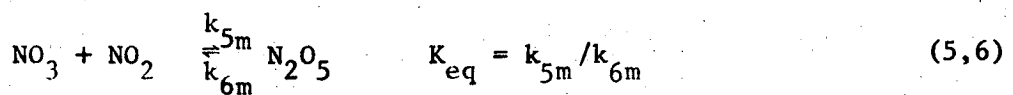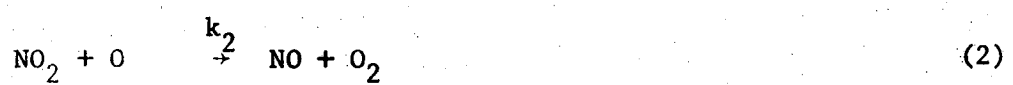
Support for this mechanism comes from several sources. The primary photolysis of $NO_2$ has been studied over the region of its absorption in the ultraviolet and visible spectrum, and the studies indicate that an excited $NO_2$ molecule is produced in the sharply structured visible region of the spectrum with dissociation occurring at wavelengths below 400 nanometers where the spectrum becomes more diffuse. (See Fig. 1). Evidence for this comes from the observation of fluorescence from $NO_2$ after absorption of visible light and the absence of fluorescence when the exciting light is below 370 nm.[2,3] Using mixtures of $NO_2$ and $O^{18}$ enriched $O_2$, Hall observed isotope scrambling after photolysis (313 nm) of this system, with $ONO^{18}$ appearing.[4] This is explained through the photolytic dissociation of $NO_2$ to NO and O, with the recombination to $NO_2$ occurring through NO and $O_3$, producing isotopically scrambled $ONO^{18}$. No isotope scrambling was observed after photolysis with light of 404.7 nm, indicating that dissociation does not occur at this wavelength. This evidence indicates that radiation of energy greater than 400 nm is required to produce dissociation of $NO_2$. In agreement with this the bond dissociation energy of $NO_2$ into $NO(^2\pi)$ and $O(^3P)$ is between 71 and 72 kcal/m corresponding to absorption of radiation of about 400 nm.[7] The limiting quantum yields for this dissociation have also been reported, with a value of unity being approached at 360 nm (Fig. 2).

After the photodissociation of $NO_2$, the major reactions in the system are the oxygen atom reactions with $NO_2$ and NO. The rapid bimolecular reaction of O atoms with $NO_2$ to produce NO and $O_2$ has been studied by several methods, including flash photolysis,[8] resonance fluorescence,[9] and the analysis of oxygen discharge flow systems.[10]
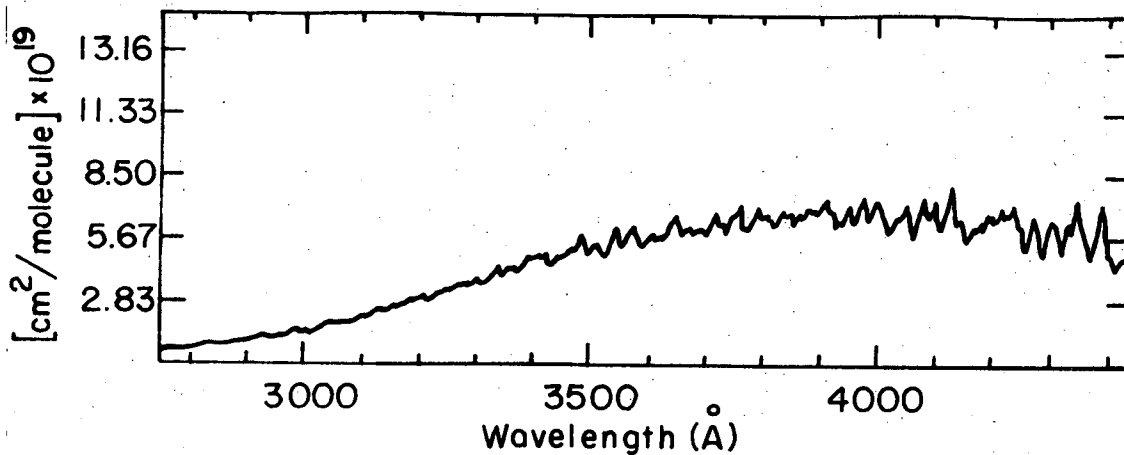
Fig. 1. Absorption coefficient of $NO_2$ base e versus wavelength in Å (5).
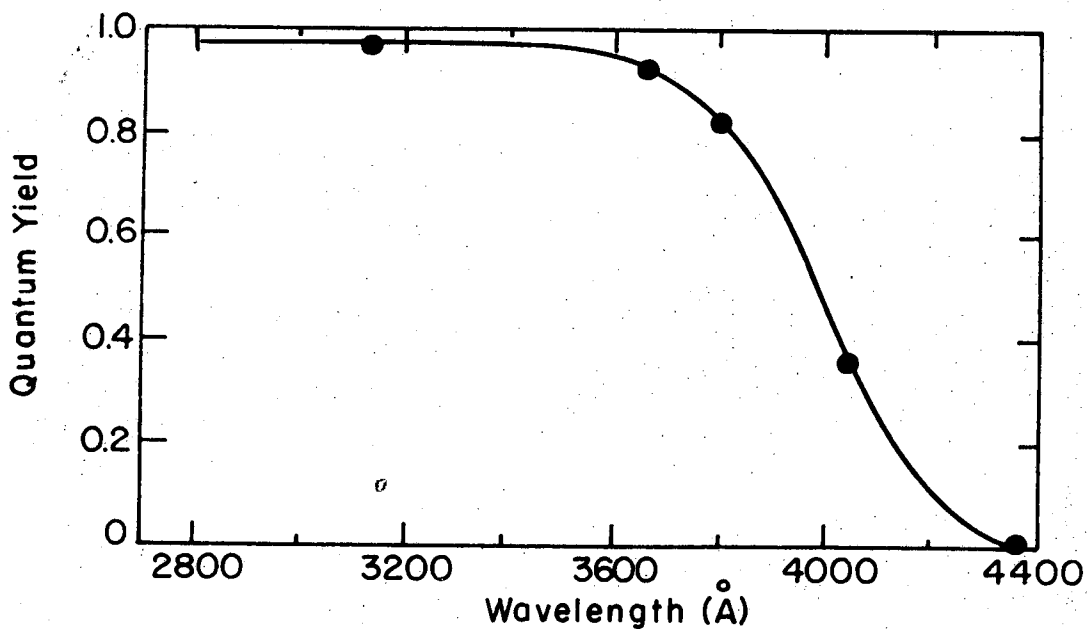


XBL 728 - 6829

Fig. 2. Quantum yield of $O_2$ in the photolysis of $NO_2$, at a total pressure of less than 5 mm/Hg. When $[M] \approx 0$, one $O_2$ molecule is produced for each molecule of $NO_2$ dissociated by light. (6)

Comparison of the mechanism of this reaction with the termolecular reaction of $NO_2$ with O atoms and a M gas to produce $NO_3$, indicates that the two reactions proceed via different intermediate forms of excited $NO_3$. This is supported by the high pressure limit rate studies done by Troe which show different limiting rates for the two reactions.[11] The literature values for these two rate constants are summarized in Table I.

The reaction of O atoms with nitric oxide to produce $NO_2$ has been studied repeatedly by monitoring the chemiluminescence of:

$O + NO + M \rightarrow NO_2^* + M \rightarrow h\nu + NO_2 + M$. The rate of this reaction has been determined often enough in oxygen discharge flow systems that a reasonably good value for $k_1$ at room temperature and 1 atm. pressure is available. The reported values for this rate constant are given in Table II.

The reactions of $N_2O_5$ and those involving the $NO_3$ free radical were studied during the 1950's. Mills and Johnston reported a value for the decay rate constant of $N_2O_5$ in 1951,[19] but no direct measurements of the individual rate constants for the $NO_3$ reactions were published. The rates of the $NO_3$ reactions were determined by relating them to the equilibrium constant for the formation of $N_2O_5$. This constant, $K_{eq}$, was reported by Schott and Davidson in 1957,[20] soon after Hisatsune, et al. published a value for $K_{eq}^{-1}k_4$.[21] The literature rate constants for these reactions are summarized in Table III, along with the accepted values for the rates of the reactions containing ozone, (7 and 8).

The kinetics of the entire $NO_2$ photolysis mechanism were reported in detail by Ford and Endow in 1957.[22] By flowing known amounts of $NO_2$, NO, $O_2$, and $N_2$ into a stirred 52 liter photolysis cell, and monitoring the exhaust gas for $NO_2$, NO, and $O_3$ they were able to carry out a steady state

Table I.  A summary of the literature values for the rate constants $k_2$ and $k_3$.

| $k_2$ (cm$^3$/part. sec) | T °K | Method & Reference | |
|---|---|---|---|
| $5.6 \pm 1.6 \times 10^{-12}$ | 298 | Flash photolysis | (8) |
| $9.2 \pm 0.5 \times 10^{-12}$ | 298 | Resonance fluorescence | (9) |
| $7.0 \pm 0.7 \times 10^{-12}$ | 297 | $O_2$ discharge flow system | (10) |
| $4.4 \pm 1.1 \times 10^{-12}$ | 300 | UV photolysis | (12) |
| $5.4 \pm 1.6 \times 10^{-12}$ | 296 | $O_2$ discharge flow system | (13) |

| $k_3$ (cm$^6$/part.$^2$ sec) | T °K | Method & Reference |
|---|---|---|

There is no literature value for this rate constant reported separately, but there are two reported ratios of $k_3$ done at 1 atmosphere with $N_2$ as the M gas.

| | | | |
|---|---|---|---|
| $k_3[M]/k_2 = 1.9$ | 300 | UV photolysis with reactant product analysis. | (22) |
| $k_3[M]/k_2 = 0.33 \pm .08$ | 296 | UV photolysis with initial slope measurement. | (25) |

Table II.  A summary of the literature values for the rate constant $k_1$.

| $k_1$ $(cm^6/part.^2-sec)$ | M gas | T °K | Ref. |
|---|---|---|---|
| $7.0 \pm 0.8 \times 10^{-32}$ | $O_2$, $N_2$, Ar | 296 | (14) |
| $7.6 \pm 0.5 \times 10^{-32}$ | Ar, $O_2$ | 300 | (15) |
| $6.4 \pm 0.8 \times 10^{-32}$ | $O_2$ | 297 | (16) |
| $7.3 \pm 0.9 \times 10^{-32}$ | $N_2$ | 297 | (16) |
| $5.1 \pm 0.2 \times 10^{-32}$ | $O_2$, He, Ar | 293 | (17) |
| $5.3 \times 10^{-32}$ | Ar | 298 | (18) |
| $6.1 \times 10^{-32}$ | $N_2$ | 298 | (18) |
| $10.0 \pm 0.14 \times 10^{-32}$ | $N_2$ | 296 | (13) |

Average literature value

$k_1 = 6.9 \times 10^{-32}$ $(cm^6/part.^2-sec)$

Table III. Literature values for the rate constants $k_4$ through $k_8$.

| Rate constants in units of $(cm^{3x}/particles^x sec)$ | T °K | Reference | |
|---|---|---|---|
| $k_4 K_{eq}^{-1}$ = 0.6 | 296 | Hisatune et al. | (21) |
| $K_{eq}$ = 1.25 × 10$^{-11}$ | 296 | Schott & Davidson | (20) |
| $k_{6m}$ = 0.104 | 296 | Mills & Johnston | (19) |
| $k_7$ = 0.624 × 10$^{-33}$ | 296 | Johnston | (23) |
| $k_8$ = 2.1 × 10$^{-14}$ | 298 | Johnston & Crosby | (24) |

Table IV. Literature values for the rate constant ratios in the $NO_2$ photolysis system at 1 atmosphere pressure with $N_2$ as the M gas.

| $k_1[M]/k_2$ | $k_3[M]/k_2$ | $k_7[M]/k_2$ | T °K | Reference | |
|---|---|---|---|---|---|
| 0.357 | 1.9 | 1.33 × 10$^{-3}$ | 300 | Ford & Endow | (22) |
| 0.18 ± .04 | 0.33 ± .08 | 1.15 × 10$^{-3}$ | 296 | Schuck et al. | (25) |

reactant-product analysis of the system. Assuming that $NO_3$ and atomic oxygen are in their steady states, that reactions (5) and (6) are negligible, and that reactions (4) and (8) have gone to completion before the analysis is performed; they obtained the expression:

$$\frac{1}{\phi_{NO_2}} = \frac{1}{2} + \frac{k_3[M]}{2k_2} + \frac{k_1[NO][M]}{2k_2[NO_2]} + \frac{k_7[O_2][M]}{2k_2[NO_2]} \tag{9}$$

where $\phi_{NO_2}$ is the overall quantum yield. By plotting their experimental values for $1/\phi_{NO_2}$ against each ratio term in (9), Ford and Endow were able to obtain linear relationships, thus supporting the form of their analysis. From this work they reported the ratios of the important rate constants: $k_1[M]/k_2$, $k_3[M]/k_2$, and $k_7[M]/k_2$.

Another measurement of these ratios comes from the work of Schuck, Stephens, and Schrock in 1966, who repeated the experiments of Ford and Endow, using IR spectroscopy to monitor the decay of $NO_2$, rather than a product analysis.[25] Using a similar steady-state analysis of the system they derive the relationship:

$$\frac{-2\alpha I[NO_2]}{d[NO_2]/dt} = 1 + \frac{k_3[M]}{k_2} + \frac{k_1[M][NO]}{k_2[NO_2]} + \frac{k_7[M][O_2]}{k_2[NO_2]} \tag{10}$$

This allows the rate constant ratios to be evaluated from monitoring the decay of $NO_2$ at various pressures and initial concentrations of $O_2$ and NO. The results of these two attempts to describe the entire kinetic system are compared in Table IV.

Examination of the literature values shows that there is substantial disagreement over the rate constants for reactions (2) and (3). There is only one reported value for the rate of reaction (4), and the two studies

of the entire system show marked disagreement in their measured ratios.
To help resolve this situation the purpose of this research is to com-
bine steady state kinetic methods with initial slope data and molecular
modulation in order to obtain quantitative relationships between the
rate constants in this system.

## II.  EXPERIMENTAL

### A.  Method

To do a more complete analysis of the $NO_2$ system than previous investigators, this investigation combines traditional steady-state analysis with more dynamic methods.  These methods include the monitoring of the intermediate species $N_2O_5$, and the molecular modulation study of $NO_2$. Combining these techniques with initial slope measurements on the $NO_2$ decay allows the system to be analyzed.

To describe the $NO_2$ photolysis system adequately requires the rate constants for reactions (1) through (6) and the wavelength integrated product of the photolytic lamp intensity, quantum yield, and absorption coefficient, $\alpha I$.  This investigation was able to produce experimental values for $\alpha I$, $k_4 K_{eq}^{-1}$, $k_1[M]/k_2$, and $k_3[M]/k_2$.  Combining these measurements with literature values for $K_{eq}$ and $k_1$ allows values to be determined for the individual rate constants.  Using these values in a coupled differential equation simulation of the system permits a check of these results against experimental concentration profiles.

The experimental results come from five measurable parameters:

a.  The low pressure initial slope of the $NO_2$ decay

b.  The 1 atm. initial slope of the $NO_2$ decay

c.  The initial slope of the $N_2O_5$ buildup at 1 atm.

d.  The maximum value of the $N_2O_5$ buildup at 1 atm.

e.  The amplitude of the concentration modulation of $NO_2$ induced by the modulation of a steady state flow system by the periodic flashing of the photolysis lamps.

The measurements of the low pressure initial decay of the $NO_2$, yield a value for the first order rate constant, $\alpha I$, which represents the wavelength integrated product of the lamp intensity, $NO_2$ absorption coefficient, and the primary quantum yield. At pressures below 50 torr the rates of the M gas dependent reactions become negligible with respect to reaction (2) which is a two-body, pressure independent reaction. This gives the following expression for the $NO_2$ decay:

$$\frac{d[NO_2]}{dt} = -\alpha I[NO_2] - k_2[NO_2][O] \tag{11}$$

Since reaction (2) is very fast this gives an effective quantum yield of two times the primary value, and the expression reduces to:

$$\ln \frac{[NO_2]}{[NO_2]_i} = -2\alpha It \tag{11'}$$

Thus measuring the low pressure initial slope of the $NO_2$ decay gives an experimental value for $\alpha I$.

The differential equation for the one atmosphere initial decay of $NO_2$ during photolysis is given by (12).

$$\frac{d[NO_2]}{dt} = -\alpha I[NO_2] + k_1[NO][O][M] - (k_2 + k_3[M])[NO_2][O]$$

$$+ 2k_4[NO_3][NO] - k_{5m}[NO_3][NO_2] + k_{6m}[N_2O_5] \tag{12}$$

$$+ k_8[NO][O_3]$$

This expression can be reduced by the following assumptions:

a. At t=0 with no initial $O_2$ there will be no ozone and reactions (7) and (8) can be neglected.

b. Since all the oxygen atom and $NO_3$ radical reactions are very fast,

these two species can be assumed to be present in their steady state concentrations.

c. The $N_2O_5$ reactions are initially very small compared to the $NO_2$ decay, and can be neglected.

With these assumptions the expression for the $NO_2$ decay reduces to:

$$\frac{d[NO_2]}{dt}_{(t\to0)} = \frac{-2\alpha I k_2 [NO_2]^2}{k_1[NO][M] + (k_2+k_3[M])[NO_2]} \qquad (13)$$

As $t\to0$, [NO] also approaches zero and (13) further reduces

$$\frac{d[NO_2]}{dt}_{(t\to0)} = \frac{-2\alpha I k_2 [NO_2]}{k_2 + k_3[M]} \qquad (13')$$

This approximation is good to better than 97% until the [NO] builds up to about 20% of the [$NO_2$]. This doesn't occur until about 30 seconds have elapsed under these experimental conditions. Integrating (13') gives the equation for the one atmosphere initial slope for the conditions of no initial oxygen or nitric oxide.

$$\ln\frac{[NO_2]}{[NO_2]} = -2\alpha I(k_2/(k_2+k_3[M]))t \qquad (14)$$

The third experimentally measurable relationship comes from the differential equation for $N_2O_5$. The $N_2O_5$ builds up until it reaches a maximum value as the $NO_2$ is photolyzed and then it also decays. At this point the first time derivative of the $N_2O_5$ concentration is equal to zero.

$$\frac{d[N_2O_5]}{dt}_{(t=t^*)} = k_{5m}[NO_3][NO_2] - k_{6m}[N_2O_5] = 0 \qquad (15)$$

$t^*$ is the time of the maximum.

At the time of the $N_2O_5$ maximum under these reaction conditions the term $k_1[NO][M]$ is still only about 1.5% of the term $(k_2+k_3[M])[NO_2]$ so the 0 atom steady state can be expressed as:

$$[0]_{ss} = \frac{\alpha I}{k_2+k_3[M]} \tag{16}$$

Using this expression for the 0 atom concentration, and assuming the $NO_3$ to also be in its steady state allows (15) to be reduced to:

$$\frac{[N_2O_5]^*}{[NO_2]} = \frac{\alpha I[NO_2]}{K_{eq}^{-1}k_4(1+k_2/k_3[M])[NO]} \tag{17}$$

Where all concentrations are evaluated at time $t=t^*$

The fourth experimental relationship comes from evaluating $d[N_2O_5]/dt$ at the limit $t=0$. Again assuming steady states for $NO_3$ and 0 atoms this gives:

$$\lim_{t \to 0} \frac{d[N_2O_5]}{dt} = \frac{\alpha I[NO_2]}{(1+k_2/k_3[M])} \tag{18}$$

The fifth relationship is derived from the behavior of the nitrogen dioxide in a steady state flow system with the photolysis lamps flashing on and off at one cycle per second. Under these conditions the $NO_3$ and oxygen atom will be at their steady state concentrations, and the $N_2O_5$ will be at equilibrium.

The behavior of the modulated $NO_2$ can be described by a differential equation with the flashing lamps represented by a Fourier series for a square wave.

$$\frac{d[NO_2]}{dt} = \frac{F}{V}(A_{in}-A_{out}) - \frac{\alpha I k_2[NO_2]^2}{k_1[NO][M]+(k_2+k_3[M])[NO_2]} \tag{19}$$

$$- \frac{2\alpha I}{\pi} \sum_{\substack{odd \\ n}}^{\infty} \frac{1}{n} \sin(n\omega t) \left( \frac{2k_2[NO_2]^2}{k_1[NO][M]+(k_2+k_3[M])[NO_2]} \right)$$

where  $F$ = flow rate

    $V$ = volume of cell

   $A_{in}$ = $NO_2$ concentration flowing into cell

   $A_{out}$ = $NO_2$ concentration flowing out of cell

   $\omega = 2\pi/T$, where $T$ is the period of the square wave

And the flashing lamps are described by:

$$f(I) = \frac{I}{2} + \frac{2I}{\pi} \sum_{\substack{\text{odd} \\ n}}^{\infty} \frac{1}{n} \sin(n\omega t) \tag{20}$$

This expression again neglects the reactions containing ozone. The ratio of [NO] to $[O_2]$ in this experimental system is approximately 10/1, and the ratio of $[NO_2]$ to $[O_2]$ is about 1/1. Since oxygen molecule competes with NO and $NO_2$ for oxygen atoms the ratio of the rate constants for the competition reactions multiplied by the concentration ratios will determine the importance of reaction (7). Using the literature values for the rate constants this gives:

$$\frac{k_1[NO]}{k_7[O_2]} = 1000/1 \quad \text{and} \quad \frac{k_2[NO_2]}{k_7[O_2]} = 550/1$$

Since less than 0.1% of the oxygen atoms could be converted to ozone and be available to combine with NO to form $NO_2$, it is a good approximation to neglect the formation of ozone under these experimental conditions.

Under these conditions the flow system has reached a steady state with respect to reactants and products, so the un-modulated or DC terms in (19) cancel. This leaves only the modulated or AC terms, giving the following expression for the modulation of the $NO_2$ concentration by the

flashing lamps:

$$\frac{d[NO_2]}{d\theta}_{(AC)} = -\frac{\alpha I}{\pi^2 f} \left( \frac{2k_2[NO_2]^2 \sum\limits_{odd\ n}^{\infty} \frac{1}{n} \sin(n\theta)}{k_1[NO][M]+(k_2+k_3[M])[NO_2]} \right) \tag{21}$$

where $d\theta = 2\pi f dt$; $\theta = \omega t$; and $f$ = flashing frequency.

If the conditions are selected so that the modulation is less than one part per 1000 then the concentrations of the reactants will be essentially constant. This gives a linear differential equation for the $NO_2$ modulation which can be integrated in closed form.

$$[NO]_{2(AC)} = \frac{\alpha I[NO_2]^2}{\pi^2 f} \left( \frac{2k_2 \sum\limits_{odd\ n}^{\infty} n^{-2}\cos(n\theta)}{k_1[NO][M]+(k_2+k_3[M])[NO_2]} \right) \tag{22}$$

The experimentally determined quantity is the peak to peak amplitude of the first harmonic of the modulation signal. An expression for this quantity can be derived from (22) and is given in (22').

$$[NO_2]_{(exp.)} = \frac{4\alpha I k_2[NO_2]^2}{\pi^2 f(k_1[NO][M]+(k_2+k_3[M])[NO_2])} \tag{22'}$$

Comparison of Eq. (22) with Eq. (20) shows the modulation wave form to be a triangular wave, phase shifted 90° from the exciting light. The modulation amplitude and phase shift can be experimentally evaluated using methods similar to the phase shift method of obtaining fluorescence life times. Since any periodic function can be expressed by a Fourier series the concentration modulation of the reacting species can be described by

$$f(\omega t) = \sum\limits_{n=1}^{\infty} A_n \sin(n\omega t) + B_n \cos(n\omega t) \tag{23}$$

Then for some phase angle $\delta$, **given by:** $B_n/A_n = \tan(\delta)$ Equation (23) can be rearranged to give:

$$f(\omega t) = \sum_{n=1}^{\infty} C_n \sin(n\omega t + \delta) \qquad (24)$$

where $C_n = (A_n^2 + B_n^2)^{1/2}$.

If just the first fundamental of equation (24) is used $C_1$ will be the modulation amplitude and $\delta$ will be the phase shift from the exciting light.

This translates into experimentally measurable quantities when the concentrations of the reacting species can be expressed in terms of Beer's law: $\exp(-\sigma c l) = I/I_o$. If the modulation concentration changes are small, they can be described by:

$$\frac{I + \Delta I}{I_o} = \exp(-\sigma l(c - \Delta c)) = \exp(-\sigma l(1 - \Delta c/c)) \qquad (25)$$

Taking the ratio of $\dfrac{(I + \Delta I)/I_o}{I/I_o}$ gives the reduced expression:

$$\frac{I + \Delta I}{I} = \exp(\sigma l \Delta c) \qquad (26)$$

Expanding $\exp(\sigma l \Delta c)$ in a power series, and neglecting all higher order terms since $\Delta c$ is much less than one, allows a further reduction of the expression. This gives: $\exp(\sigma l \Delta c) = 1 + \alpha l \Delta c$

which when substituted into (26) gives the experimentally measurable quantity:

$$\frac{\Delta I}{I} = \sigma l \Delta c \qquad (26')$$

By using lock-in amplification techniques it is possible to measure the magnitude of the sine and cosine components of the modulation

signal as well as the absolute DC intensity of the monitoring radiation, I. Then the concentration modulation, $\Delta c$, can be determined since $\Delta I = (A^2 + B^2)^{1/2}$ as in equation (24). The phase shift is then given experimentally by the relationship $\delta = \tan^{-1}(B/A)$.

By solving these five experimental relationships, (11'), (14), (17), (18), and (22'), simultaneously, and combining them with experimentally measured values it is possible to obtain values for $\alpha I$, $k_4 K_{eq}^{-1}$, $k_1[M]/k_2$, and $k_3[M]/k_2$, with one equation redundant to use as a check.

Once these ratios were determined, a further check was available by using these ratios along with literature values for $K_{eq}$ and $k_1$ in a set of coupled differential equations to give reaction profiles for $NO_2$ and $N_2O_5$. Comparison of the calculated curves with the experimental ones will give another measure of the accuracy of the analysis.

## B.  Apparatus

The 40 m. path molecular modulation infrared spectrophotometer used for this work was constructed in this laboratory. A block diagram of the instrument is shown in Fig. 3a. The monochromator is a McPherson model 2051, one meter grating monochromator, equipped with interchangeable gratings and order sorting filters. The four gratings are blazed at 18, 12, 8, and 3.5 microns to give maximum light through put over the range 500 to 4000 $cm^{-1}$.

The detectors are cooled photoconductors from the Santa Barbara Research Center, mounted on the two exit slits of the monochromator. The main detector is a copper doped germanium photoconductor cooled to liquid helium temperature (4°K). It is used for the region 500 to 3000 $cm^{-1}$. The second detector is a lead sulfide photoconductor cooled
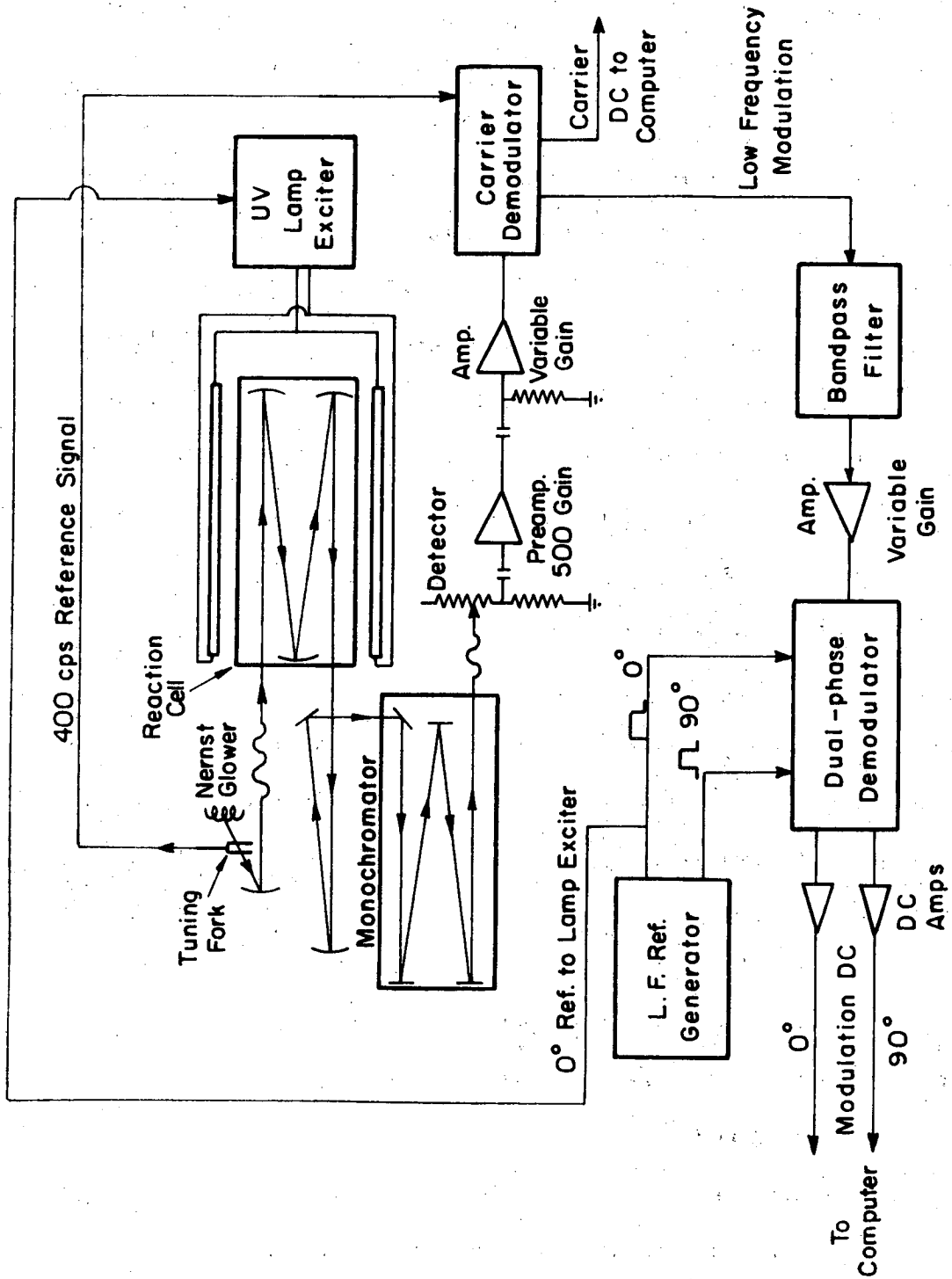
Fig. 3a.   Schematic diagram of experimental apparatus

XBL 728-6830

to -76°C with a dry ice propanol slush, and is used for the region 3000 to 4000 cm$^{-1}$.

The detectors are mounted in interchangeable vacuum dewars designed to permit the use of liquid nitrogen cooled filters and field of view reduction shields. The detector noise is greatly reduced by the exclusion of room temperature radiation, so the field of view is made as narrow as the input optics will allow. This is about 40° for the copper doped germanium detector, but no reduction in view is necessary for the PbS detector since it is not sensitive to room temperature radiation. Though both of these detectors are highly sensitive in their respective wavelength regions, they are still the major source of electrical noise in the system. This noise is due to background radiation, Johnson noise, and shot noise.

1. Reaction Cell

The reaction cell is a cylindrical quartz tube 91 cm long and 28.7 cm in diameter. The quartz tube is mounted in a massive stainless steel and covar bracket to form a closed cell with an overall volume of 67.0 liters. The cell has three gold coated multiple reflection mirrors mounted in it to give an optical path variable from 4 to 40 meters. The entrance and exit slits of the cell are covered with KBr windows, and the end plates of the cell are O-ring fitted to allow the cell to be evacuated.

Temperature control in the cell is maintained by convection cooling, with the temperature being monitored by a mercury theromometer mounted inside the cell. Any temperature changes within the cell can be offset by using a fan to circulate room air around the cell. The laboratory

air conditioning allows the temperature in the cell to be regulated to 24 ± .5°C.

## 2. Photolysis Lamps

The photolytic light for these experiments was supplied by four, 32 inch, G.E., 30 watt, F30T8/BL black lamps. These are low pressure mercury fluorescent lamps coated with a phosphor that emits light in the region 300. to 420. nanometers. The manufacture's output curve for the lamps is shown in Fig. (3b). The four lamps are mounted symmetrically around the outside of the cell and parallel to it at a distance of about two inches from the cell wall. Around the whole cell and the lamps is an "Alzak" aluminum reflective shield. This highly polished aluminum reflects 85 percent in the 300 to 400 nm region and increases the light passing through the cell as well as making the photon flux much more uniform. The photon flux in the cell is on the order of $10^{16}$ photons/cm$^2$-sec.

The filaments of the lamps are heated to a red glow by five volt transformers to prolong lamp life and to insure rapid firing of the lamps at low flashing frequencies. The lamps are powered by a 700 volt regulated power supply, which electrically switches the 700 volts across the lamps' electrodes in response to a reference square wave. This reference square wave is supplied by dividing down a crystal oscillator to frequency multiples of 0.25 cps.

The lamp output can be monitored by a permanently mounted phototransistor pointed toward the center of the cell. This photo-transistor shows the flashing lamp output to be a square wave with a
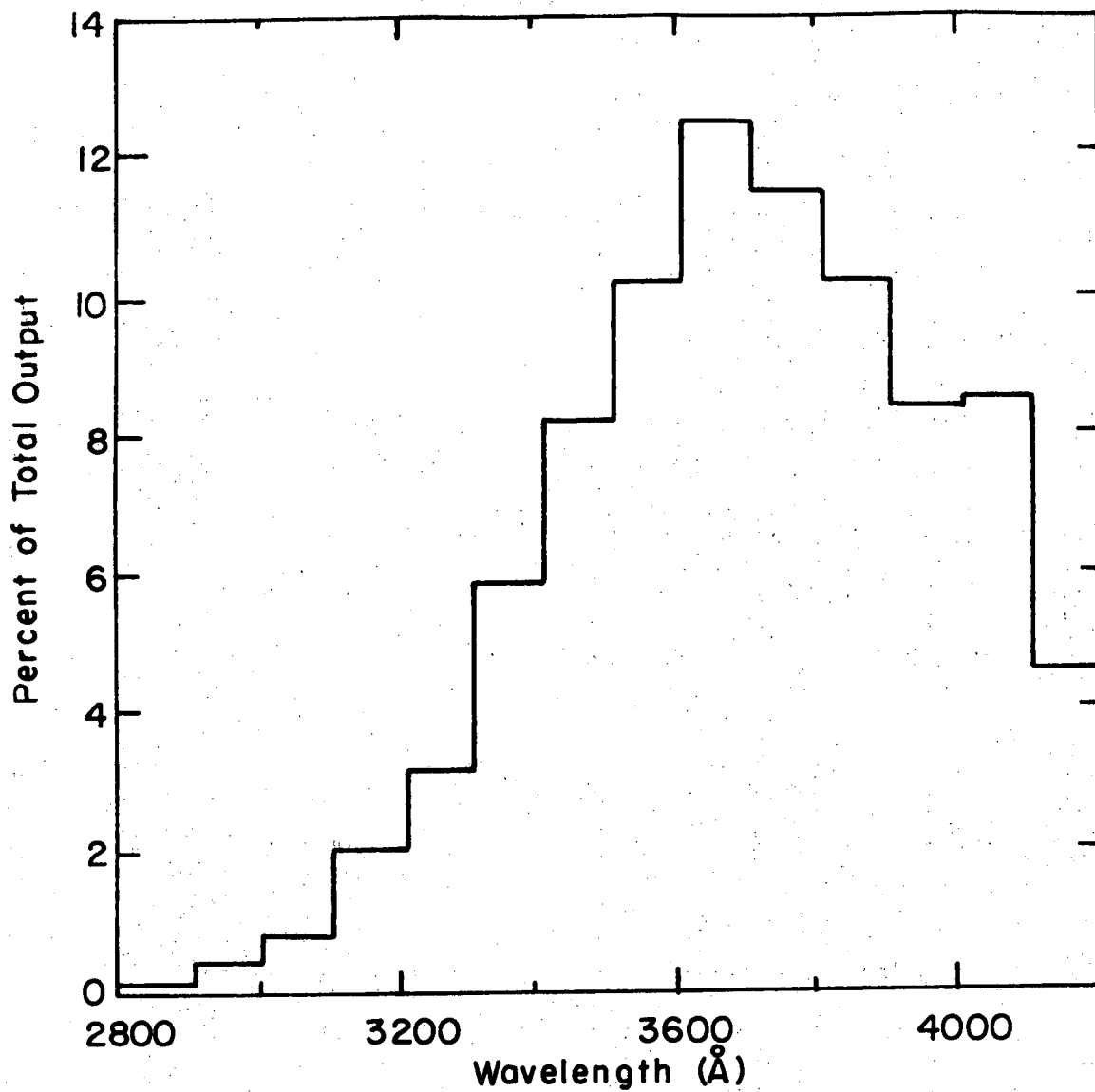
XBL728-6831

Fig. Black Lamp emission spectrum.

spike at the initial firing. This asymmetry has less than 0.01 percent

of the total area of the light output under it, so the lamp output

can be considered a true square wave. The phototransistor also gives

a measure of the overall output of the photolysis lamps. It can monitor

any changes in the lamp intensity due to aging or temperature change,

and give a reference value to which the lamp output can be corrected.

3. IR Source

The infrared source is a 2 by 12 mm Nernst glower element powered

by an Infrared Industries AC power supply isolated from the wall

current by a Sola regulating transformer. The source element is

contained in a nitrogen gas purge box with a steady rate of gas flow

to provide convection cooling. The source beam is chopped at 400 cps

by an American Time Products tuning fork to have the signal information

carried at a frequency well above the region of electronic 1/f noise.

4. Electronics

A diagram of the detector circuit is shown in Fig. (3c). The

photodetector is balanced by a metal film resistor of approximately

equal value, and the whole circuit is biased at 135 volts. The bias

voltage was selected to give an optimum signal to noise output from

the detector circuit. The signal is AC coupled to remove the low

frequency noise, and then fed into a LM308 operational amplifier set

for a gain of 500. This gives an output signal on the order of 0 to

10 volts AC. This signal is filtered to pass frequencies from 200 to

1000 cps to further reduce the low frequency noise and to remove the

higher harmonics of the 400 cps carrier signal.
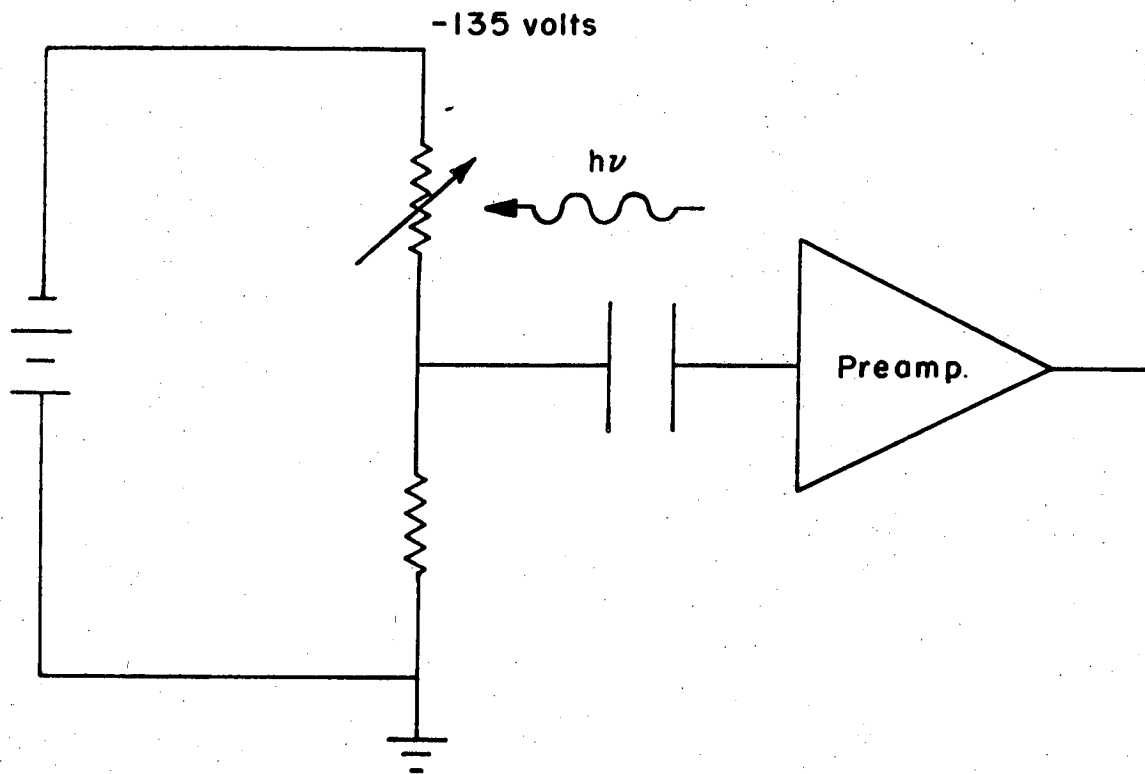
Fig. 3c.  Photodetector circuit.

XBL728-6832

5. Carrier Demodulator

The amplified 400 cps signal is rectified by a lock in amplifier operating from a 400 cps reference supplied by the tuning fork chopper. The output of this lock in passes through an integrating filter which can be set for a time constant of .001, .01, or .1 second with a 12 DB per octave roll off slope. These filters smooth the rectified carrier signal without attenuating the low frequency modulation signal which the 400 cycle signal carries on side bands at $400 \pm f$ cps when the apparatus is operating in the modulation mode.

The DC voltage produced by the carrier demodulator is directly proportional to the intensity of the infrared radiation striking the detector.

6. Low Frequency Dual Demodulator

When the instrument is used as a modulation device, the flashing photolysis lamps cause periodic concentration fluctuations in the absorbing gases in the cell. These concentration fluctuations amplitude modulate the 400 cps carrier signal, where the modulation information is carried at $400 \pm f$ cps and f can be varied from 0.25 to 32 cps.

When the signal passes through the carrier demodulator the output is a DC signal on the order of 2 volts carrying a $10^{-4}$ to $10^{-3}$ AC ripple at frequency f with the modulation information contained in the ripple. This modulation information is retrieved in the low frequency dual demodulator (Fig. 3d). The DC signal from the carrier demodulator is split with one signal going to a signal averaging computer, and the other going into a set of high Q band pass filters.
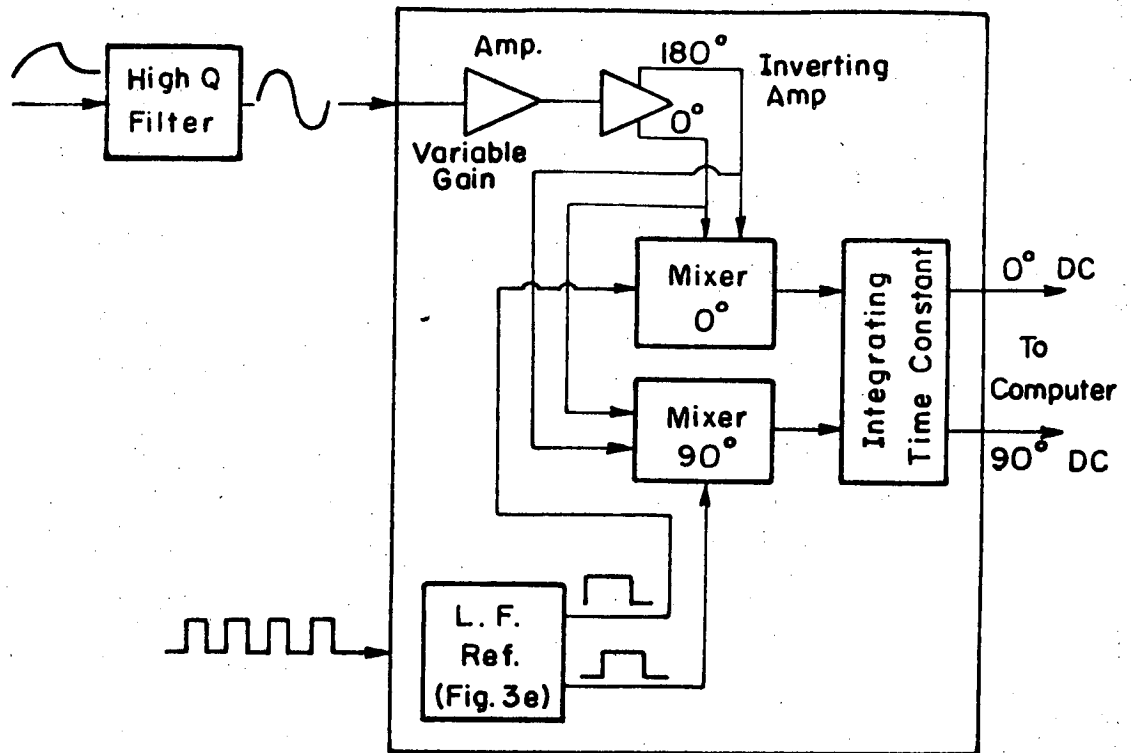
Fig. 3d.  Low frequency dual demodulator
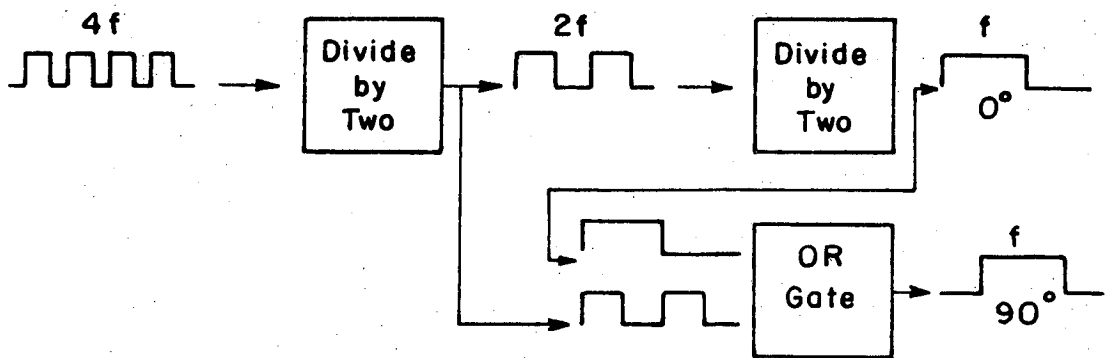


XBL 728-6833

Fig. 3e.  Low frequency reference generator

The band pass filters select for the low frequency, f, of the modulation signal. These filters reduce the third harmonic of the low frequency signal by a factor of eight.

After the filtering the low frequency signal goes into a variable gain amplifier with settings from a gain of 100 to 100,000. The modulation signal on the detector is between 0.1 and 10 micro volts, and this is amplified up to the millivolt level by the detector preamplifier. By setting the dual demodulator amplifier for a gain of 500 or 1000 it is then possible to bring the modulation signal up to the level of 1 volt AC. This is the maximum value possible for the modulation signal since it is buried in about $\pm$ 15 volts of noise at this level, which is the maximum swing for the demodulators.

The AC signal is then split and sent into two separate lock in mixers. The two mixers operate on references which are 90° phase shifted from one another. One mixer then produces a DC voltage for the "in phase" or sine component of the modulation signal, and the other mixer gives a voltage for the "quadrature" or cosine component.

The timing and symmetry of the references for the low frequency mixers are critical for measuring phase shifts. To produce these 90° phase shifted references a square wave at 4 times the flashing frequency, f, is frequency divided by 2 in two steps Fig. (3e). The resulting square waves are at frequencies 2f and f, and are completely symmetrical. The square wave at frequency f is used to drive the lamp flasher, and it is used as the reference for the "in phase" or sine component mixer. The quadrature reference is then generated from an exclusive OR circuit

operating on the square waves at f and 2f. This produces a square wave 90° phase shifted and perfectly symmetrical to the square wave driving the flashing lamps.

The output signals from the dual demodulator are then integrated through filters with time constants adjustable from 0.1 to 20 seconds, with 12 DB roll offs. The integrated signals are then sent into a signal averaging computer.

## 7. Filtering

The purpose of the low frequency band pass filtering is to reduce the higher harmonics of the modulation signal. The higher harmonics contain kinetic information, but they are discriminated against by the lock in amplifiers, since they switch on square wave references. The even harmonics of the modulation signal cancel each other in the lock in mixer, and the odd harmonics are reduced by 1/3, 1/5, . . ., 1/n, where n is the number of the odd harmonic. Rather than trying to include these reduced higher harmonics in the data analysis it is much simpler to filter them out electronically. This shortens the time required for averaging the modulation signal, and makes the differential equation analysis of the results much more tractable.

The reduction of the third harmonic is 1/8 due to the filters, and 1/3 due to the lock in mixers. This gives 1/24 for the total electronic reduction of the third harmonic, but the third harmonic is usually less than one third of the first harmonic due to the modulation signal having been produced from the square wave flashing of the photolysis lamps. This gives an overall reduction of approximately

1/72 for the third harmonic with respect to the fundamental frequency. This makes the higher harmonics negligible in the final results since the modulation data are **seldom** better than ± 5 percent.

## C. Computer Coupling

Once the DC voltages from the lock in amplifiers are available the method of handling the data must be considered. There are three forms of experimental data provided by this instrument and the data handling device must be able to record all three adequately.

(1) The apparatus is a single beam spectrometer and requires a simple method of storing a background and an absorption spectra to calculate a ln $I_o/I$ versus wavelength plot.

(2) When doing DC photolysis experiments the IR light intensity must be recorded as a function of time.

(3) When operating the apparatus in the modulation mode, there are three channels of data which must be recorded simultaneously and averaged over long periods of time.

In order to meet these requirements and to have the ability to manipulate the data, the experiment is coupled to a combination of two small computers, Fig. (4). The first computer is a Fabritek 1074 hardwired signal averaging computer, the second is a PDP 8/L, Digital Equipment general purpose computer. Each of the computers has 4096 words of addressable memory and the two computers are linked together so that all the memory is accessable to the operator.

The data input to the computer is through either of two analog-to-digital converters which are plug in units for the 1074 signal averager.
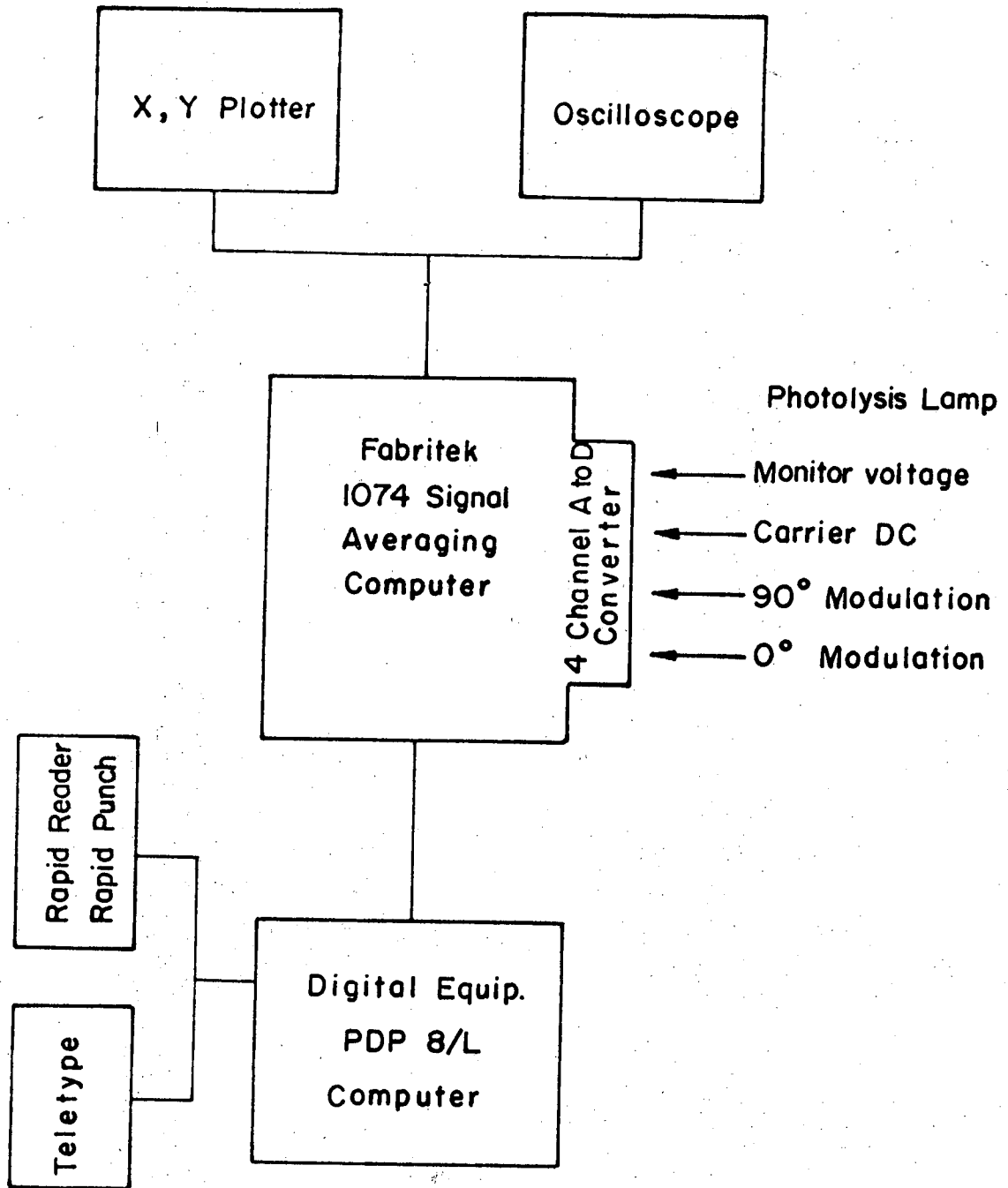
XBL728-6834

Fig. 4. Schematic diagram of computer coupling.

One is a 12 bit A to D converter which allows 1 part in 2048 accuracy
for high sensitivity in spectrum scanning, and the other is a 9 bit,
4 channel input A to D which is used for monitoring 1, 2, or 4 signals
simultaneously with lower sensitivity for signal averaging.

By using the computer memory for storage of background spectra,
it is possible to calculate the $\ln(I_o/I)$ for an absorption spectra
and plot this out on an X,Y recorder as a function of wavelength.

The modulation data can be taken on 3 channels at once and
averaged for any desired length of time, with oscilloscope display of
the computer memory giving direct access to monitor the progress of the
experiment. When the sine and cosine components of the modulation
signal have been sufficiently characterized by averaging, the data
can be manipulated in the general purpose computer to print or plot
out the phase and amplitude information.

When doing photolysis experiments the voltage as a function of
time can be stored in the computer, with the time scale selected on
the computer to give maximum resolution to the curvature of interest.
For permanent storage of data, it is possible to have the computer
punch out the data on paper tape.

### D.  Modulation Standard

Since the modulation signals pass through several stages of
amplification and attenuation due to filtering, it is necessary to
have some means to calibrate the absolute gain of the system for each
frequency of interest. It is also necessary to have an absolute

calibration of the phase shift introduced onto the fundamental

modulation frequency due to the filtering out of the higher harmonics.

To calibrate the system it was necessary to produce a modulation

on a 400 cps carrier signal of known amplitude and phase shift with

respect to the flasher reference. The circuit shown in Fig. (5)

produces a zero degree phase shifted square wave modulation on the car-

rier signal with an amplitude of $\Delta I/I = 2.0 \times 10^{-3}$. Since the

electronics will select only the fundamental frequency of the square

wave, the absolute modulation of the carrier by the fundamental is

$\Delta I/I = 8.0 \times 10^{-3}/\pi$, where $\Delta I/I$ is defined as:

$$\frac{\Delta I}{I} = \frac{(A^2 + B^2)^{1/2}}{V_{carrier}}$$

A = amplitude of sine component voltage

B = amplitude of cosine component voltage

V = amplitude of carrier signal voltage

The total phase shift of the system is then given by $\delta = \tan^{-1}(B/A)$.

By comparing the data taken on chemical systems to the modulation

standard it is possible to determine exact amplitudes and phase shifts

for the chemical modulation.

## E.  Gases and Flow System

The chemicals used in the $NO_2$ experiments were flowed into the

reaction cell at rates of 2 to 5 liters per minute through a 2.5 foot

long glass tube extended into the cell with small holes placed in the

**From Tuning Fork Reference**

20 K

500 K

Output

Input

0

-10

1 K
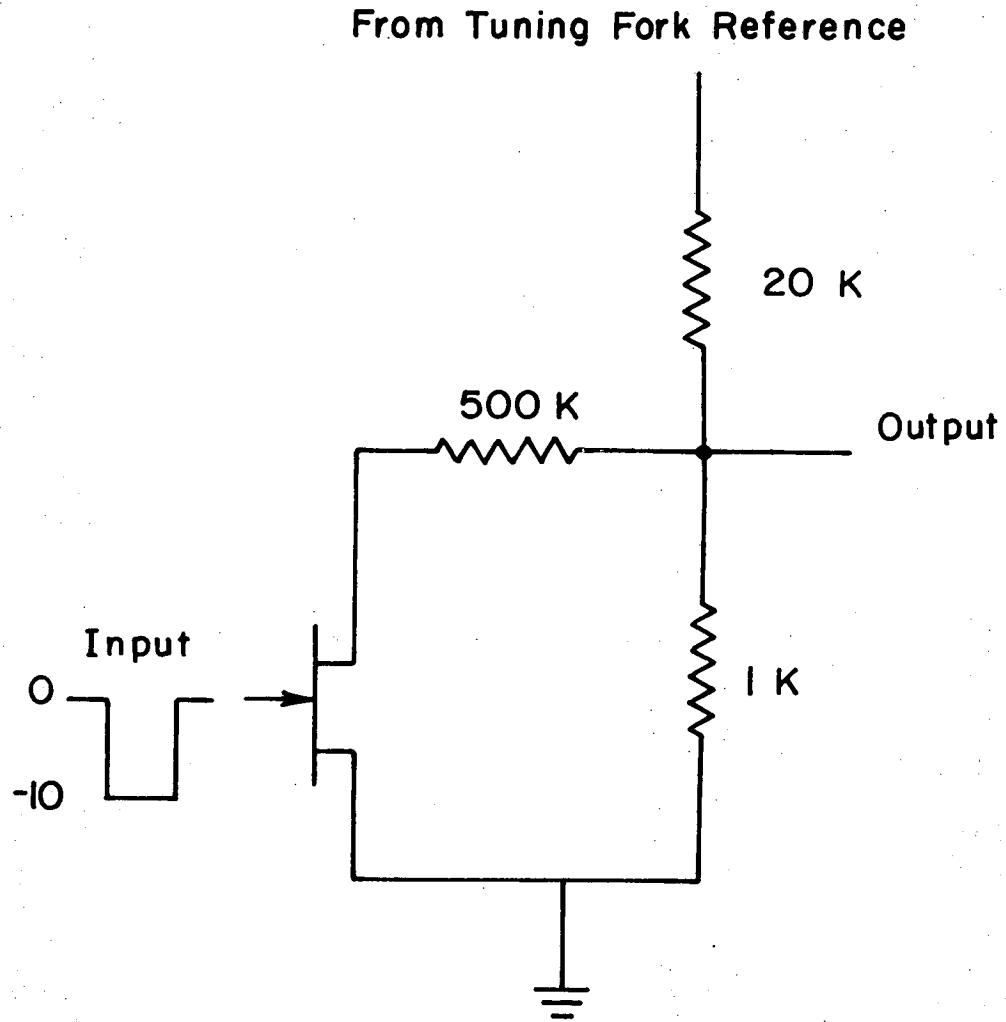
XBL 728-6835

Fig. 5.  Circuit used as modulation standard, all
resistors are accurate to 1 percent.

tube every four inches.  This causes a jetting of the chemicals into the cell giving a more even mixing throughout.  The exit flow is through a similar tube with larger holes to reduce the chance of a pressure buildup within the cell.

Flow rates into the reaction cell were measured by Hastings Mass Flow Meters, and Manostat Predictability flow meters.  Each of the flow meters was calibrated for the gas being flowed through it by measuring the water the flow would displace in a wet test flow meter.

The carrier gas used in the experiments was High Dry grade nitrogen supplied by the Lawrence Berkeley Laboratory.  The only purification was to pass the gas through a Matheson particulate and water removal filter.  The analysis of the nitrogen supplied by the dealer is given below.

<div align="center">

High Dry Nitrogen

</div>

| | | |
|---|---|---|
| $N_2$ | 99.999 | percent |
| $O_2$ | 0.1 | ppm |
| $H_2O$ | 0.25 | ppm |
| $CO_2$ | 0 | |

<div align="center">

Argon less than 5 ppm

</div>

The nitrogen dioxide used in the closed cell photolysis experiments was prepared by vacuum distillation from bulk liquid $N_2O_4$.  The $N_2O_4$ was stored in one atmosphere of oxygen at 0°C for 24 hours to convert any NO into $NO_2$.  Then the material was condensed in a dry ice bath and the non-condensible gases were pumped off.  The material was then distilled from -20°C to -76°C several times with the first portion

being discarded in an attempt to remove $HNO_3$. The remaining solid $N_2O_4$ was stored as a white solid at $-76°C$.

The $NO_2$ used in the flow experiments was mixed gas supplied by Matheson. The gas was analyzed by IR and UV spectroscopy in this laboratory to contain $970 \pm 5$ ppm $NO_2$ and $38 \pm 4$ ppm NO, with the remainder being $N_2$. The nitric oxide was also supplied by Matheson and was analyzed in this laboratory to contain $1030 \pm 20$ ppm NO and $160 \pm 4$ ppm $NO_2$, with the remainder being $N_2$.

The concentrations of all $NO_x$ species were determined from absorption coefficients measured in this laboratory. The basis for these absorption coefficients was the determination of the $NO_2$ absorption coefficient in the ultra violet by a coworker, Richard Graham. He expanded known amounts of purified $NO_2$ into a 45.6 liter calibrated volume u.v. cell and determined the absorption coefficient at several wavelengths. From these measurements the Matheson mixed $NO_2$ in $N_2$ was calibrated and used as a standard for obtaining infrared absorption coefficients through flow experiments.

Using the measured $NO_2$ absorption coefficient it was possible to calibrate the tank of mixed NO in $N_2$ by flowing a known amount of the gas into the IR cell and then photolyzing the NO to $NO_2$.

The absorption coefficient of $N_2O_5$ was determined by reacting a known amount of $NO_2$ with ozone. The reaction mechanism is given by:

$$NO_2 + O_3 \rightarrow NO_3 + O_2$$

$$NO_3 + NO_2 \rightleftharpoons N_2O_5$$

$$NO_2 + NO_3 \rightarrow NO + O_2 + NO_2$$

$$NO + NO_3 \rightarrow 2NO_2$$

$$NO + O_3 \rightarrow NO_2 + O_2$$
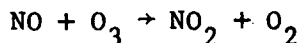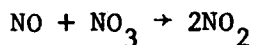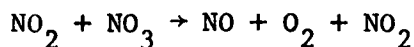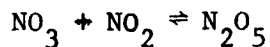
In a steady state flow system with excess $NO_2$, there is a conversion of the $NO_2$ to $N_2O_5$ with a small steady state concentration of $NO_3$ maintained. The $NO_3$ concentration is given by:[26] $[NO_3]_{ss} =$ $7.6 \times 10^3 [O_3]_{ss}^{1/3} [N_2O_5]_{ss}^{1/3}$ molecules $cm^{-3}$. With an excess of $NO_2$ the $O_3$ is kept very small so that $[NO_3]_{ss}$ is negligable with respect to $[N_2O_5]_{ss}$. This gives the relationship: $[N_2O_5]_{ss} = ([NO_2]_i - [NO_2]_{ss})/2$. This would allow the measurement of the $N_2O_5$ absorption coefficient. Unfortunately there was always a source of hydrogen in the ozone stream, due apparently to small amounts of a hydrocarbon in the oxygen used to form the $O_3$. This hydrocarbon reacted with the $NO_3$ in the reaction cell to produce nitric acid.

Attempts to remove the hydrocarbon impurity with cold traps and an Engelhard, palladium hydrocarbon conversion catalyst were unsuccessful. Running the catalyst at 450°C supposedly gives 100 percent conversion of hydrocarbons to $CO_2$ and water which can then be trapped out or absorbed on Ascarite and $P_2O_5$. All attempts along this line met with only limited success, so it was decided to subtract out the amount of $HNO_3$ formed. This gives the equation: $[N_2O_5]_{ss} = ([NO_2]_i - [NO_2]_{ss} - [HNO_3]_{ss})/2$.

The nitric acid absorption coefficient was obtained by the expansion of purified $HNO_3$ into the IR cell with the pressure then brought up to 1 atm. with $N_2$.

The reaction of $NO_2$ with $O_3$ was carried out at several different sets of reactant conditions, with the resulting $N_2O_5$ absorption coefficient being reproducable to within five percent.

All the absorption coefficients were measured as a function of optical density to assure that they were constants over the range of conditions used in these experiments. The absorption coefficients used in this work are listed in Table V, and the absorption versus wavelength plots of $NO_2$, $N_2O_5$, and $HNO_3$ are shown in Fig. 6. The spectra shown in Fig. 6 were done with a 150 line/mm grating and 2 mm slit widths. The resolution of these spectra is wavelength dependent, being limited by the monochromator. The resolution is 2 $cm^{-1}$ at 1200 $cm^{-1}$ and 3.5 $cm^{-1}$ at 1600 $cm^{-1}$.

Table V.  Absorption coefficients determined in this research, for

individual wavelengths.

| Species | Wavelength | Absorption Coefficient[*] base e in units of $(cm^2/particle)$ |
|---------|-----------|----------------------------------------------------------------|
| $NO_2$ | 6.25 microns | $9.6 \times 10^{-19}$ |
| $HNO_3$ | 7.604 microns | $1.06 \times 10^{-18}$ |
| $N_2O_5$ | 8.032 microns | $1.84 \times 10^{-18}$ |
| $NO_2$ | 355.0 nm | $5.42 \times 10^{-19}$ |
| $NO_2$ | 346.8 nm | $4.74 \times 10^{-19}$ |
| $NO_2$ | 348.6 nm | $5.32 \times 10^{-19}$ |

[*]Total pressure was 1 atm. with $N_2$ as the m gas.  Measured absorption
coefficients were constant over the optical density range 0.0 to 1.0.
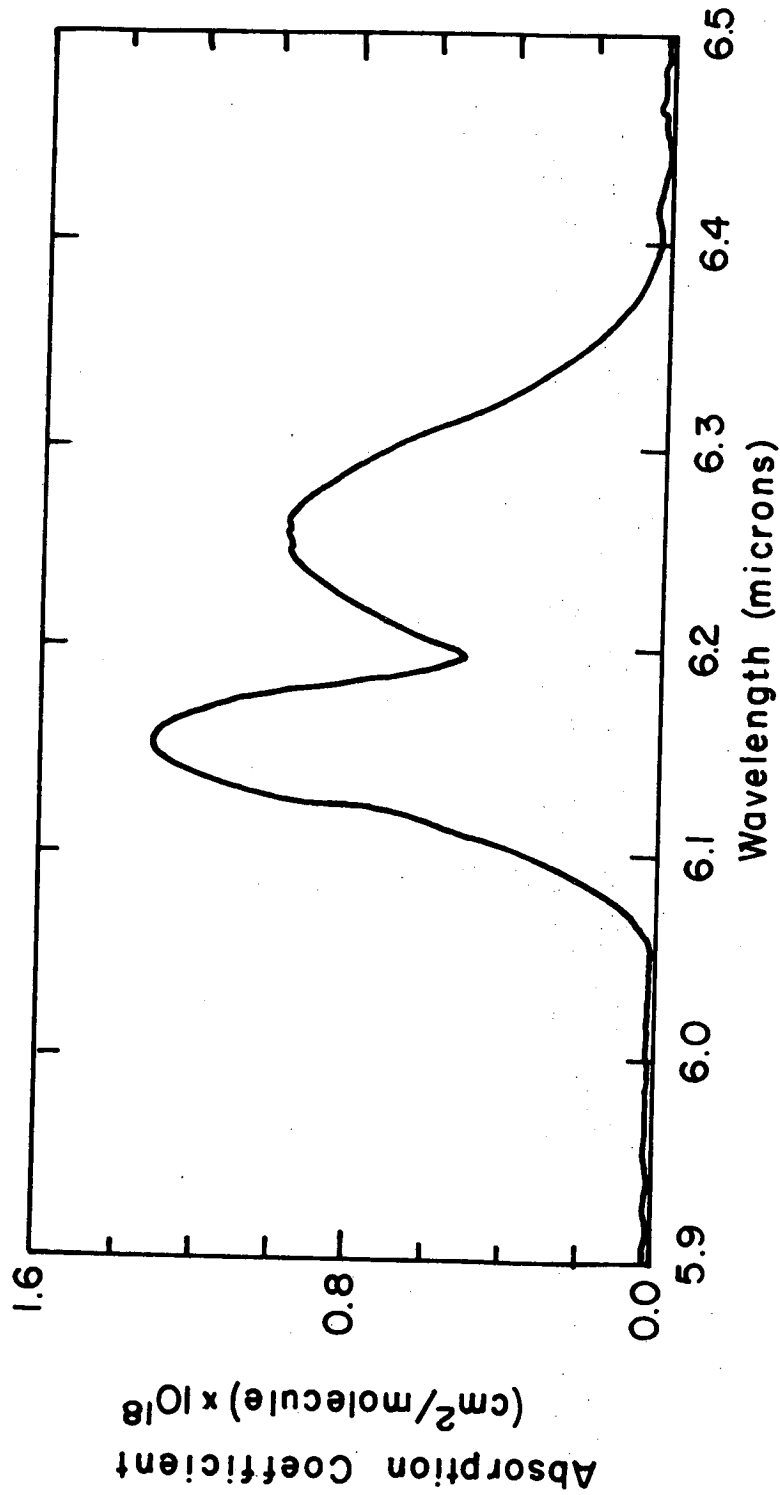
Fig. 6a. Absorption coefficient of $NO_2$ versus wavelength.
Total pressure = 1 atmosphere with $N_2$ as the M gas
Spectral Resolution = 0.014 microns

XBL728-6836
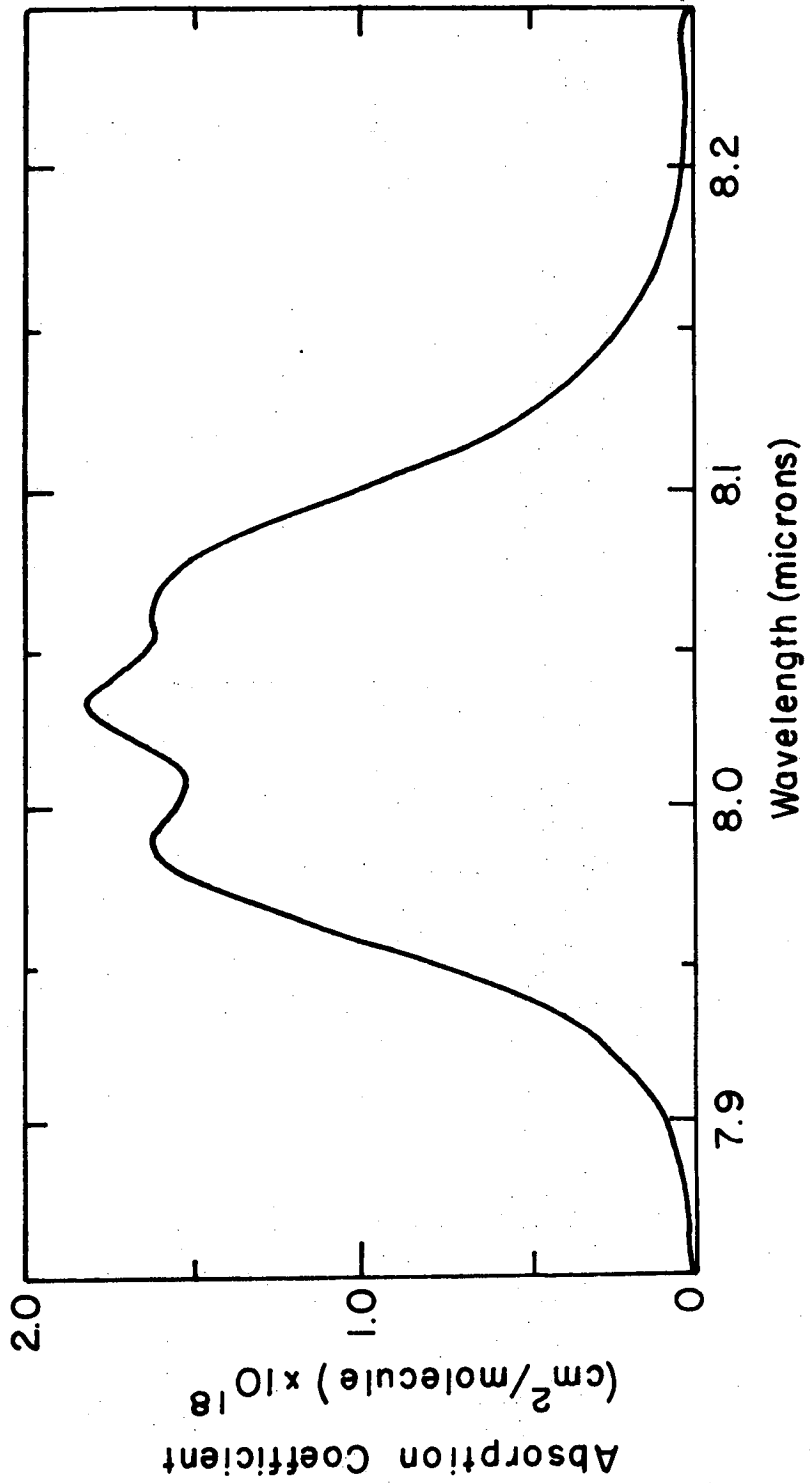
Fig. 6b. Absorption coefficient of $N_2O_5$ versus wavelength.
Total pressure = 1 atmosphere with $N_2$ as the M gas
Spectral Resolution = 0.014 microns
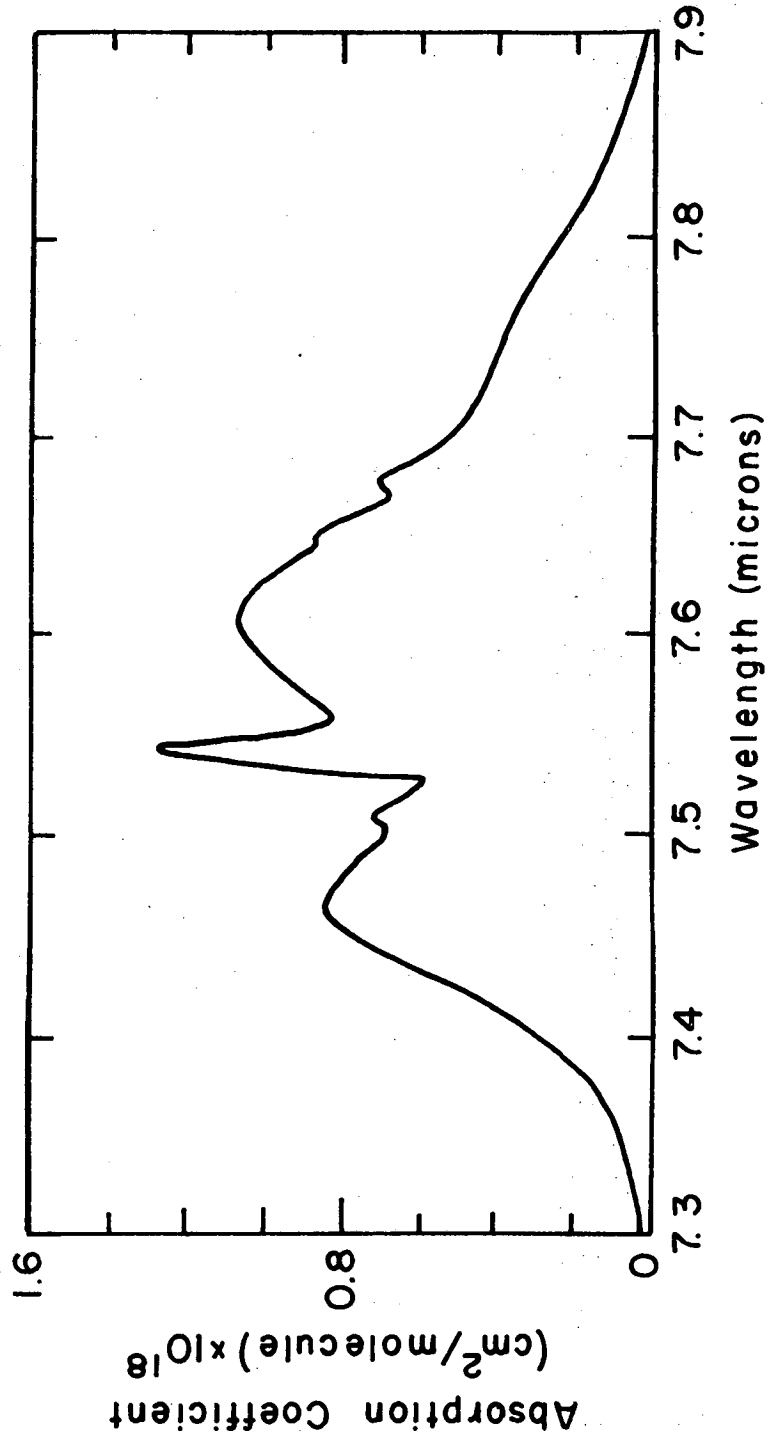
XBL 728-6837

XBL728-6838

Fig. 6c. Absorption coefficient of $HNO_3$ versus wavelength
Total pressure = 1 atmosphere with $N_2$ as the M gas.
Spectral Resolution = 0.014 microns

## III. EXPERIMENTAL PROCEDURE AND DATA

The first series of experiments was the closed cell photolysis of nitrogen dioxide at low pressures. Equation (11') shows that at pressures low enough for all M gas dependent reactions to be negligible the initial slope of the $NO_2$ decay gives a value for $2\alpha I$.

The experiments were carried out at pressures ranging from 10 to 50 mm of mercury, where the M gas was $N_2$. The $NO_2$ partial pressure was always less than 0.1 mm of Hg so that its photolysis would not cause any significant pressure change in the reaction cell. This was done to avoid any change in the $NO_2$ absorption coefficient due to pressure broadening of the rotational lines.

The experiments were carried out at 24°C with the $NO_2$ decay being monitored at 1600 $cm^{-1}$. The $NO_2$ was prepared by vacuum distillation and injected into the evacuated cell before the cell was brought up to the desired pressure with nitrogen. During these experiments the photolysis lamps were monitored by a phototransistor and their intensity was found to be constant to ± 2% over the period of measurement, which was the first twenty seconds of the photolysis. The absolute value of the lamp intensity could be related from one set of experiments to the next by the voltage output of the phototransistor.

The initial conditions of the experiments and the results are listed in Table VI.

The second series of experiments was the one atmosphere, closed cell photolysis of $NO_2$. The chemicals and procedure were the same as in the first series of experiments, only all runs were done at room

pressure. The reaction conditions and the measured first order decay

rate constant of $NO_2$ for each run are recorded in Table (VI).

As shown in Table (VI) there were two sets of experiments run

at one atmosphere total pressure. Set II was run with four photolytic

lamps, and Set III with only two lamps. The experiments with two

lamps were performed to give a longer period in which the initial

slope could be monitored. The photolytic light increase is not linear

between the 2 and 4 lamp experiments, due to the variation between

individual lamps, and possibly due to some loading down of the power

supply. The two sets of experiments can be correlated by comparing

the measurements of the phototransistor which was used to monitor the

photolytic light intensity.

The third series of experiments was conducted to monitor the

build up of $N_2O_5$ during the $NO_2$ photolysis. The $N_2O_5$ experiments

were run at 24°C and 1 atm. pressure, with the $N_2O_5$ being monitored

at either 1245 or 1238 $cm^{-1}$. The $N_2O_5$ was observed at two different

wavelengths to assure that the overlap of the very small $N_2O_4$ absorption

centered at 1265 $cm^{-1}$ was having no effect on the measurements. The

behavior of the $N_2O_5$ at each of these wavelengths is typified by the

concentration versus time curves shown in Fig. (7). The $N_2O_5$ builds

up to a maximum in about 21 seconds and then decays to approach a

steady state concentration.

The comparison of the two curves in Fig. (7c) shows some asymmetry

in their decay slopes. This is probably due to the experimental error

envolved in these measurements. The data was taken by monitoring the

Table VI. Initial slope measurements for $NO_2$ decay as a function of pressure.

| Set I | $[NO_2]_i$ (molecules/cm$^3$) | Total Pressure mm/Hg | Number of Photolysis Lamps | ka* sec$^{-1}$ |
|---|---|---|---|---|
| 1 | $8.8 \times 10^{14}$ | 27 | 4 | $1.52 \times 10^{-2}$ |
| 2 | $4.8 \times 10^{14}$ | 22 | 4 | $1.50 \times 10^{-2}$ |
| 3 | $1.2 \times 10^{15}$ | 56 | 4 | $1.52 \times 10^{-2}$ |
| 4 | $8.8 \times 10^{14}$ | 19.5 | 4 | $1.44 \times 10^{-2}$ |
| 5 | $8.6 \times 10^{14}$ | 19.5 | 4 | $1.47 \times 10^{-2}$ |

relative light intensity = 1.0**; average $k_a$ = 1.49 ± .03 × $10^{-2}$ sec$^{-1}$

| Set II | $[NO_2]_i$ | Total Pressure | # of Lamps | ka sec$^{-1}$ |
|---|---|---|---|---|
| 1 | $6.7 \times 10^{14}$ | 756 | 4 | $1.23 \times 10^{-2}$ |
| 2 | $9.6 \times 10^{14}$ | 756 | 4 | $1.20 \times 10^{-2}$ |
| 3 | $1.16 \times 10^{15}$ | 756 | 4 | $1.22 \times 10^{-2}$ |
| 4 | $1.05 \times 10^{15}$ | 756 | 4 | $1.25 \times 10^{-2}$ |

relative light intensity = 1.0; average $k_a$ = 1.22 ± .02 × $10^{-2}$ sec$^{-1}$

| Set III | $[NO_2]_i$ | Total Pressure | # of Lamps | ka sec$^{-1}$ |
|---|---|---|---|---|
| 1 | $1.97 \times 10^{15}$ | 756 | 2 | $0.68 \times 10^{-2}$ |
| 2 | $3.1 \times 10^{14}$ | 756 | 2 | $0.685 \times 10^{-2}$ |
| 3 | $2.1 \times 10^{14}$ | 756 | 2 | $0.69 \times 10^{-2}$ |
| 4 | $2.4 \times 10^{14}$ | 756 | 2 | $0.706 \times 10^{-2}$ |

relative light intensity = 0.56; $k_a$ = 0.69 ± .01 × $10^{-2}$ sec$^{-1}$

*ka = first order decay rate constant for $NO_2$

**Relative light intensity measured by phototransistor.

changes in the $\ln(I_o/I)$ during photolysis runs on an A to D converter
connected to the 1074 signal averager. Due to the small amounts of
$N_2O_5$ being formed the maximum optical density reached during most of
the runs was $\ln(I_o/I) = 0.06$ to $0.08$. The sensitivity of the electronics
was limited by the number of bits in the A to D converter used. In
order to be able to monitor the photolytic light intensity simultaneously,
the data was normally taken on the 4 input, 9 bit A to D converter.
With this A to D converter, an optical density of 0.08 corresponds to
a change of about 20 digital counts in the monitoring light intensity.
This means that in an average run the accuracy of the measurements
was $\pm$ 5 percent at the maximum of the $N_2O_5$ concentration profile, but
the accuracy drops with the optical density. The noise of the
electronics is $\pm$ 1 count on the A to D converter, so during the decay
when the optical density gets down to about 0.01 the signal to noise
ratio is only 3/1. So at these small optical densities the percentage
error in the measurements is inversely proportional to the amount of
absorption.

The $N_2O_5$ profile shown in Fig. (7a) was done at 1245 $cm^{-1}$ at the
peak of the $N_2O_5$ Q branch. The maximum optical density reached was
0.08 with an $I_o$ of 250 digital counts. This corresponds to a change
of 21 counts at the $N_2O_5$ concentration maximum with a signal to noise
ratio of 21/1. The curve in Fig. (7b) was done at 1238 $cm^{-1}$, and has
a maximum signal to noise ratio of 17/1. The relative experimental
error is indicated on the curves showing the percentage increase in
experimental error at low optical densities.
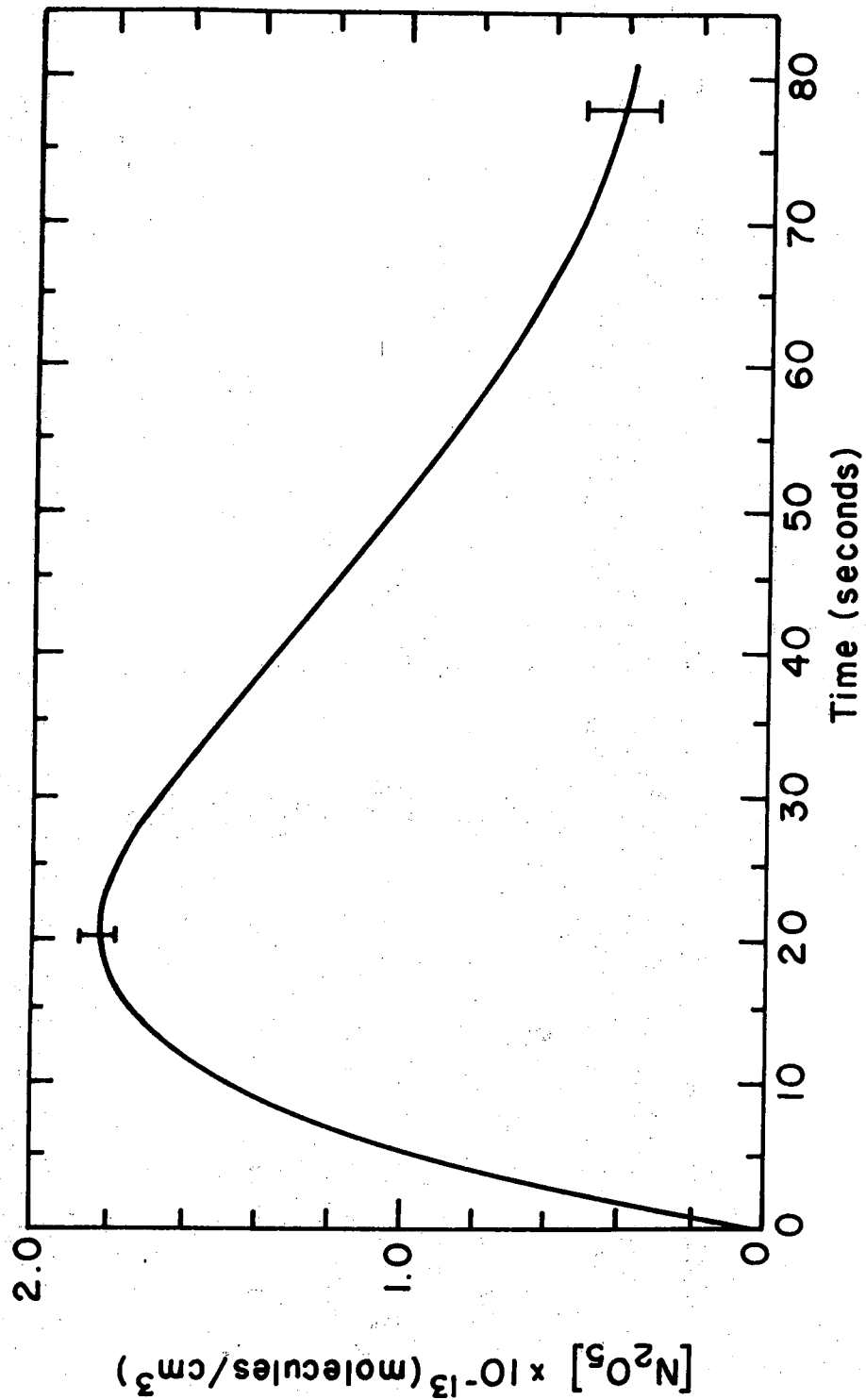
Fig. 7a. $N_2O_5$ concentration profile at 1245 cm$^{-1}$. $[NO_2]_i = 4.2 \times 10^{15}$, $[NO] = 2.05 \times 10^{14}$. The error bars show how the accuracy of the measurement improves with increasing $N_2O_5$ concentration.
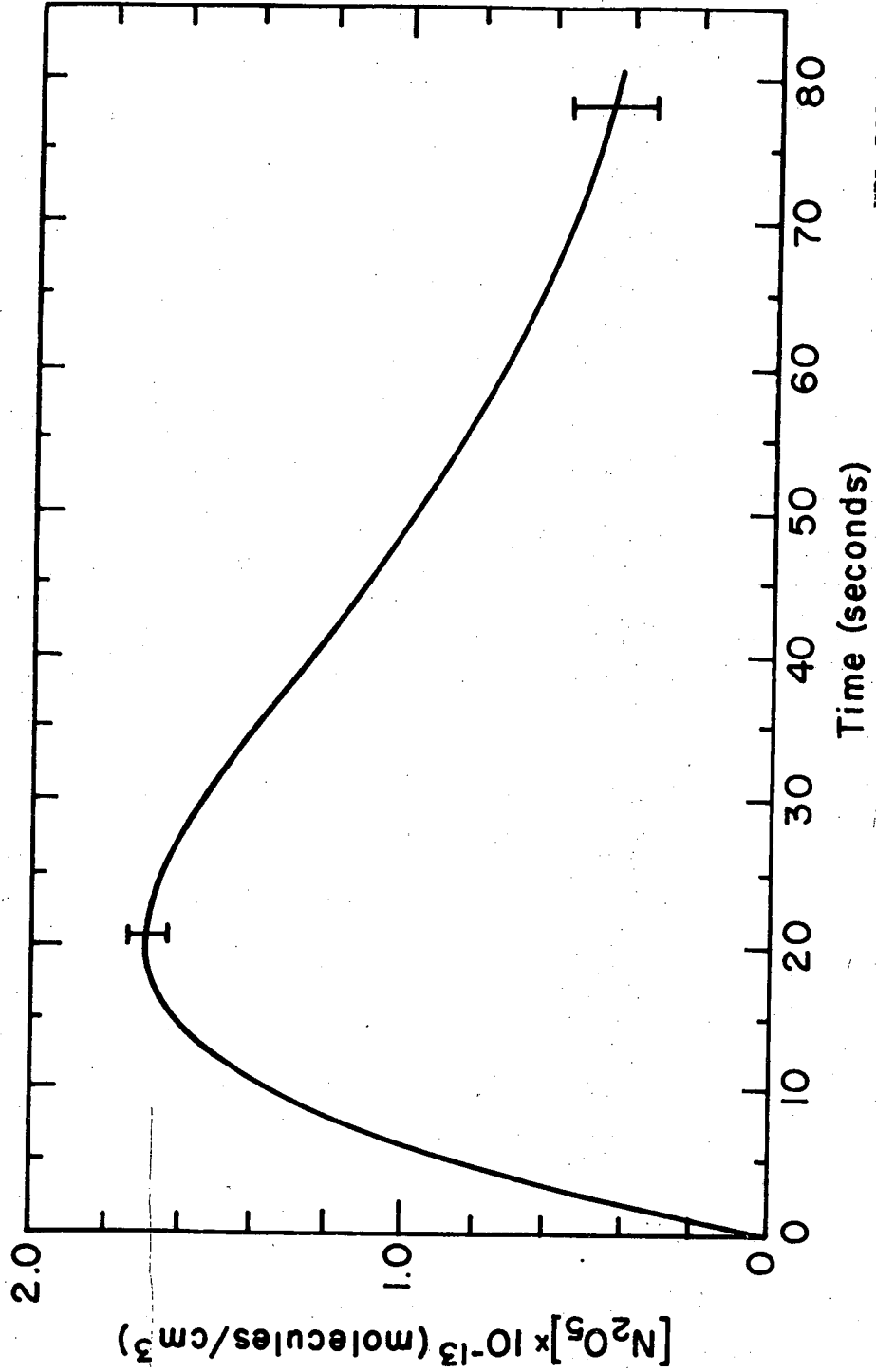
XBL 728-6839

Fig. 7b. $N_2O_5$ concentration profile at 1237 cm$^{-1}$. $[NO_2]_i = 2.84 \times 10^{15}$, $[NO] = 0.0$. The error bars show how the accuracy of the measurement improves with increasing $N_2O_5$ concentration.
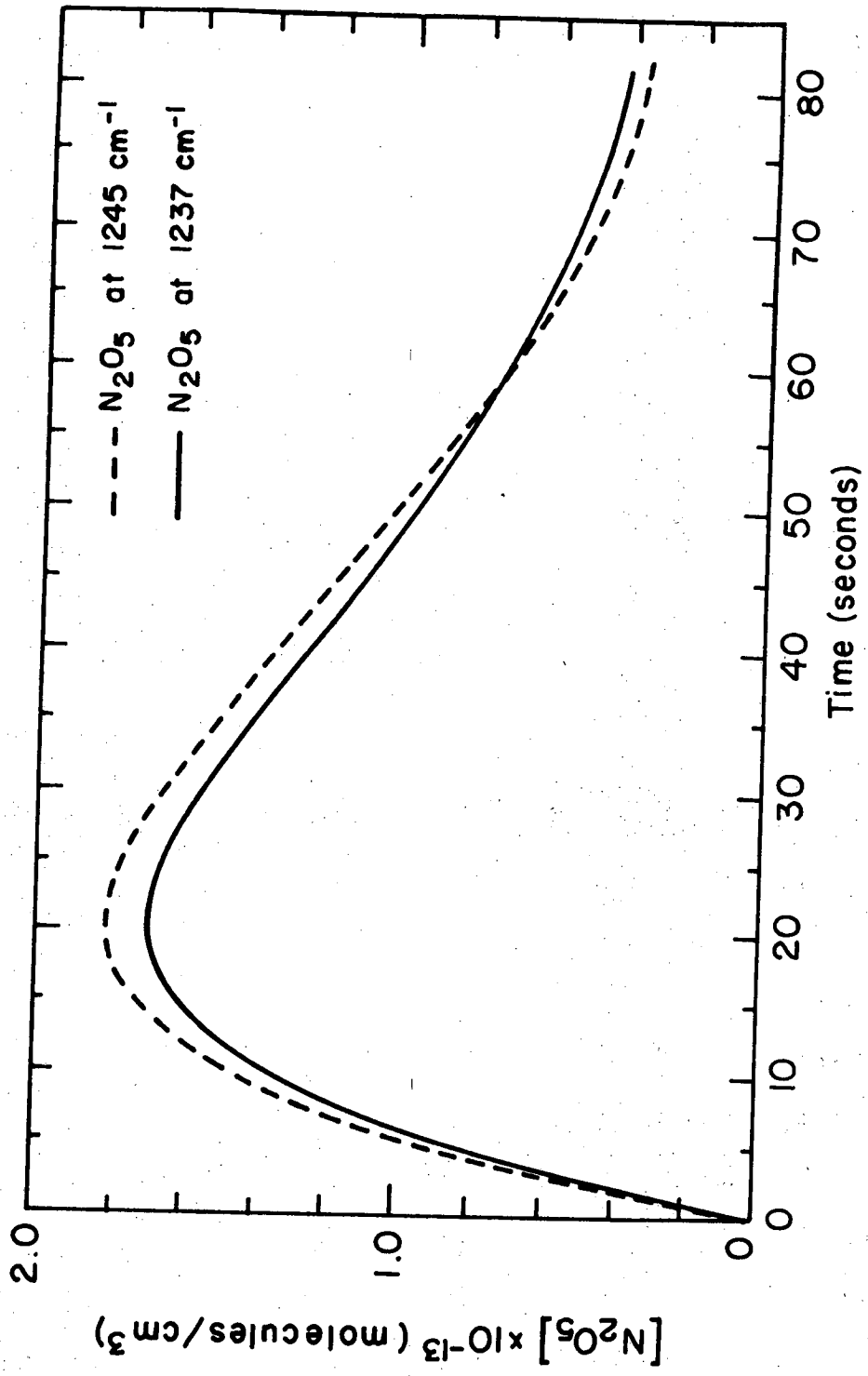
XBL 728-6840

Fig. 7c. Overlay of Figs. 7a and 7b.

XBL728-6841

On the basis of this sensitivity, the asymmetry between the two curves during the decay portion can be attributed to experimental error, rather than to a kinetic effect or overlap by $N_2O_4$.

The data of interest in the $N_2O_5$ experiments are the slope of the initial build up, and the amplitude of the maximum. The initial slopes divided by the $NO_2$ concentration at time zero of the $N_2O_5$ runs done with no initial nitric oxide are recorded in Table (VII).

The amplitude of the $N_2O_5$ maximum is controlled by the ratio $[NO_2]^2/[NO]$ as can be seen from Eq. (17). To test this relationship, experimental runs with varying amounts of initial NO were done. In these experiments distilled $NO_2$ was injected into the cell and the concentration measured. Then some of the $NO_2$ was converted to NO by photolysis, and the NO concentration determined by the amount of $NO_2$ destroyed. After the cell had equilibrated the photolysis lamps were turned on again and the $N_2O_5$ concentration monitored.

The initial concentrations and amplitude of the $N_2O_5$ maxima are recorded in Table (VIII). The graph in Fig. (8) shows $[N_2O_5]_{max}/[NO_2]$ versus $[NO_2]/[NO]$. The plot shows the linear relationship predicted by the mechanism, with the proper limiting behavior of $[N_2O_5]_{max}/[NO_2]$ approaching zero as initial NO becomes large with respect to initial $NO_2$.

The fourth series of experiments were flow experiments with the photolysis lamps being flashed at 1 cycle per second. Steady state flows of $NO_2$, NO, and $N_2$ were established with the photolysis lamps flashing; then the modulation of the $NO_2$ absorption at 1600 $cm^{-1}$ was monitored to determine its amplitude and phase shift from the exciting

Table VII.  Data for the initial slope measurement on $N_2O_5$ buildup.

| # | $[NO_2]_i$ | # of Lamps | $\dfrac{\Delta[N_2O_5]/\Delta T}{[NO_2]_i}$ sec$^{-1}$ |
|---|---|---|---|
| 1 | $2.84 \times 10^{15}$ | 2 | $0.63 \times 10^{-3}$ |
| 2 | $2.5 \times 10^{15}$ | 2 | $0.69 \times 10^{-3}$ |
| 3 | $3.28 \times 10^{15}$ | 2 | $0.79 \times 10^{-3}$ |
| 4 | $1.91 \times 10^{15}$ | 2 | $0.73 \times 10^{-3}$ |
| 5 | $2.58 \times 10^{15}$ | 2 | $0.64 \times 10^{-3}$ |
| 6 | $3.26 \times 10^{15}$ | 2 | $0.70 \times 10^{-3}$ |

$$\text{ave } \frac{\Delta[N_2O_5]/\Delta T}{[NO_2]_i} = 0.70 \pm .06 \times 10^{-3} \text{ sec}^{-1}$$

Table VIII. Data for graph in Fig. 8.

| # | (part/cc) $[NO_2]_1$ | (part/cc) $[NO]_1$ | (part/cc) $[N_2O_5]_{max}$ | $\dfrac{[N_2O_5]_{max}}{[NO_2]^*}$ | $\dfrac{[NO_2]^*}{[NO]^*}$ | $T\,°K = 296$ |
|---|---|---|---|---|---|---|
| 1 | $3.28 \times 10^{15}$ | $0.0$ | $2.06 \times 10^{13}$ | $0.73 \times 10^{-2}$ | $6.39$ | |
| 2 | $3.26 \times 10^{15}$ | $0.0$ | $2.0 \times 10^{13}$ | $0.718 \times 10^{-2}$ | $6.38$ | |
| 3 | $2.5 \times 10^{15}$ | $0.0$ | $1.43 \times 10^{13}$ | $0.67 \times 10^{-2}$ | $6.32$ | |
| 4 | $2.84 \times 10^{15}$ | $0.0$ | $1.66 \times 10^{13}$ | $0.684 \times 10^{-2}$ | $6.34$ | |
| 5 | $1.85 \times 10^{15}$ | $8.1 \times 10^{13}$ | $0.89 \times 10^{13}$ | $0.56 \times 10^{-2}$ | $5.02$ | |
| 6 | $1.61 \times 10^{15}$ | $1.02 \times 10^{14}$ | $0.65 \times 10^{13}$ | $0.472 \times 10^{-2}$ | $4.24$ | |
| 7 | $2.56 \times 10^{15}$ | $1.65 \times 10^{14}$ | $0.84 \times 10^{13}$ | $0.38 \times 10^{-2}$ | $4.19$ | |
| 8 | $2.56 \times 10^{15}$ | $2.52 \times 10^{14}$ | $0.68 \times 10^{13}$ | $0.31 \times 10^{-2}$ | $3.57$ | |
| 9 | $2.26 \times 10^{15}$ | $2.58 \times 10^{14}$ | $0.8 \times 10^{13}$ | $0.41 \times 10^{-2}$ | $3.52$ | |
| 10 | $2.36 \times 10^{15}$ | $4.08 \times 10^{14}$ | $0.57 \times 10^{13}$ | $0.285 \times 10^{-2}$ | $2.71$ | |

* = concentration at time of $N_2O_5$ maximum
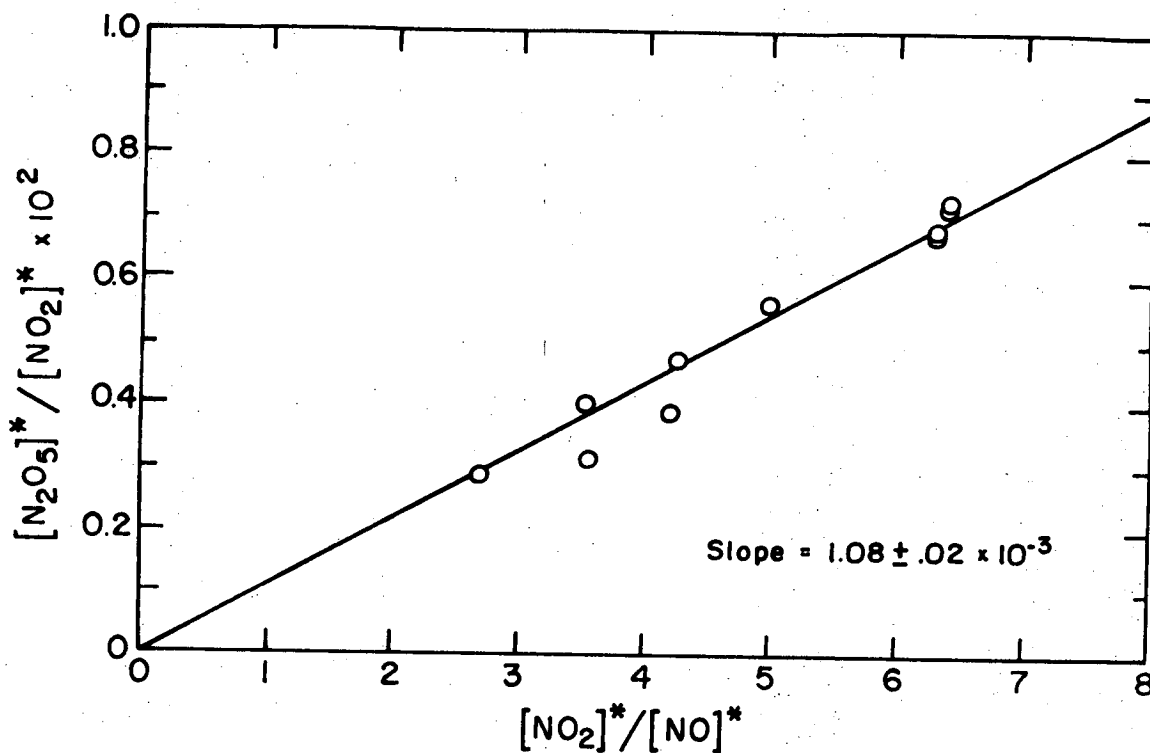
The * indicates the concentration at the time of the $N_2O_5$
concentration maximum, $t^*$

XBL 728-6842

Fig. 8.  Plot of $[N_2O_5]^*/[NO_2]^*$ versus $[NO_2]^*/[NO]^*$ ,
with the slope giving a value of

$$\frac{\alpha I}{k_{eq}^{-1}\, k_4\, (1+k_2/k_3[M])} \ .$$

lights. A summary of the steady state concentrations with the phase and amplitude measurements are recorded in Table (IX). The photolytic light intensity for the modulation experiments was found to be 11.2 percent greater than in the initial slope experiments, when measured by the phototransistor mounted on the cell. This is due to the lamps warming up over the hours of firing required for each modulation experiment. To normalize the results the value of $\alpha I$ used in the analysis of the modulation data was 11.2 percent greater than that measured in the initial slope experiments.

Table IX. Data for $NO_2$ modulation experiments done at 1 atmosphere pressure and 24°C.

| Exp. # | M gas | Lamps | $\alpha I$ (sec$^{-1}$) | $[NO_2]_{AC}$ (molecules/cm$^3$) | Phase Shift | $[NO_2]_{ss}$ (molecules/cm$^3$) | $[NO]_{ss}$ (molecules/cm$^3$) | $\dfrac{k_1[m]}{k_2}$ |
|---|---|---|---|---|---|---|---|---|
| 1 | $N_2$ | 4 | $.83 \times 10^{-2}$ | $1.43 \times 10^{11}$ | 93.6° | $1.02 \times 10^{14}$ | $7.4 \times 10^{14}$ | 0.163 |
| 2 | $N_2$ | 4 | $.83 \times 10^{-2}$ | $1.31 \times 10^{11}$ | 89° | $1.19 \times 10^{14}$ | $1.22 \times 10^{15}$ | 0.179 |
| 3 | $N_2$ | 4 | $.83 \times 10^{-2}$ | $1.4 \times 10^{11}$ | 70° | $0.68 \times 10^{14}$ | $1.49 \times 10^{14}$ | 0.189 |
| 4 | $N_2$ | 4 | $.83 \times 10^{-2}$ | $8.32 \times 10^{10}$ | 82° | $1.13 \times 10^{14}$ | $2.04 \times 10^{15}$ | 0.185 |
| 5 | $N_2$ | 4 | $.72 \times 10^{-2}$ | $1.62 \times 10^{11}$ | 80° | $1.87 \times 10^{14}$ | $2.12 \times 10^{15}$ | 0.19 |
| 6 | $N_2$ | 4 | $.72 \times 10^{-2}$ | $1.68 \times 10^{11}$ | 94° | $1.68 \times 10^{14}$ | $1.6 \times 10^{15}$ | 0.178 |
| 7 | Ar | 4 | $.83 \times 10^{-2}$ | $1.78 \times 10^{11}$ | 88.2° | $1.55 \times 10^{14}$ | $1.38 \times 10^{15}$ | 0.19 |
| 8 | Ar | 2 | $.46 \times 10^{-2}$ | $1.65 \times 10^{11}$ | 87.8° | $2.18 \times 10^{14}$ | $1.3 \times 10^{15}$ | 0.206 |
| 9 | Ar | 4 | $.83 \times 10^{-2}$ | $1.41 \times 10^{11}$ | 91.8° | $1.34 \times 10^{14}$ | $1.34 \times 10^{15}$ | 0.198 |

For m = $N_2$ average $\dfrac{k_1[m]}{k_2}$ = 0.18 ± .01

For M = Argon average $\dfrac{k_1[m]}{k_2}$ = 0.20 ± .01

## IV. RESULTS

By comparing the results of these four sets of experiments, it is possible to characterize the kinetics of the $NO_2$ photolysis system.

The first set of experiments, the low pressure photolysis of $NO_2$, yields a value for $\alpha I$, the product of the integrated absorption coefficient, quantum yield, and light intensity. Using this value for $\alpha I$ with the published values for the absorption spectrum of $NO_2$, primary quantum yields of $NO_2$, and the photolysis lamp output; it is possible to obtain a value for the photon flux in the reaction cell.

The quantity $\alpha$ is essentially a rate constant for the photolytic decomposition of $NO_2$, and it can be expressed as a product of the absorption coefficient (base e) and quantum efficiency for photo decomposition. This is assuming that since less than 0.7% of the total photolytic light was absorbed in each experiment, the light intensity can be treated as a constant throughout a photolysis run. This product can be written as an integral over wavelength of the product of the discrete values for the absorption coefficient and quantum yield at wavelength $\lambda$. This integral is given by:

$$\alpha_{NO_2} = \frac{\int (\sigma_{NO_2})_\lambda P_\lambda (Q_{NO_2})_\lambda d\lambda}{\int (Q_{NO_2})_\lambda P_\lambda d\lambda}$$

Where $(Q_{NO_2})_\lambda$ is the quantum yield, $P_\lambda$ is the percentage of the total photon flux, and $(\sigma_{NO_2})_\lambda$ is the absorption coefficient of $NO_2$, all at wavelength $\lambda$. These integrals can be approximated by the summations:

$$\alpha_{NO_2} = \frac{\sum\limits_{i} (\sigma_{NO_2})_{\Delta\lambda i} \bar{P}_{\Delta\lambda i} (\bar{Q}_{NO_2})_{\Delta\lambda i}}{\sum\limits_{i} \bar{P}_{\Delta\lambda i} (\bar{Q}_{NO_2})_{\Delta\lambda i}}$$

where the bar indicates an average value over the interval $\Delta\lambda i$. The wavelength dependence of $\sigma_{NO_2}$ and $Q_{NO_2}$ can be obtained from the literature (Figs. (1) and (2)), and $P_\lambda$ can be taken from the manufacturer's lamp output spectra Fig. (3b). Evaluating this summation over 100 Å intervals gives the value $\alpha_{NO_2} = 5.41 \times 10^{-19} cm^2$. The data for this calculation are shown in Table (X).[27] Dividing the measured value for $\alpha I$ by the calculated value for $\alpha_{NO_2}$ yields the light flux in the reaction cell.

$$I = \alpha I / \alpha_{NO_2} = 1.5 \times 10^{16} \text{ photons/cm}^2 \text{ sec}$$

Where $\alpha I$ was taken as $.83 \times 10^{-2}$, the value corresponding to four lamps flashing at 1 cps.

The data in Table (VI) for the 1 atmosphere photolysis of $NO_2$ gives an average value for the first order decay rate constant, $k_a$. Equation (14) gives:

$$k_a = 2k_2 \alpha I / (k_2 + k_3 [M]) \tag{28}$$

Since a value for $\alpha I$ under these same reaction conditions is available from the low pressure $NO_2$ photolysis runs the ratio $2k_2/(k_2+k_3[M])$ can be calculated from Eq. (28).

Table X. Calculation of average $NO_2$ photolytic rate constant.

| Spectral Range | Mean $p_\lambda$ | Mean $Q_\lambda$ | $p_\lambda Q_\lambda$ | Mean $\sigma_\lambda$ (1./mole-cm) | $p_\lambda Q_\lambda \sigma_\lambda$ |
|---|---|---|---|---|---|
| 2700-2800Å | .00065 | 0.97 | .00063 | 18. | .0113 |
| 2800-2900 | .00190 | 0.97 | .00184 | 23. | .0423 |
| 2900-3000 | .00405 | 0.97 | .00393 | 31. | .1218 |
| 3000-3100 | .00785 | 0.97 | .00761 | 47. | .3577 |
| 3100-3200 | .0196 | 0.97 | .0190 | 67. | 1.273 |
| 3200-3300 | .0319 | 0.97 | .0309 | 88. | 2.72 |
| 3300-3400 | .0578 | 0.97 | .0561 | 109. | 6.115 |
| 3400-3500 | .0820 | 0.965 | .0791 | 128. | 10.12 |
| 3500-3600 | .1018 | 0.955 | .0972 | 143. | 13.89 |
| 3600-3700 | .1250 | 0.92 | .1150 | 154. | 17.71 |
| 3700-3800 | .1149 | 0.86 | .0988 | 160. | 15.80 |
| 3800-3900 | .1023 | 0.74 | .0757 | 165. | 12.49 |
| 3900-4000 | .0846 | 0.57 | .0482 | 169. | 8.15 |
| 4000-4100 | .0850 | 0.35 | .0298 | 169. | 5.035 |
| 4100-4200 | .0457 | 0.12 | .00548 | 165. | 0.904 |
| 4200-4300 | .0306 | 0.03 | .00092 | 156. | 0.1434 |
| 4300-4400 | .0763 | 0.005 | .00038 | 146. | 0.0555 |
| | | | $\Sigma = .6706$ | | $\Sigma = 94.941./$ mole-cm (base 10) |

Therefore, $(\alpha)_{NO_2} = \dfrac{\Sigma\, p_\lambda Q_\lambda \sigma_\lambda}{\Sigma\, p_\lambda Q_\lambda} = \dfrac{(94.94)(2.303)}{(0.6706)(6.02 \times 10^{20}} = 5.41 \times 10^{-19} cm^2$

From Table (VI):  $k_a = 1.22 \times 10^{-2}$ sec$^{-1}$ (1 atm. and 4 lamps)

$\alpha I = 7.45 \times 10^{-3}$ sec$^{-1}$ (low pressure, 4 lamps)

Using these values and rearranging Eq. (28):

$$\frac{k_3[M]}{k_2} = \frac{2\alpha I}{k_a} - 1.0 = .221 \pm .005 \tag{29}$$

A check for this value is available from the initial slope of the $N_2O_5$ build up. Equation (18) shows:

$$\lim_{t \to 0} \frac{\Delta[N_2O_5]/\Delta T}{[NO_2]} = \frac{\alpha I}{1 + k_2/k_3[M]}$$

From Table (VI):  $\alpha I = 0.42 \times 10^{-2}$ sec$^{-1}$ (2 lamps)

From Table (VII):  $\dfrac{\Delta[N_2O_5]/\Delta T}{[NO_2]} = 7.0 \times 10^{-4}$ sec$^{-1}$ (2 lamps)

Using these values in Eq. (18):

$$\frac{k_3[M]}{k_2} = 0.20 \pm .02 \tag{30}$$

Of these two values for the ratio $k_3[M]/k_2$, the value obtained from the $NO_2$ photolysis at 1 atm is the more accurate result. The $N_2O_5$ build up is much smaller than the $NO_2$ decay, and there was consequently greater experimental error envolved in its measurement. Thus the preferred value is $k_3[M]/k_2 = 0.221 \pm .005$.

A value for $K_{eq}^{-1}k_4$ can be determined from the linear plot in Fig. (8). The slope of this line is given by Eq. (17) to be:

$$\text{Slope} = \frac{\alpha I}{K_{eq}^{-1}k_4(1+k_2/k_3[M])}$$

Under the conditions of 24°C and 2 photolysis lamps:

$$\alpha I = .42 \times 10^{-2} \; sec^{-1}$$

$$k_3[M]/k_2 = 0.22$$

Slope of Fig. (8) = $1.08 \pm .02 \times 10^{-3}$

Then: $K_{eq}^{-1}k_4 = 0.71 \pm .02 \; (sec^{-1})$

The final experimentally determined value is $k_1[M]/k_2$. Equation (22') relates the $NO_2$ modulation amplitude to $\alpha I$, $k_1$, $k_2$, and $k_3$. This equation can be rearranged to give:

$$\frac{[NO_2]_{(exp.)} \pi^2 f}{\alpha I [NO_2]} = \frac{4k_2[NO_2]}{k_1[NO][M] + (k_2 + k_3[M])[NO_2]}$$

By letting $\beta = [NO_2]_{(exp.)} \pi^2 f/\alpha I[NO_2]$, and using the measured values for $\alpha I$ and $k_3[M]/k_2$ this equation can be reduced to:

$$\frac{k_1[M]}{k_2} = \frac{(4-1.22\beta)[NO_2]}{\beta[NO]} \tag{32}$$

Using the data in Table (IX) to evaluate (32) gives:

$$\frac{k_1[M]}{k_2} = 0.18 \pm .01 \text{ for } M = N_2$$

and

$$\frac{k_1[M]}{k_2} = 0.20 \pm .01 \text{ for } M = \text{Argon}$$

A summary of these experimentally determined values is shown in Table (XI), along with the results of other investigators who have measured the same quantities.

Table XI.   Comparison of the results of this work with the literature
values.

| $k_1[M]/k_2$ | $k_3[M]/k_2$ | $k_4 K_{eq}^{-1} (sec^{-1})$ | T °K | Ref. |
|---|---|---|---|---|
| 0.18 ±.01 | 0.221 ±.005 | .71 ± .014 | 296 | This work |
| 0.18 ±.004 | 0.33 ±.08 | | 296 | Schuck et al.   (25) |
| 0.357 | 1.9 | | 300 | Ford & Endow   (22) |
| | | .60 ± .06 | 296 | Hisatsune et al. (21) |

Total pressure = 1 atmosphere

M gas = Nitrogen

Another means of checking the validity of these results is available. By using a set of coupled differential equations to represent the photolysis system, it is possible to calculate the concentration versus time profiles for $NO_2$ and $N_2O_5$. Comparison of the calculated curves with the experimentally measured ones will give an indication of the accuracy of the analysis.

To do such a calculation requires individual values for each of the rate constants. The rate constant $k_1$ is fairly well known, and its average literature value is shown in Table (II). By using this value for $k_1$, the rate constants $k_2$ and $k_3$ can be determined from the experimental ratios. Using the value reported for $K_{eq}$ by Schott and Davidson which is listed in Table (III) allows the calculation of $k_4$ from the measured value of $K_{eq}^{-1}k_4$. Combining these rate constants with the literature values for $k_{6m}$, $k_7$, and $k_8$ (Table (III)) gives all the necessary parameters for the calculation of the reaction profiles.

The coupled differential equations used in the calculation are given below:

$$\frac{d[NO_2]}{dt} = -\alpha I[NO_2] + k_1[NO][O][M] - (k_2+k_3[M])[NO_2]$$

$$+ 2k_4[NO][NO_3] - k_{5m}[NO_2][NO_3] + k_{6m}[N_2O_5] + k_8[NO][O_3]$$

(33)

$$\frac{d[NO]}{dt} = \alpha I[NO_2] - k_1[NO][O][M] + k_2[NO_2][O] - k_4[NO][NO_3]$$

(34)

$$- k_8[O_3][NO]$$

$$\frac{d[N_2O_5]}{dt} = k_{5m}[NO_2][NO_3] - k_{6m}[N_2O_5] \qquad (35)$$

$$\frac{d[O_2]}{dt} = k_2[NO_2][O] + k_8[NO][O_3] - k_7[O_2][O][M] \qquad (36)$$

$$\frac{d[O_3]}{dt} = k_7[O_2][O][M] - k_8[O_3][NO] \qquad (37)$$

$$[O]_{ss} = \alpha I[NO_2]/(k_7[O_2][M] + k_1[NO][M] + (k_2+k_3[M])[NO_2]) \qquad (38)$$

$$[NO_3]_{ss} = \frac{k_3[NO_2][O][M] + k_{6m}[N_2O_5]}{k_{5m}[NO_2] + k_4[NO]} \qquad (39)$$

The steady state approximation for the oxygen atoms and the $NO_3$ was tested by computing the reaction profile with and without this assumption, and the results of both calculations were identical. Since the computer time was reduced by a factor of $10^3$ when the steady states were used it was economical to include this assumption in the calculation.

The values of the rate constants used for the calculation are listed in Table (XII). The calculated and experimental reaction profiles for $NO_2$ and $N_2O_5$ are shown in Fig. (9) for the three wavelengths monitored.

There are three parameters with which to check the sensitivity of these calculations to changes in the rate constants, the $NO_2$ decay rate, the time of the $N_2O_5$ maximum, and the amplitude of the $N_2O_5$ maximum.

Table XII. Rate constants used in computer simulation of $NO_2$ photolysis.

| Rate Constant | $T = 296°K$ | Ref. |
|---|---|---|
| $k_1 = 6.9 \times 10^{-32}$ | $(cm^6/part.^2 \, sec)$ | Lit. average |
| $k_2 = 9.2 \times 10^{-12}$ | $(cm^3/part. \, sec)$ | exp. ratio this work |
| $k_3 = 0.82 \times 10^{-31}$ | $(cm^6/part.^2 \, sec)$ | exp. ratio this work |
| $K_{eq} = 1.24 \times 10^{11}$ | $(cm^3/particles)$ | (20) |
| $k_{6m} = 0.104$ | $(sec^{-1})$ | (19) |
| $k_4 = 0.87 \times 10^{-11}$ | $(cm^3/part. \, sec)$ | exp. ratio this work |
| $k_{5m} = k_6/K_{eq}$ | $1.29 \times 10^{-12}$ | $(cm^3/part. \, sec)$ |
| $k_7 = 0.624 \times 10^{33}$ | $(cm^6/part \, sec)$ | (23) |
| $k_8 = 2.1 \times 10^{-14}$ | $(cm^3/part \, sec)$ | (24) |

Total pressure = 1 atmosphere

M gas = Nitrogen

Units = $(cm^{3x}/particle^x\text{-}sec)$
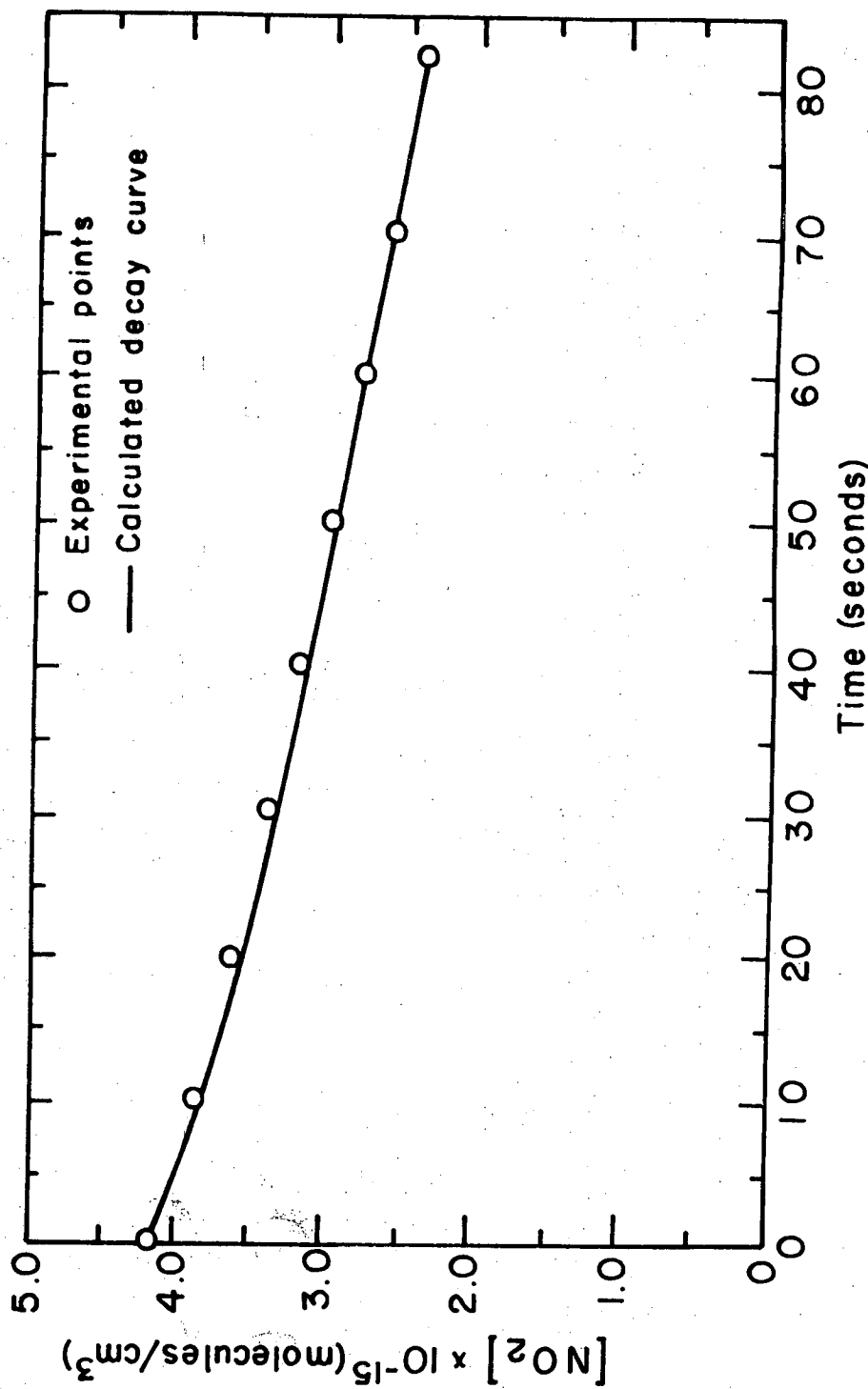
Fig. 9a. NO$_2$ decay; comparison of experimental points with calculated decay curve.

$[NO_2]_i = 4.2 \times 10^{15}$, $[NO]_i = 2.05 \times 10^{14}$
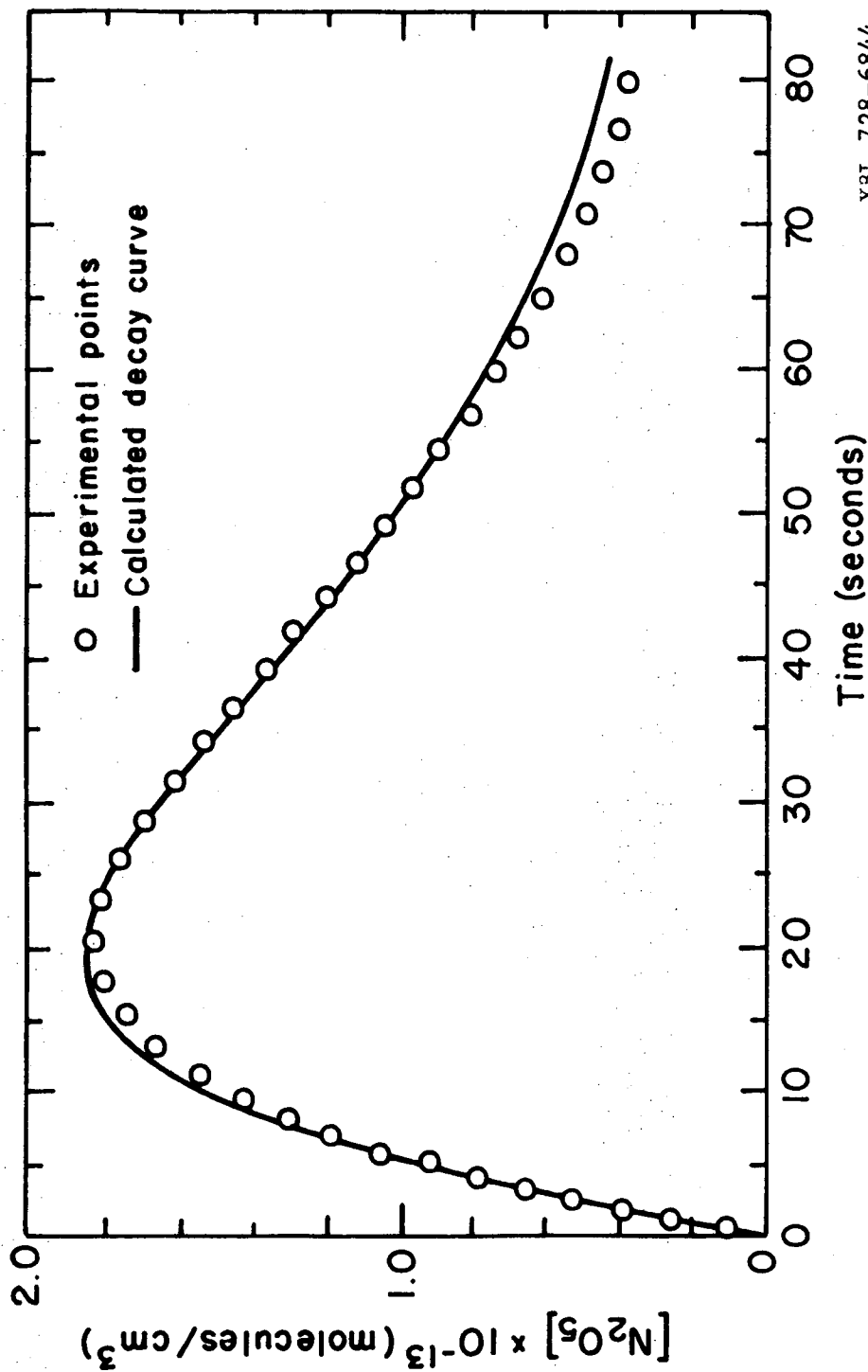
XBL 728-6843

Fig. 9b. $N_2O_5$ decay at 1245 $cm^{-1}$; comparison of experimental points with calculated decay curve.

$[NO_2]_i = 4.2 \times 10^{15}$, $[NO]_i = 2.05 \times 10^{14}$
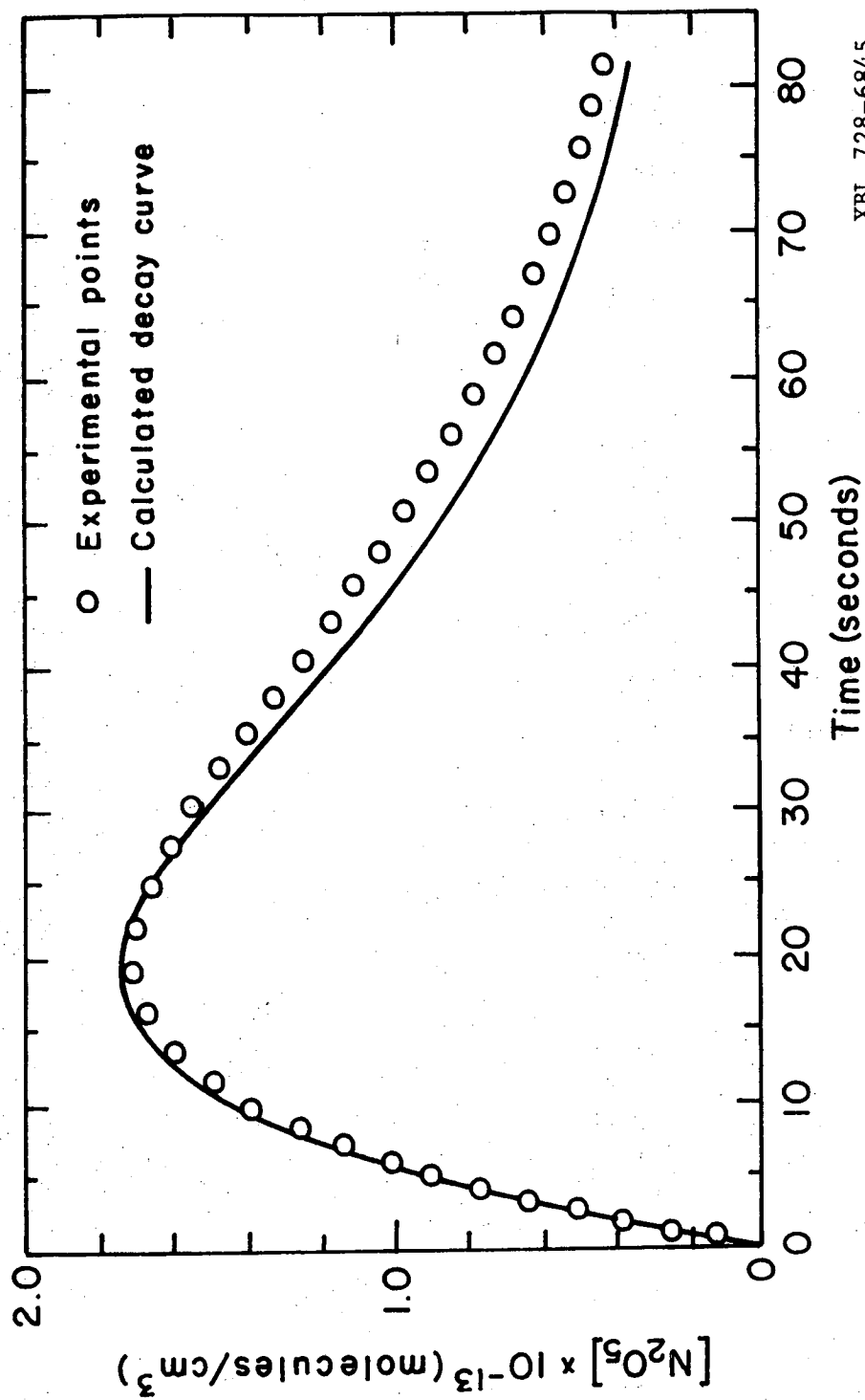
XBL 728-6844

Fig. 9c. $N_2O_5$ decay at 1237 $cm^{-1}$; comparison of experimental points with the calculated decay curve.

$[NO_2]_i = 2.84 \times 10^{15}$, $[NO]_i = 0.0$

XBL 728-6845

Increasing the value of $k_1$ by 20 percent had little effect upon the calculated profiles. Reaction (1) was very small since there was no initial nitric oxide. The only noticable effect of varying $k_1$ was a change in the $NO_2$ decay slope after the NO had built up sufficiently. Thus these simulation calculations were not a good test for the accuracy of $k_1$.

Increasing $k_2$ by 20 percent caused the $N_2O_5$ to reach its maximum 1 second sooner and this maximum was 15 percent lower than in the calculation with $k_2$ at its predicted value. The slope of the $NO_2$ decay was increased by only 1 percent by this change, as would be expected since $k_2$ is in both the numerator and denominator of the initial slope expression, Eq. (13'). This calculation shows that the amplitude and time dependence of the $N_2O_5$ concentration provide a test of $k_2$ which is useful to about $\pm 10\%$.

The shape of the $N_2O_5$ profile is also sensitive to $k_3$. Increasing $k_3$ by 20 percent raised the $N_2O_5$ maximum by 16 percent and made the peak come a half second later. In this calculation the $NO_2$ decay slope was decreased by 2 percent.

When $k_4$ was increased by 20 percent the amplitude of the $N_2O_5$ maximum was increased by 11 percent, and the peak occurred 2 seconds early. The $NO_2$ decay is very insensitive to this rate constant, but since reaction (4) is the major removal step for $NO_3$ the shape of the $N_2O_5$ curve is directly related to $k_4$.

From these calculations it becomes apparent that under the condition of no initial nitric oxide the simulation calculations are a good test

for the relative values of $k_2$, $k_3$ and $k_4$, but they are not sensitive to $k_1$. The decay slope of $NO_2$ is controlled by the ratio $2k_2/(k_2+k_3[M])$ and responds to changes in either $k_2$ or $k_3$, but the $N_2O_5$ curve is the more sensitive test of these rate constants. The time and amplitude of the $N_2O_5$ maximum are determined by the ratio $k_3[M]/k_4(k_3[M]+k_2)$, so a change in any of these three rate constants can change the $N_2O_5$ profile significantly.

The good agreement between the predicted and measured concentration profiles indicates that the ratios containing $k_2$, $k_3$, and $k_4$ are accurate to within 10 percent, since any greater error would cause noticable shifting of the $N_2O_5$ maxima and amplitude. The good match up for the $NO_2$ decay also confirms the ratio of $k_2$ to $k_3$.

## V. DISCUSSION AND CONCLUSIONS

The good agreement between the experimental and calculated $NO_2$ and $N_2O_5$ concentration profiles shows the assumptions and equations used in deriving the rate constant ratios to be consistant with the proposed mechanism for the photolysis system. Since no adjustable parameters were involved in these calculations, the good agreement with the experimental data also indicates the validity of the results.

The most notable result of this investigation comes from the comparison of these measured ratios with the literature values. The measured value for $K_{eq}^{-1}k_4$ is quite close to that reported by Hisatsune in 1957, and the ratios of $k_1$ to $k_2$ and $k_3$ to $k_2$ compare very well with those determined by Schuck et al in 1966. (see Table XI) The most marked disagreement with the literature is between these results and those of Ford and Endow. Their results give a value of 1.9 for the ratio $k_3[M]/k_2$; this is a factor of 8.6 greater than the value found in this investigation. Their result of 0.36 for the ratio $k_1[M]/k_2$ is larger by a factor of 2.0.

Another evaluation of the literature can be made if the averaged literature value used for $k_1$ is assumed to be accurate. Using $k_1 = 0.69 \times 10^{-31}$ $cm^6$/particles$^2$-sec in the ratio $k_1[M]/k_2$ predicts a value of $9.2 \times 10^{-12}$ $cm^3$/particles-sec for $k_2$. This is in good agreement with the value reported by Davis and that of Westenberg and de Haas. This investigation then supports their work over the lower values for $k_2$ reported by other investigators. (see Table I)

With the increasing pollution of the lower atmosphere and the impending pollution problem posed by the introduction of commercial stratospheric flight, it is becoming imperative that scientists provide a description of the mechanisms of photochemical smog reactions. The full importance of the reactions of $NO_2$ in atmospheric pollution is just beginning to be recognized, and as work progresses more researchers are going to turn to the literature for knowledge of the reaction rate constants. It is hoped that this research will help to clarify some of the disagreements which exist in the present literature on the $NO_2$ photolysis system.

The rate constant ratios determined in this investigation confirm the work of Schuck, Stephens, and Schrock, and that of Hisatsune et al, while disagreeing with the earlier work of Ford and Endow. Based on an averaged literature value for the rate constant $k_1$, this work provides the following values for the important rate constants in the $NO_2$ photolysis system in nitrogen at 24°C:

$$k_1 = 0.69 \times 10^{-31} \qquad cm^6/particles^2\text{-sec}$$

$$k_2 = 9.2 \times 10^{-12} \qquad cm^3/particles\text{-sec}$$

$$k_3 = 0.82 \times 10^{-31} \qquad cm^6/particles^2\text{-sec}$$

$$K_{eq}k_4 = 0.71 \qquad sec^{-1}$$

if

$$K_{eq} = 1.23 \times 10^{-11} \qquad particles/cm^3$$

From Schott and Davidson 1957

then

$$k_4 = 0.87 \times 10^{-11} \qquad cm^3/particles\text{-sec}$$

## PART II.  THE SPECTRA AND REACTION KINETICS OF THE FREE RADICALS IN THE PHOTOLYSIS OF THE $Cl_2-O_2-CO$ SYSTEM

### I.  INTRODUCTION

Another reaction system of interest in this laboratory has been the production of carbon dioxide from the photolysis of $Cl_2 + O_2 + CO$. Due to the complexity of this system, it has been investigated many times since it was first reported in the literature in 1920 by Bütefisch.[28]

The first quantitative study of the system was done in 1927 by H. J. Schumacher.[29] He measured the rate law for the formation of $CO_2$ by monitoring the pressure changes in the reaction vessel at approximately 1/2 atmosphere pressure and room temperature.  He found that the $CO_2$ was produced by a chain reaction with a quantum yield reaching 1,000 molecules of $CO_2$ for every molecule of $Cl_2$ dissociated by photolysis.  The observed rate law was:

$$\frac{d(CO_2)}{dt} = k[Cl_2]^{0.71} [CO]^{1/2} \tag{40}$$

He found no noticeable dependence of the rate upon oxygen as long as it was present in excess.

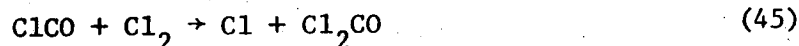In 1928, Bodenstein and Onoda did a product analysis on the system over a range of temperatures.[30]  They found that $CO_2$ production predominates over the formation of phosgene ($Cl_2CO$) at room temperatures, but that the rate of $CO_2$ production slows down markedly around 150°C. They reported that by 300°C the $CO_2$ production had all but ceased with the only product of the photolysis being phosgene.

In an extensive work in 1931, Schumacher and Stieger examined the chlorine dependence of the rate law at total pressures ranging from 240 to 760 mm of Hg.[31] They found that the chlorine dependence of the rate law changed with pressure; with the chlorine power being approximately one at a total pressure around 240 mm of Hg, and approaching a value of 1/2 at one atmosphere total pressure. That is:

$$\frac{dCO_2}{dt} = k[Cl_2]^x[CO]^{1/2} \tag{41}$$

with x varying from approximately 1 at low pressures to 1/2 at one atmosphere total pressure. Throughout this pressure range, Schumacher found that the half power dependence on CO was maintained.

Bodenstein, Lenher and Wagner in 1929 had proposed the following adaptation of the phosgene production mechanism in an attempt to describe this system.[32]

$$Cl_2 + h\nu \rightarrow 2Cl \tag{42}$$

$$Cl + CO + M \rightarrow ClCO + M \tag{43}$$

$$ClCO + M \rightarrow Cl + CO + M \tag{44}$$

$$ClCO + Cl_2 \rightarrow Cl + Cl_2CO \tag{45}$$

$$ClCO + O_2 \rightarrow CO_2 + ClO \tag{46}$$

$$ClO + CO \rightarrow CO_2 + Cl \tag{47}$$

$$ClCO + Cl \rightarrow Cl_2 + CO \tag{48}$$

Under the conditions of a long chain reaction with excess oxygen, the ClCO radical can be considered to be in its steady state. This gives:

$$[ClCO]_{ss} = \frac{k_{43}[Cl][CO][M]}{k_{44}[M] + k_{45}[Cl_2] + k_{46}[O_2]} \qquad (49)$$

Since very little phosgene is produced at room temperature, reaction (45) can be neglected. And with $O_2$ large enough, reaction (44) will be small compared to (46). This yields:

$$[ClCO]_{ss} \approx \frac{k_{43}[Cl][CO][M]}{k_{46}[O_2]} \qquad (50)$$

In a long chain reaction, the chain initiation rate is equal to the chain termination rate. This approximation gives:

$$k_{42}I[Cl_2] = k_{48}[Cl][ClCO], \qquad (51)$$

(for small percentages of total photolytic light absorption). This can be rearranged to produce the following expression for chlorine atoms:

$$[Cl] = \left\{ \frac{k_{42}I[Cl_2] \, k_{46}[O_2]}{k_{48} \, k_{43} \, [CO][M]} \right\}^{1/2} \qquad (52)$$

So long as the ClO free radical decays only by step (47), the expression for carbon dioxide production will be:

$$\frac{d[CO_2]}{dt} = 2k_{46}[ClCO][O_2] \qquad (53)$$

which can be rearranged to give:

$$\frac{d[CO_2]}{dt} = 2k_{43}[M](k_{42}I[Cl_2])^{1/2}[CO]^{1/2} \left\{ \frac{k_{46}[O_2]}{k_{48} \, k_{43}[M]} \right\}^{1/2} \qquad (54)$$

If $[O_2]$ is large enough where $[O_2] \approx [M]$, then this reduces to:

$$\frac{d[CO_2]}{dt} = K(I[Cl_2])^{1/2}[CO]^{1/2}[M] \tag{55}$$

where

$$K = 2 \left(\frac{k_{43}k_{42}k_{46}}{k_{48}}\right)^{1/2}$$

This is the correct form for the rate law at pressures around 1/2 atmosphere, assuming that the oxygen dependence can be approximately cancelled out by the M gas dependence in the square root term. Bodenstein then attempted to explain the rate law change with pressure by assuming that at low pressures, the termination reaction would become: Radical + wall → termination. This would explain the change of the chlorine dependence from the 1/2 power to first power at low pressures, but this would also predict that the rate law should become first order in carbon monoxide at low pressures.

To test this mechanism experimentally, Franke and Schumacher extended the rate law measurements down to 10 mm of Hg total pressure, checking for any change in the carbon monoxide dependence.[33] They reported that the rate law for the formation of $CO_2$ remained proportional to carbon monoxide to the 1/2 power, down to at least 10 mm total pressure. This experiment showed that the Bodenstein mechanism did not fully account for the $CO_2$ production reactions, though it does give a complete description for the photochemical phosgene production chain.

In an experimental attempt to clarify the role of the proposed
free radical ClCO in this system, G. K. Rollefson in 1937 ran a series
of experiments testing for the formation of both phosgene and carbon
dioxide as a function of $[O_2]/[Cl_2]$.[34] If the ClCO radical was
actually the intermediate precursor to both products, then there should
be a relationship between $d[CO_2]/dt$ and $d[Cl_2CO]/dt$.

$$\text{If} \quad \text{(a)} \quad \frac{d[CO_2]}{dt} = 2k_a[ClCO][O_2] \tag{55}$$

$$\text{and} \quad \text{(b)} \quad \frac{d[Cl_2CO]}{dt} = k_b[ClCO][Cl_2]$$

$$\text{then} \quad \frac{k_a[ClCO][O_2]}{[ClCO](2k_a[O_2] + k_b[Cl_2]} = \frac{d[CO_2]/dt}{d[Cl_2CO]/dt + d[CO_2]/dt}$$

$$\frac{d[CO_2]/dt}{d[Cl_2CO]/dt + d[CO]/dt} = \frac{1}{1 + k_b[Cl_2]/2k_a[O_2]} \tag{56}$$

Rollefson varied the initial concentration of all three reactants at
approximately 20°C and 20 mm total pressure. His results matched the
curve predicted by Eq. (56), indicating that the rate of formation of
$CO_2$ and phosgene was only a function of the ratio $[Cl_2]/[O_2]$.

Rollefson reported that the rate of formation of $CO_2$ was five
times greater than the rate of phosgene formation at this pressure
and temperature. When he repeated the experiments at higher tempera-
tures, he found that the rates of production of $CO_2$ and $Cl_2CO$ were
equal at lower values of the ratio $[Cl_2]/[O_2]$. His quantitative results

indicated the reaction of $O_2$ with ClCO to have a heat of activation

2.9 kcal/mole higher than the reaction of $Cl_2$ with ClCO.

Further experiments comparing phosgene to $CO_2$ formation were

carried out by Brenschede.[35] Using the same experimental analysis as

Rollefson, he derived the relationship:

$$\frac{[CO_2]}{[COCl_2]} = \frac{A[O_2]}{[Cl_2]} \qquad \text{with } \frac{1}{A} = \frac{1}{1 + k_b[Cl_2]/2k_a[O_2]} \tag{57}$$

Measuring the value of A over a wide range of pressure and temperature,

he found that A increases with pressure towards a limiting high pres-

sure value. His data are diagrammed in Fig. 10. This behavior can be

expressed in the limit, by $A = ae^{-q/RT}$. In a series of experiments

measuring A as a function of temperature, Brenschede tested this

relationship and found that a and q changed values at 200°C, as shown

in Fig. 11.

To explain these results, Brenschede postulated the presence of

a new intermediate species, a peroxy radical formed from ClCO and $O_2$.

His theory was that this $ClCO_3$ radical could explain the temperature

dependency of the A factor by having two different decay mechanisms.

At low temperatures, the radical could dissociate by: $ClCO_3 + M \rightarrow$

$ClO + CO_2 + M$; and at temperatures above 200°C, it could decay by:

$M + ClCO_3 \rightarrow ClCO + O_2 + M$. This predicts the carbon dioxide production

to be controlled by the rate of $ClCO_3$ formation at low temperatures,

and by the rate of $ClCO_3$ decomposition at temperatures over 200°C,

when the reaction $ClCO_3 \rightarrow ClCO + O_2$ becomes important.
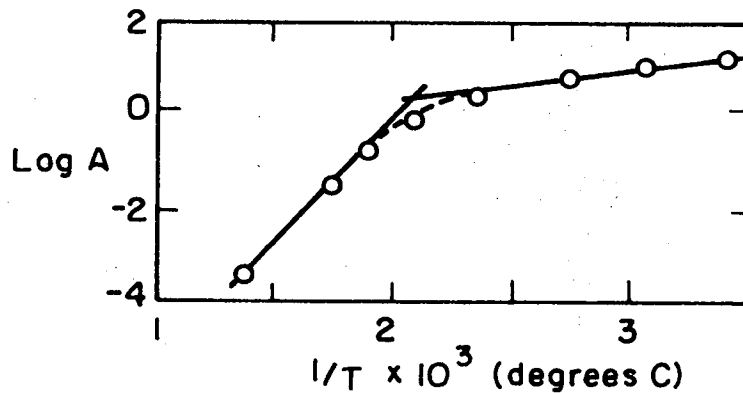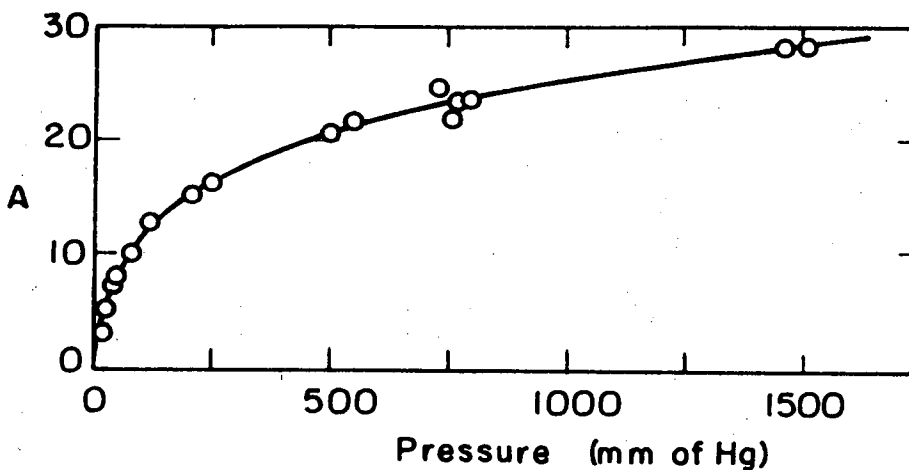
Fig. 11. Brenschede's A factor as a function of 1/T.
The x's are experimental points, and the lines
are calculated values from two sets of adjustable
parameters.

Brenschede's arguments met with some acceptance, but proof for the presence of a new intermediate could not be obtained by the techniques available at the time.

A full description of the kinetics of this system requires the ability to determine the identity and kinetic behavior of all the free radical intermediates. This ability has been developed through the use of flash photolysis, matrix isolation, and molecular modulation spectroscopy.

In 1965, Milligan and Jacox confirmed the presence of the ClCO free radical by observing its infrared spectrum in an argon matrix after photolysis of $Cl_2$ and CO.[36] The ultraviolet spectrum of the ClO radical was observed by G. Porter in 1950.[37] The ClOO free radical was observed in a nitrogen matrix by Rochkind and Pimentel in 1967[38] and in the gas phase by infrared and ultraviolet molecular modulation spectroscopy by Johnston, Morris and Van den Bogaerde in 1969.[39] With the existence of these three free radicals confirmed, the mechanism for the $Cl_2 + O_2$ + CO photolysis becomes even more complicated.

In 1953, Porter and Wright added carbon monoxide to the $Cl_2 + O_2$ + hν system and observed an increase in the absorption at 265 nm by the ClO radical.[40] This led Morris and Van den Bogaerde in this laboratory to examine this system in hopes of obtaining the gas phase infrared spectrum of the ClO radical. In their study of the $Cl_2 + O_2$ + hν system, Morris and Van den Bogaerde observed molecular modulation absorption spectra in the ultraviolet for the ClOO and ClO free radicals, and an infrared absorption for ClOO. Upon the addition of

carbon monoxide to this system, five new modulation absorption peaks were discovered. These consisted of an ultraviolet absorption band with a maximum at 220 nm, a strong infrared absorption centered at 937 $cm^{-1}$ with a weaker side band at 970 $cm^{-1}$, and a pair of moderate infrared absorptions at 1835 and 1905 $cm^{-1}$. All five of these molecular modulation absorption peaks showed the kinetic behavior of intermediate species.

The purpose of this research is to identify these new absorbing species, and to combine the new kinetic information obtained from studies of the $Cl_2 + O_2$ system with the observations made during the 1930's on the $Cl_2 + O_2 + CO$ system. With the ability to monitor free radical species through molecular modulation, it is possible to describe the role of some of the intermediate species in this reaction system, and to infer the role of the other free radicals. It is hoped that a combination of new and old research with the data gathered in this work will allow a complete kinetic description of this reaction system.

## II.  EXPERIMENTAL

### A.  Experimental Method

The major difficulty in using reactant-product analysis to explain the kinetics of photochemical reactions is the inability to experimentally determine the behavior of the intermediate species.  In a system proceeding solely through $\underline{n}$ free radical intermediates, there are $n^2$ possible disproportionation reactions and only $2n$ possible products.  So for a system with three or more intermediates, $n > 3$, the number of unknowns exceeds the measurable quantities.  In this case, it becomes impossible to determine the mechanism uniquely from simple reactant-product analysis.[41]  Due to this difficulty, it is desirable to be able to observe the intermediates in a complex reaction by direct spectroscopic means.

The methods of flash photolysis, matrix isolation, and rapid scan spectroscopy are valuable in obtaining the absorption spectra of intermediate species, but they do not yield much kinetic data about room temperature, one atmosphere gas phase reactions.

Flash photolysis typically uses a high intensity flash of exciting ultraviolet light on the order of $10^{20}$ photons $cm^{-2}sec^{-1}$ to produce high initial concentrations of free radicals.  The decay processes of these radicals can then be monitored.  However, these processes are usually dominated by radical-radical reactions, due to the high concentrations of free radical species.  Reactions taking place under moderate light conditions with approximately $10^{15}$ photons $cm^{-2}sec^{-1}$

have typical radical concentrations on the order of $10^{10}$ to $10^{13}$ molecules/cc. Since the gas concentration at one atmosphere of pressure is $2.45 \times 10^{19}$ molecules/cc, the predominant reactions are between radicals and molecules. These radical-molecule reactions are the type of interest in this work.

The molecular modulation method is designed to work with reactions occurring at moderate exciting light intensity, with intermediate species present at approximately $10^{12}$ molecules/cc. This makes it ideally suited for studying the chlorine sensitized photolytic production of $CO_2$, since the system contains a minimum of five free radical intermediates.

The concentration modulation behavior of a reaction species can be calculated by representing the photolysis light by a Fourier series square wave, and integrating the differential equation for the species of interest; as was done for the $NO_2$ modulation in Part I. Calculations of this nature have been carried out in this laboratory by T. Paukert for a number of different types of kinetic species.[42] Included among these are a radical formed by the photo-dissociation of a reactant and destroyed by reaction with a stable molecule; and a radical species formed by the photo-dissociation of a reactant, and decaying by a reaction "second order" in its own concentration.

1. Radical species closely following the photolytic light, decaying by a process first-order in radical concentration.

The first of these examples is that of the radical species formed from the photolytic dissociation of a reactant, or from a fast radical produced by the initial photolytic act, and decaying by a reaction with a reactant molecule. This can be expressed for a steady-state flow system as:

$$A + h\nu \xrightarrow{\alpha I} 2X$$

$$X + B \xrightarrow{fast} Y + P_1$$

$$Y + C \xrightarrow{k_r} P_2$$
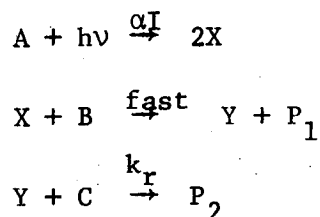
A, B, and C are reactants in constant concentrations, with X and Y representing the radical intermediates. $P_1$ and $P_2$ are the products of the reaction.

Assuming the X radical to be in a steady state, the differential equation for Y is:

$$\frac{d[Y]}{dt} = 2\alpha I[A] - k_r[Y][C] - (\text{flow out term}) \qquad (58)$$

Replacing I by the Fourier series representation of a square wave gives the result:

$$\frac{d[Y]}{dt} = 2\alpha[A](\frac{I_o}{2} + \frac{2I_o}{\pi} \sum_{n,odd}^{\infty} \frac{1}{n} \sin(n\omega t)) - k_r[C][X] \qquad (59)$$

$$- \ (\text{flow out term})$$

with: $I_o$ = the magnitude of the photolysis light in photons $cm^{-2} sec^{-1}$

$\omega$ = flashing frequency in radians/sec

$f$ = flashing frequency in cycles/sec

$\alpha$ = integrated absorption cross-section and quantum yield of the reactant in $cm^2$/molecule

$t$ = time in seconds

Since the flow out term is generally much smaller than the chemical decay term, it will be dropped. Substituting $\omega = 2\pi f$ and $\theta = \omega t$, this reduces to a linear differential equation which can be integrated to give:

$$[Y] = \frac{2\alpha I_o}{\pi^2 f} \sum_{n,odd}^{\infty} \frac{\left(\frac{k_r [C]}{2\pi f} \frac{1}{n} \sin(n\theta) - \cos(n\theta)\right)}{\left(\left(\frac{k_r}{2} \frac{[C]}{\pi f}\right)^2 + N^2\right)} + \frac{\alpha I_o [A]}{k_r [C]} \qquad (60)$$

The low frequency limiting behavior of the radical concentration, [Y], gives the form of a square wave.

$$\lim_{f \to 0} [Y] = \frac{4\alpha I [A]}{\pi k_r [C]} \sum_{n,odd}^{\infty} \frac{1}{n} \sin(n\theta) + \frac{\alpha I [A]}{k_r [C]} \qquad (61)$$

The maximum radical concentration is twice the amplitude of the square wave function, or $2\alpha I [A]/k_r [C]$, which is equivalent to the "steady state" concentration of the radical. The phase shift of the wave form from the exciting light is $0°$.

Looking at the high frequency limit of the equation:

$$\lim_{f \to \infty} [Y] = \frac{2\alpha I_o [A]}{\pi^2 f} \sum_{n,\text{odd}}^{\infty} \frac{1}{n^2} \cos(n\theta) + \frac{\alpha I [A]}{k_r [C]} \qquad (62)$$

This shows the [Y] concentration to be a triangular wave form oscillating about a level of half the "steady state" concentration, and phase shifted -90° from the exciting light.

At intermediate flashing frequencies, the amplitude and phase shift of the radical species will be a function of the flashing frequency. Since Eq. (60) is in the form of a Fourier series, the phase shift and amplitude of the first harmonic can be calculated for any flashing frequency from the first Fourier coefficients, $a_1$ and $b_1$. From Eq. (60):

$$a_1 = \frac{\alpha I_o k_r [C]}{\pi^3 f^2} \left/ \left( \left( \frac{k_r}{2} \frac{[C]}{\pi f} \right)^2 + 1 \right) \right.$$

$$b_1 = \frac{2\alpha I_o}{\pi^2 f} \left/ \left( \left( \frac{k_r}{2} \frac{[C]}{\pi f} \right)^2 + 1 \right) \right.$$

The phase shift is given by $\delta = \tan^{-1}(b_1/a_1)$, or $\delta = \tan^{-1}\left( \frac{2\pi f}{k_r [C]} \right)$ and the amplitude is given by:

$$[Y]_{\text{mod}} = \sqrt{a_1^2 + b_1^2}$$

The "lifetime" of the radical, Y, is defined to be $\tau = 1/k_r [C]$, the time necessary to drop to a level of $1/e$ times the initial

concentration. This "lifetime" can be determined from a single experimental phase shift measurement, since $\frac{1}{\tau} = k_r[C] = \frac{-2\pi f}{\tan \delta}$ . This is a good example of how the kinetic "lifetime" of a free radical can be determined by the modulation method, and it also shows how a phase shift varying with flashing frequency between 0 and-90° can characterize an absorbing species as a free radical closely following the exciting light. Figure (12) shows the modulation phase shift and amplitude of this radical behavior as a function of flashing frequency.

2.  Radical closely following the photolytic light and decaying second order in its own concentration.

   A second example of radical behavior is that of a radical closely following the exciting light and decaying by a process that is second order in radical concentration.

$$A + h\nu \rightarrow 2X$$

$$X + B \xrightarrow[\text{fast}]{k_a} Z$$

$$Z + Z + M \xrightarrow{k_r} P + M$$
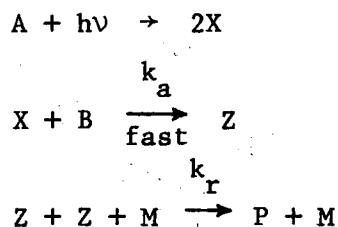
The radical, Z, is formed from a fast radical precursor, X, reacting with a molecule, B, and then it decays by a process second order in itself. If the radical X is assumed to be in its steady state, the differential equation for Z is:

$$\frac{d[Z]}{dt} = 2\alpha I[A] - 2k_r[Z]^2 - (\text{flow out term}) \tag{63}$$
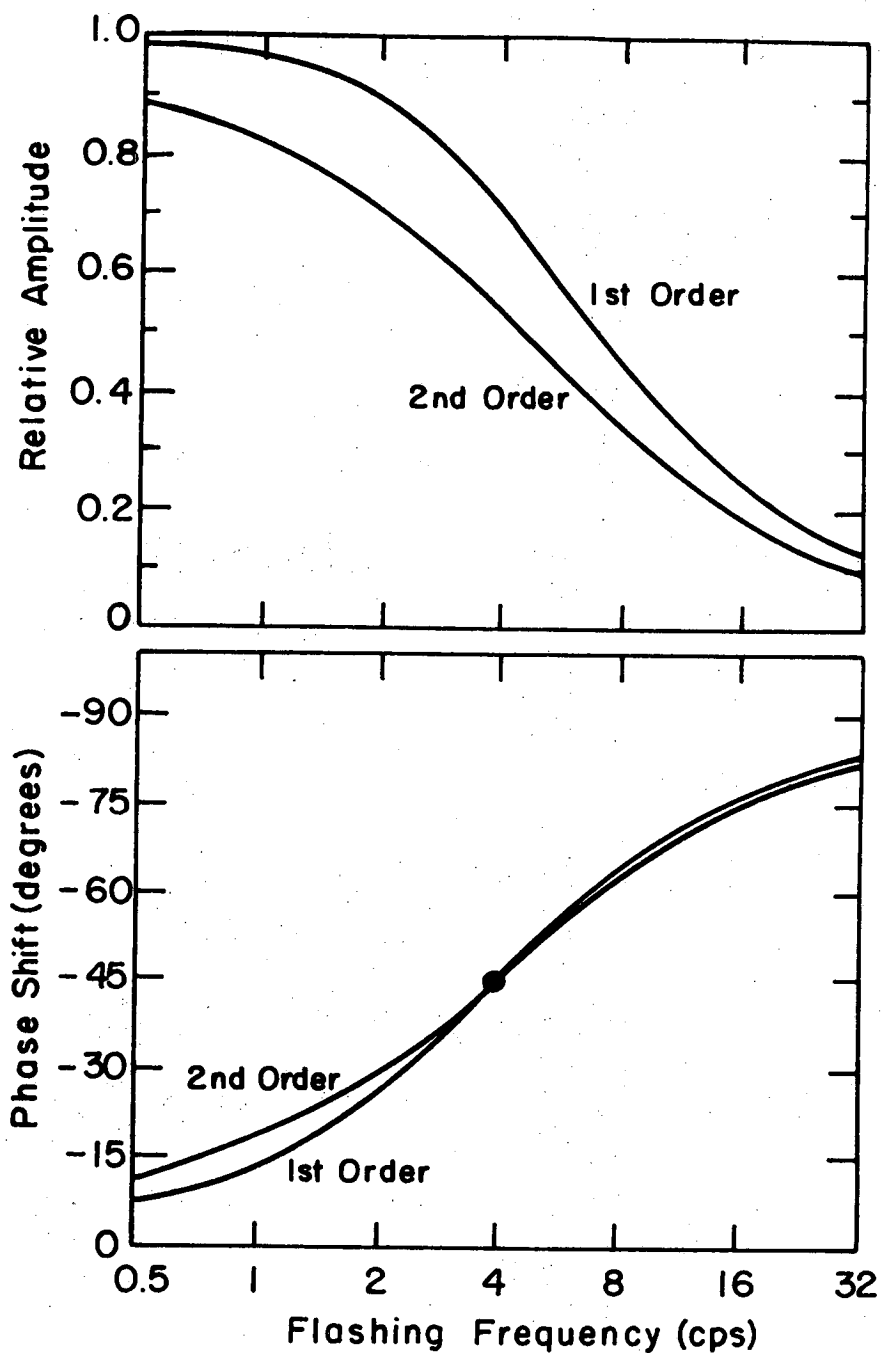
XBL 6812-7456 A

Fig. 12. Theoretical phase shift and relative amplitude
of the fundamental component of the periodic concen-
tration modulation. Both the first and second order
decaying radical behavior were calculated for the
case of the -45° phase angle occurring at 4 cps.

Again, the flow out term can be neglected.

This differential equation can be solved by breaking the equation down into two parts, one describing the light-on period, and one the light-off period. Making the same substitution as in case 1, the equations for Z are:

$$\frac{d[Z]}{dt} = \frac{1}{2\pi f}(2\alpha I_o[A] - 2k_r[Z]^2) \text{ for } -\pi \leqslant \theta \leqslant 0 \tag{64}$$

and

$$\frac{d[Z]}{dt} = \frac{1}{2\pi f}(-2k_r[Z]^2) \text{ for } 0 \leqslant \theta \leqslant -\pi \tag{65}$$

The light, I, is represented by a Fourier series square wave at frequency f, and the build up rate is controlled by the initial photodissociation of A.

Each of these equations can be integrated separately, giving:

$$[Z]_\theta = \left(\frac{2\alpha I_o[A]}{2k_r}\right)^{1/2} \tanh \frac{(\theta + \pi)(2\alpha I_o[A]2k_r)^{1/2}}{2\pi f} \tag{66}$$

$$\tan^{-1} \frac{[Z]_{-\pi}}{(2\alpha I_o[A]/2k_r)^{1/2}} \text{ for the lamp on period}$$

and

$$[Z]_\theta = \frac{2\pi f[Z]_0}{2\pi f + 2k_r\theta[Z]_0} \text{ for the lamp off period} \tag{67}$$

By assuming an initial value for $[Z]_{-\pi}$, values can be calculated for $[Z]_0$ and $[Z]_\pi$. By successively setting $[Z]_{-\pi} = [Z]_\pi$ and

recalculating, the profile of [Z] versus $\theta$ can be calculated to any degree of accuracy. Once this profile is obtained, a numerical Fourier analysis can be performed upon it to obtain the Fourier coefficients, using the formulas:

$$a_n = \frac{1}{\pi} \sum_{i=1}^{m} [Z]_{\theta_i} \sin(n\theta i)\Delta\theta$$

$$b_n = \frac{1}{\pi} \sum_{i=1}^{m} [Z]_{\theta_i} \cos(n\theta i)\Delta\theta$$

m is the number of increments of $\theta$. From the first Fourier coefficients, the amplitude and phase shift of the first fundamental can be obtained. The behavior of the amplitude and phase shift of the first fundamental as a function of flashing frequency are shown in Fig. (12). Like the radical species in case 1, this radical also has a phase shift varying from $0°$ to $-90°$ with flashing frequency.

The steady state concentration of the radical Z is given by:

$$[Z]_{ss} = \left(\frac{Z\alpha I_o [A]}{2k_r}\right)^{1/2} \tag{68}$$

and if the "lifetime", $\tau$, of the radical is defined as the half-life of the radical concentration, this gives:

$$\tau = \frac{1}{2k_r [Z]_{ss}} \tag{69}$$

with

$$\tau = \frac{1}{2k_r \left(\dfrac{2\alpha I_o [A]}{2k_r}\right)^{1/2}} = \frac{1}{2(\alpha I_o [A] k_r)^{1/2}} \qquad (70)$$

In comparison, the radical decaying first order in radical concentration shows:

$$\tau = \frac{1}{k_r [C]}$$

This radical's lifetime is inversely proportional to the concentration of the reactant involved in the radical's decay, while the radical decaying second order in its own concentration has its lifetime inversely proportional to the square root of its own steady state concentration. Thus, varying reactant concentration and photolytic light intensity will give a means of distinguishing between these two forms of radical species.

Calculations of phase angle versus flashing frequency behavior for other types of reacting species can be carried out by using these same methods. The graph in Fig. (13) shows how this behavior can characterize other reacting species. Using this approach, then, the absorptions in the ultraviolet and infrared spectra taken during the photolysis of $Cl_2 + O_2 + CO$ can be characterized by their phase shifts as to the role of the absorber in the reaction; and their kinetics can be studied.

The experiments performed on this system were of two different varieties. The first was a series of qualitative experiments carried out over a wide range of reaction conditions to characterize the
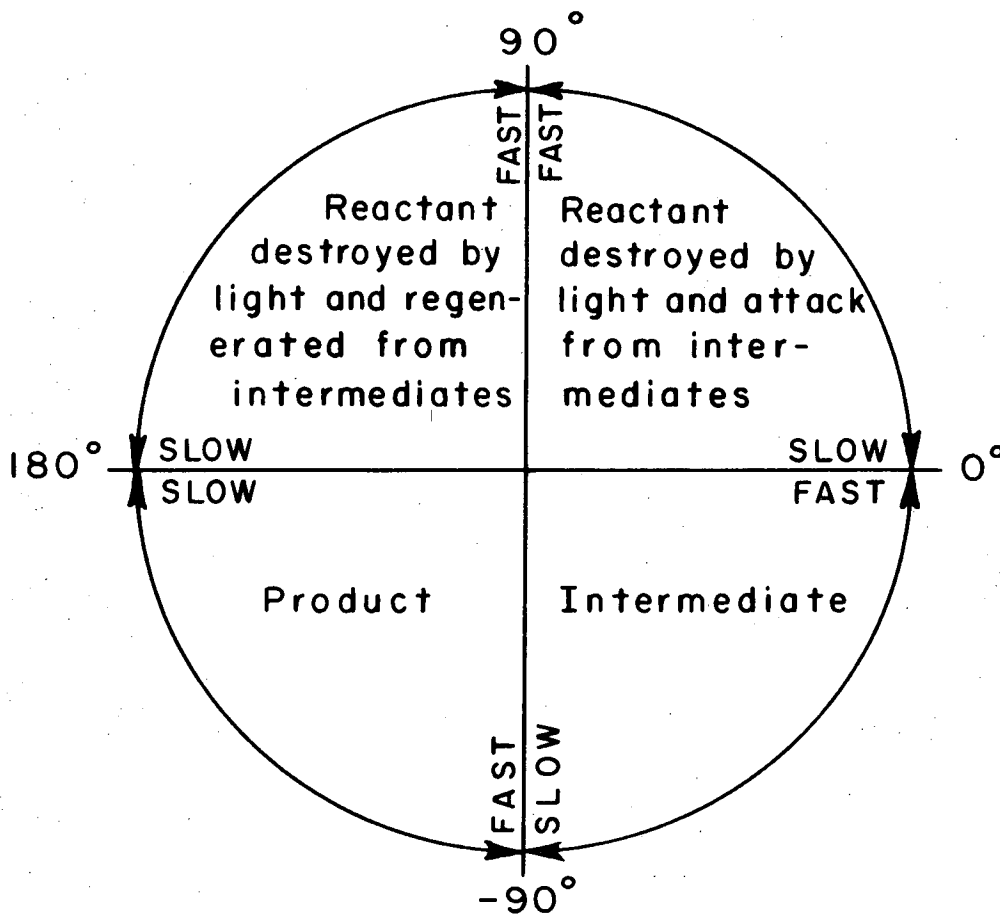
XBL68I2-7446

Fig. 13. Phase shift relationships of modulated
concentration signals associated with various
reaction species.

behavior of each of the ultraviolet and infrared absorption bands as a function of reactant concentrations and modulation flashing frequency. The hope in these experiments was to find which absorption bands corresponded to the same species, and if possible, to identify the absorbers as products or intermediates in the reaction sequence.

The second series was a group of experiments run in both ultraviolet and infrared photolysis cells under as nearly the same conditions as possible. In these experiments, the reactants, products and intermediates were monitored for quantitative kinetic data. This series included simple DC photolysis experiments in which the photolysis light was turned on and the decay of CO was monitored under various conditions, and modulation experiments over a range of flashing frequencies.

By comparing the experimental flashing frequency versus phase shift and amplitude data with simulation calculations, it is possible to obtain "lifetimes" for the intermediate species in the reaction; and to postulate a mechanism to explain their roles in this reaction system.

B. Experimental Apparatus

The two instruments used in this series of experiments are similar molecular modulation spectrometers. One instrument uses infrared spectroscopic analysis, and the other employs ultraviolet detection. The infrared spectrometer was described in Part I of this paper.

## 1. Ultraviolet Reaction Cell

The ultraviolet apparatus is diagramed in Fig. (14). The reaction cell consists of a 35 liter cylindrical quartz tube, 1.8 meters long and 15 cm. in diameter. The cell is mounted in a heavy nickel plated, stainless steel bracket. The cell is O-ring fitted to the mounting bracket so that it can be evacuated.

The reaction cell has a single reflecting mirror in one end to give a 3.96 meter optical path. This mirror has an aluminium reflecting surface with an overcoating of magnesium fluoride to maximize the ultraviolet reflectivity. The two optical windows in the cell are O-ring mounted disks of calcium fluoride.

The ultraviolet spectroscopic light is supplied by a deuterium arc lamp (Bausch and Lomb DE-50A) powered by a current regulated DC power supply. The light from this arc lamp is chopped at 400 cps by an American Time Products tuning fork before it enters the reaction cell.

When the spectroscopic beam exits from the reaction cell it passes through a McPherson model 218 monochromator which has a 0.3 meter optical path. This monochromator is equipped with a 2400 line/mm. grating blazed at 150 nanometers. The photodetector is an EMI Phototube (9526B) mounted on the exit slit of the monochromator. The phototube is biased by a Fluke model 408B high voltage power supply.

## 2. Photolysis Lamps

The photolytic light for the ultraviolet reaction cell was supplied by two General Electric 64 inch, F64T5-BL, black lamps. These
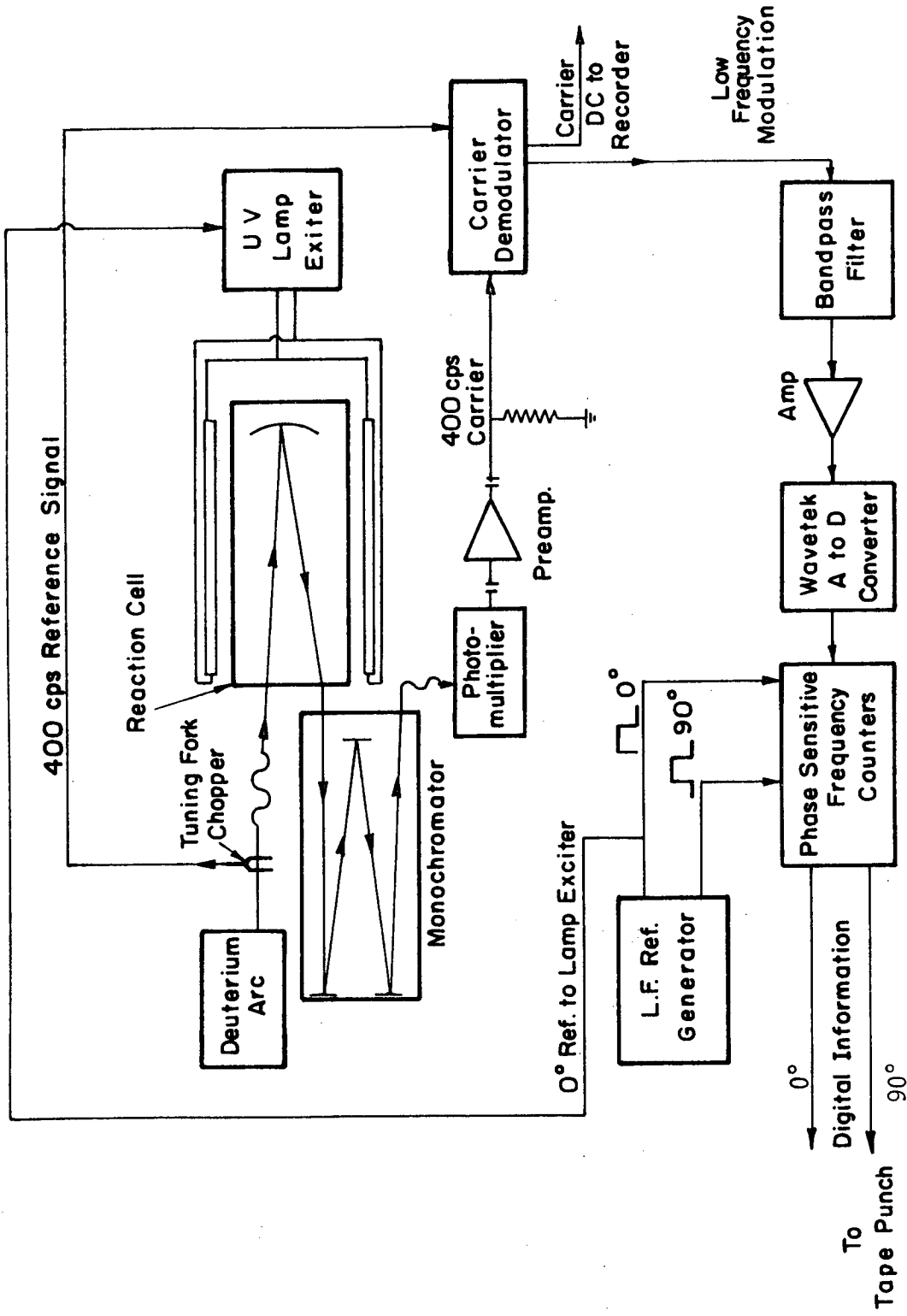
Fig. 14. Schematic diagram of ultraviolet apparatus.

XBL728-6847

lamps are mounted outside the cell and parallel to it. Surrounding the cell and the photolysis lamps is a highly reflective shield made of "Alzak" aluminum to give a greater and more uniform light flux through the cell.

The photolysis lamps are powered by a 700 volt regulated supply. The power supply operates from a three phase 440 volt source with the ripple of the three lines multiplied together in a three phase transformer to reduce the overall line noise. The power supply can electronically switch the lamps on and off at a rate set by a low frequency square wave reference. The reference generator is a crystal oscillator divided down to give a square wave signal at frequency multiples of 0.306 cps. The flashing lamp output was shown to be a square wave with a short initial spike when the lamps were monitored by a phototransistor.

The output spectrum for the photolysis lamps is the same as that shown in Fig. (3b) of Part I for the photolysis lamps in the infrared cell. The major output of the lamps is between 320 and 380 nm which gives a good overlap of the $Cl_2$ absorption band.

3. Electronics

The electronics are basically the same as those described in Part I for the infrared apparatus. There are again two stages of demodulation: one for the 400 cps carrier signal, and a phase sensitive dual demodulation stage for the low frequency modulation signal.

a. Carrier demodulator. The first stage of demodulation is a 400 cps lock-in amplifier. It receives the 400 cps AC signal from the

preamplifier of the photomultiplier tube. This signal carries the modulation information on side bands at 400 ± f cps. In the lock-in the 400 cps signal is beat against a 400 cps reference produced by the tuning fork chopper. This rectifies the 400 cps signal and produces a DC signal proportional to the spectroscopic light intensity. The modulation information is carried on top of this DC signal as a low frequency ripple.

This DC signal is then split with one output going through a set of integrating filters to a strip chart recorder, and the other going into a set of low frequency band pass filters. The band pass filters select for the first fundamental of the frequency of interest.

b.  Dual phase demodulator.  The signal that comes out of the low frequency band pass filters carries the first fundamental of the modulation signal. This low frequency AC signal is amplified and sent into a Wavetek model 11 voltage controlled oscillator which functions as an analog-to-digital converter. The Wavetek is set to have an output of 5,000 cps, and this signal is frequency modulated by the low frequency voltage changes of the AC modulation signal. This frequency modulated signal is then sent into two "up-down" frequency counters which perform the function of digital lock-in amplifiers.

The digital frequency counters are controlled by the same low frequency reference that flashes the photolysis lamps. The "in phase" or sine component frequency counter  counts up for the first half of a modulation cycle and down for the second half cycle. The "quadrature" or cosine component counter counts up for a quarter cycle, counts down for the next half cycle, and then counts up for the last quarter

cycle. The result of this counting method is diagrammed in Table (13).

The effect of counting up and down for the same period of time is to produce zero counts for the 5000 cps carrier signal and any random noise present in the signal. Any coherent signal at the same frequency as the switching reference will register as a number of digital counts at the end of a cycle.

The output of the sine component counter is proportional to the amplitude of the first fundamental sine component of the modulation signal. The output of the quadrature or cosine counter is proportional to the amplitude of the first fundamental cosine component. The experimental amplitude and phase shift from the flashing lamps can be calculated for the modulation signal, just as they were in the case of the analog demodulator in Part I. The phase shift $\delta = \tan^{-1}(b/a)$, and the amplitude is given by $\Delta I/I = (a^2 + b^2)^{1/2}/DC$.

  a  = number of counts on the in phase counter

  b  = number of counts on the quadrature counter
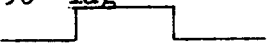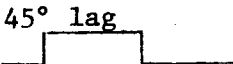
  DC = the number of counts equivalent to the background DC voltage level.

The switching mechanism for these up-down counters was designed by E. D. Morris, a former graduate student in this laboratory, and it is described in more detail elsewhere.[43]

The output of these digital counters is punched out on tape in a BCD format to be analyzed later by computer.

c.  Calibration. The output of the dual phase digital demodulator is directly proportional to the modulation signal amplitude. The amplitude proportionality factor and the proper electronic phase correction for

Table 13. Output of the digital lock-in for various simulated signals.

| | | First quarter cycle | Second quarter | Third quarter | Fourth quarter | Result |
|---|---|---|---|---|---|---|
| | A.<br>B. | add<br>subtract | add<br>add | subtract<br>add | subtract<br>subtract | |
| no signal | A.<br>B. | +100<br>-100 | +100<br>+100 | -100<br>+100 | -100<br>-100 | 0<br>0 |
| In-phase signal | A.<br>B. | +110<br>-110 | +110<br>+110 | -90<br>+90 | -90<br>-90 | +40<br>0 |
| 90° lag | A.<br>B. | +90<br>-90 | +110<br>+110 | -110<br>+110 | -90<br>-90 | 0<br>+40 |
| 45° lag | A.<br>B. | +100<br>-100 | +110<br>+110 | -100<br>+100 | -90<br>-90 | +20<br>+20 |

Signals in other quadrants will have the appropriate signs.

A. Counter with in-phase reference.
B. Counter with 90° lag reference.

the apparatus are obtained by using the modulation simulator diagrammed in Fig. (5) of Part I. The zero degree phase shifted, $2 \times 10^{-3}$ amplitude square wave modulation is run into the electronics to calibrate the instrumental phase shift caused by the filters. This calibration signal also gives a proportionality factor to relate the number of digital counts to the absolute modulation amplitude.

### 4. Gases and Flow System

The carrier gases used in the experiments were Extra Dry grade Oxygen and High Pure nitrogen from the Lawrence Berkeley Laboratories. The chlorine was Matheson research grade, which was diluted in the laboratory with Matheson ultra high purity oxygen. The carbon monoxide was Matheson ultra high purity grade. The analysis of these tank gases are given below.

Extra Dry $O_2$

| | | | |
|---|---|---|---|
| $O_2$ | 99.65 percent | $O_2$ | 99.986 percent |
| Argon | 0.3 percent | Argon | 60 ppm |
| $N_2$ | 0.05 percent | $N_2$ | 25 ppm |
| $CO_2$ | 2 ppm | Krypton | 13 ppm |
| Hydrocarbons | | $CO_2$ | 7 ppm |
| as methane | 20 ppm | Xenon | 4 ppm |
| $H_2O$ | 10 ppm | $H_2O$ | 6 ppm |
| | | Total Hydrocarbons | |
| | | as methane | 16 ppm |

| High Purity Nitrogen | | Research Grade Chlorine | |
|---|---|---|---|
| $N_2$ | 99.9976 percent | $Cl_2$ | 99.965 percent |
| $O_2$ | 80 ppm | $O_2$ | 30 ppm |
| $H_2O$ | 50 ppm | $N_2$ | 80 ppm |
| $CO_2$ | 10 ppm | $CO_2$ | 140 ppm |
| Argon | 100 ppm | $H_2O$ | 3 ppm max. |

Carbon Monoxide, Ultra High Purity

| $CO$ | 99.8 | percent min. |
|---|---|---|
| $N_2$ | 0.05 | percent max. |
| $CO_2$ | 0.2 | percent max. |
| $H_2$ | 0.025 | percent max. |
| $O_2$ | 0.0025 | percent max. |

The oxygen was normally used as the carrier gas at approximately one atmosphere pressure. The flow was passed through a four foot long copper turnings furnace to convert the hydrocarbons to water and carbon dioxide. These impurities were then removed by successive columns of calcium chloride, ascarite, and $P_2O_5$.

Infrared analysis of the carbon monoxide showed an impurity absorption that was ascribed to a FeCO type band. The CO was then passed through a five foot column of activated charcoal on glass wool to remove this impurity. After purification the carbon monoxide was free of this impurity to the limit of the infrared spectrometers sensitivity. Since the spectrometer has a maximum sensitivity of

$\ln(I_o/I) = 0.002$ at a 40 meter path length, the maximum impurity concentration would be about 1 to 10 parts per million.

The chlorine gas was diluted with ultra high purity oxygen in stainless steel tanks to form a five percent $Cl_2$ in $O_2$ mixture. This was used in the flow system with no purification, since the analysis of the research grade chlorine showed no reactive impurities.

All flows were monitored by calibrated Hastings Mass flow meters and Predictability Tri Flat flow meters. The calibration of each flow meter for its specific gas was done by measuring the amount of water the gas flow would displace per minute in a wet test flow meter.

The gasses were introduced to the reaction cells through glass dispersal tubes. The dispersal tubes are lengths of glass tubing with small holes placed every four inches along their length. These holes cause a jetting of the gasses into the cell producing more uniform mixing. The gasses exit from the cells through similar tubing.

## 5. Concentration Determinations

The concentrations of the chlorine and carbon monoxide in the cells were measured by spectroscopic absorption. The carbon monoxide Beer's Law absorption coefficient was determined as a function of optical density in the infrared cell by using calibrated flows to determine concentrations. From this absorption coefficient curve, the CO concentration during the reaction runs could be determined in the infrared cell. To measure the carbon monoxide in the ultraviolet reaction cell, the exhaust gas was piped into the infrared cell and monitored. The measured carbon monoxide absorption coefficient is
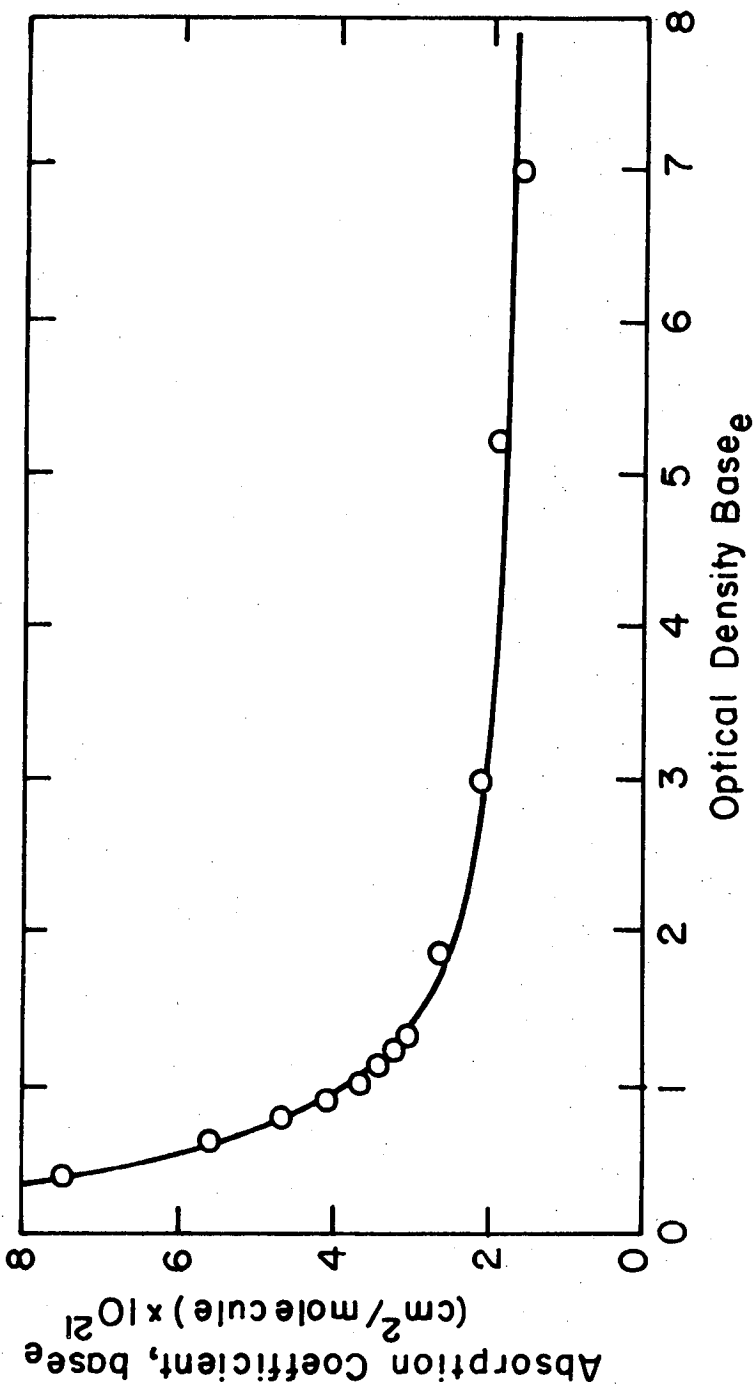
plotted as function of optical density in Fig. (15). The measurements were made at 4.811 microns with a 150 line/mm grating and a 0.8 mm slit width. The total pressure was one atmosphere with oxygen as the M gas.

The chlorine concentrations were determined by flow rates and checked by measuring the $Cl_2$ absorption around 330 nm in the ultraviolet apparatus. The $Cl_2$ absorption coefficients were taken from the work of Gibson and Bayliss.[44] Figure (16) shows this absorption coefficient as a function of wavelength. To check the chlorine concentration in the infrared cell, the exhaust gas was passed into the ultraviolet cell for analysis.

## 6. Experimental Procedure

Two groups of experiments were performed, with all experiments being run at 1 atmosphere total pressure and 298°C. The first group was a qualitative set of modulation flow experiments run in both the infrared and ultraviolet reaction cells over a wide range of initial conditions. The purpose of these experiments was to characterize the modulation behavior of each of the individual modulation absorptions with respect to the different reaction conditions. On the basis of their kinetic behavior, the absorptions belonging to a single absorber could be identified; and the absorbing species could be characterized as to their role in the reaction mechanism.

The second group of experiments were quantitative in nature. These included initial slope measurements of the carbon monoxide decay in a static cell over a wide range of initial conditions. There were

XBL 728 - 6848

Fig. 15. Infrared absorption coefficient of carbon monoxide at 4.811 microns plotted as a function of optical density, with the optical density, with the optical density defined as $\ln(I_0/I)$. The measurements were made at one atmosphere total pressure, with $O_2$ as the M gas. The spectral resolution was 0.0056 microns.
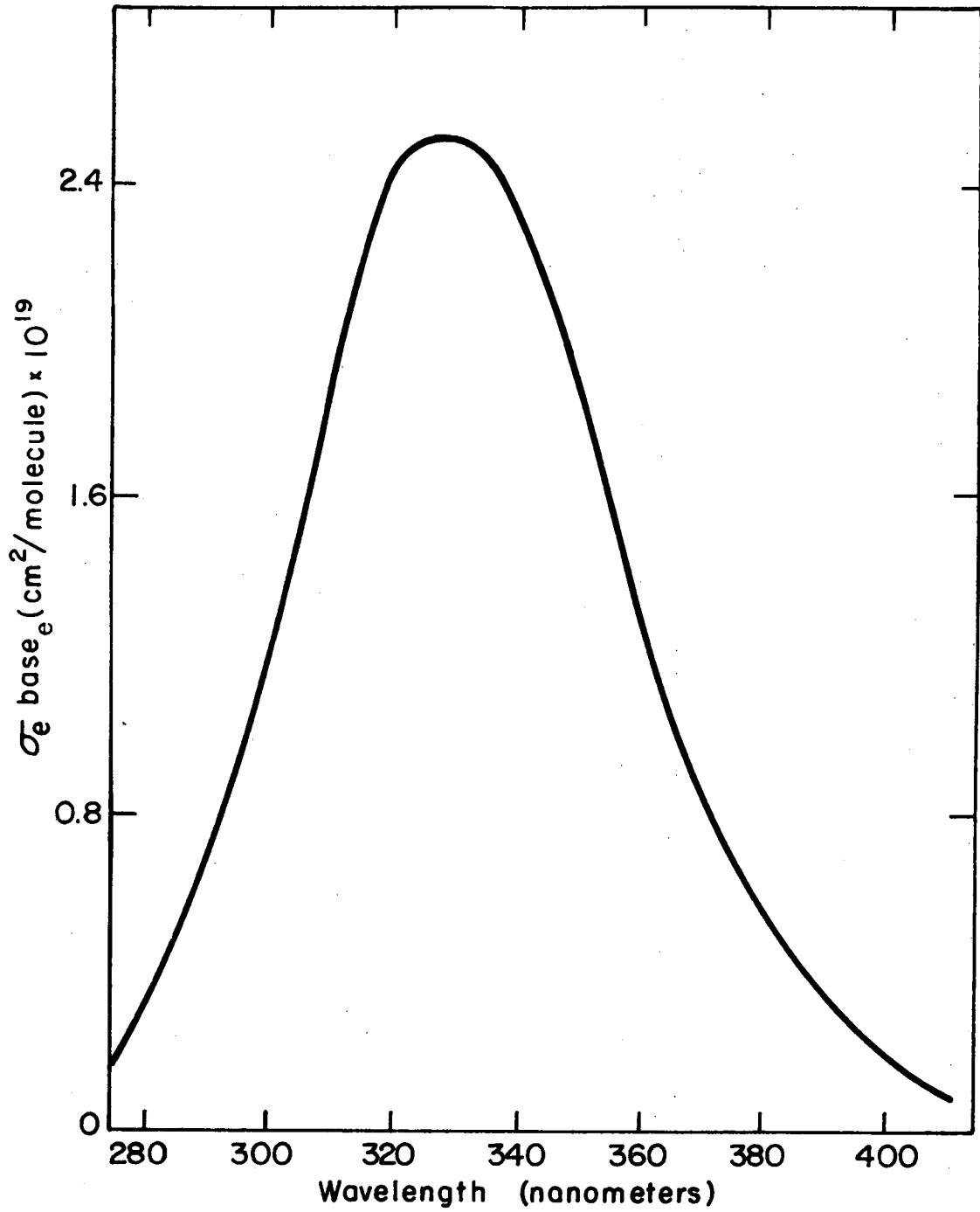
XBL728-6849

Fig. 16.   The ultraviolet absorption spectrum of chlorine
molecule. (44)

also a number of steady state flow experiments carried out with the photolysis lamps flashing. During these flow experiments the quantum yields of the $CO_2$ production were measured, and the modulation aborptions were monitored to determine their phase shifts and amplitudes.

The modulation experiments allowed each of the free radical absorptions to be characterized as to its decay mechanism. Once the decay behavior of an absorption could be established as first or second order in radical concentration, the kinetic lifetime of the absorber could be determined.

On the basis of these experiments, a general reaction mechanism for the $Cl_2-O_2-CO$ system can be proposed; and several of the major rate constants for the chain reaction determined.

## III.  SPECTROSCOPIC RESULTS

### A.  Ultraviolet Spectroscopic Results

The modulation studies of the $Cl_2 + O_2 + h\nu$ system carried out in this laboratory by Johnston et al. in 1969 showed two modulation absorption peaks in the 200 → 300 nanometer region belonging to the ClO and ClOO free radicals.[39]  In the same work they reported an infrared modulation absorption peak for the ClOO free radical at 1443 $cm^{-1}$.

In the first series of qualitative experiments carried out on the addition of carbon monoxide to the chlorine-oxygen system, it was noted by Van den Bogaerdo and Morris[45,46] that the amplitude of the 265 nm ClO absorption had increased by a factor of six to ten.  Further scanning of the ultraviolet and infrared spectra indicated that $CO_2$ was rapidly being generated by this system, and that there were five new modulation absorption bands.  These new bands consisted of a large absorption in the ultraviolet centered at 220 nanometers and four infrared peaks at 937, 970, 1835, and 1905 $cm^{-1}$.  All five of these new modulation absorption bands displayed phase shifts in the fourth quadrant, characteristic of free radical intermediates.

### 1.  Ultraviolet Spectrum

In this investigation, the studies of the $Cl_2$-$O_2$-CO system's ultraviolet modulation spectra showed two strong absorption bands; one at 220 nm. and the other at 265 nm.  Studies of the phase shifts and amplitudes of these two peaks indicate that these absorptions belong to two different free radical species.

Figure (17) shows a plot of the modulation amplitude and phase shift in the region 195 to 280 nm. The plot shows that the two absorption maxima have different phase shifts. These phase shifts are -60.5° and -51° at a flashing frequency of 2 cps. for the 265 and 220 nm peaks respectively. These phase shifts are far enough apart to be well outside of any experiemntal error. These two different phase shifts indicate that the peaks are definitely due to two different absorbing species, and the fact that both phases are in the fourth quadrant indicates that these two species are both free radicals.

These two overlapping spectra can be resolved by utilizing the relationships between the observed phase shifts and modulation amplitudes. Since each absorption is characterized by a phase angle and an amplitude they can be treated as vector quantities. When the spectrum is composed of two overlapping absorptions, the measured value of the amplitude is the vector sum of the two individual absorptions. That is:
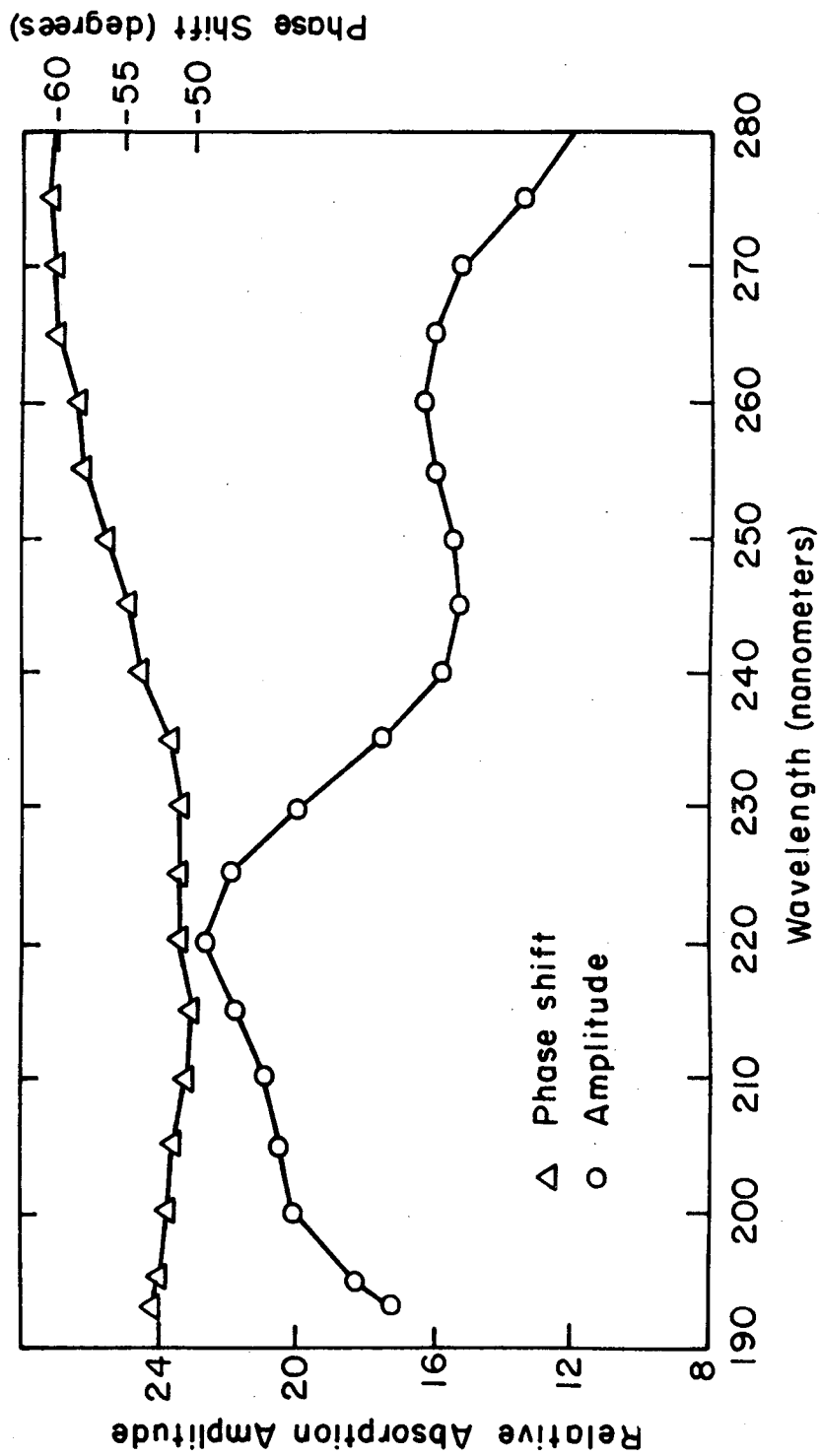
$$\vec{V}_{obs} = \vec{V}_1 + \vec{V}_2$$

$$\delta_{obs} = \text{arctangent } (b_{obs}/a_{obs}) \tag{71}$$

$$|\vec{V}_{obs}| = (a_{obs}^2 + b_{obs}^2)^{1/2}$$

These equations can be reduced to their components by vector algebra.

$$b_{obs} = b_1 + b_2 = |\vec{V}_1| \text{ sine}(\delta_1) + |\vec{V}_2| \text{ sine}(\delta_2)$$

$$\tag{72}$$

$$a_{obs} = a_1 + a_2 = |\vec{V}_1| \text{ cosine}(\delta_1) + |\vec{V}_2| \text{ cosine}(\delta_2)$$

Fig. 17. Ultraviolet modulation phase shift and amplitude spectrum.

XBL728-6850

Since $b_1 = a_1 \text{tangent}(\delta_1)$ and $b_2 = a_2 \text{tangent}(\delta_2)$, then:

$$|\vec{v}_1| = (a_1^2 + a_1^2 \text{tangent}^2(\delta_1))^{1/2}$$

$$|\vec{v}_2| = (a_2^2 + a_2^2 \text{tangent}^2(\delta_2))^{1/2} \tag{73}$$

The values of $\delta_1$ and $\delta_2$ can be obtained from the modulation spectrum, as can the values of $\delta_{obs}$, $a_{obs}$, and $b_{obs}$. Combining these measured values with Eqs. 71 → 73 makes it possible to calculate $|\vec{v}_1|$ and $|\vec{v}_2|$. Figures (18a) and (18b) show the resolved ultraviolet spectrum calculated in this manner. The -60.5° component has the published spectrum of ClO overlaid on it.[47] The good correspondence between the measured and the literature spectra reconfirm the 265 nm. absorption to be that of ClO. The new absorption at 220 nm. is not recognizable as any known intermediate species. The ClOO absorption band at 230 nm. is so small in comparison to these two large peaks that its size cannot be determined from these spectra.

With the 265 nm. absorption definitely confirmed to be caused by the ClO free radical, a number of experiments were carried out to relate the kinetic behavior of the 220 nm. absorber to that of ClO.

2. Variation of the Modulation Phase Shift and Amplitude with Reaction Conditions for the Ultraviolet Absorptions

Figure (19) shows a graph of the modulation phase shift and amplitude measurements for the two ultraviolet absorptions as a function of the relative carbon monoxide concentration for a fixed amount of chlorine and oxygen. The graph shows that the phase shifts
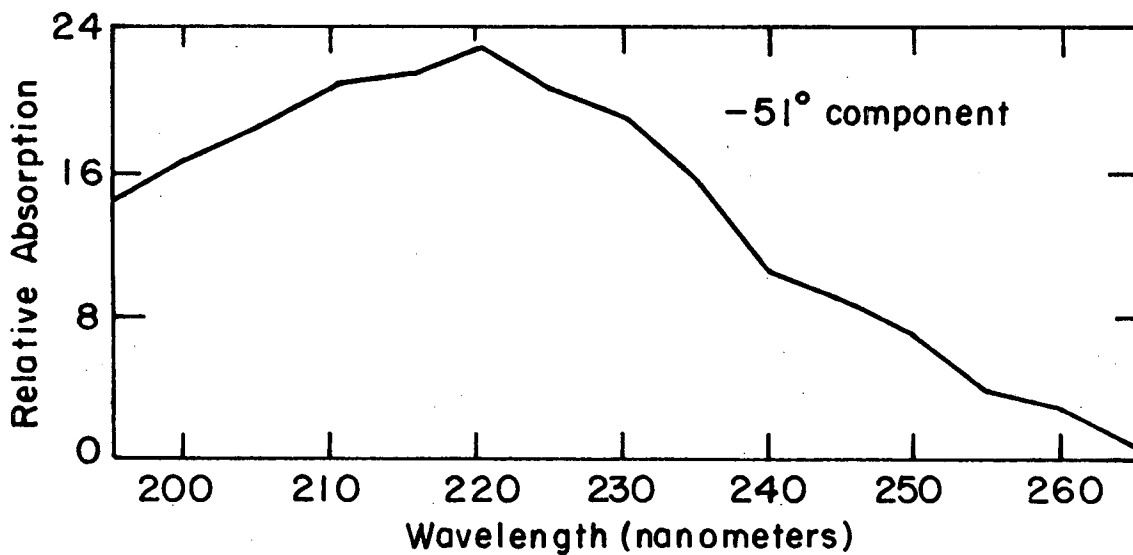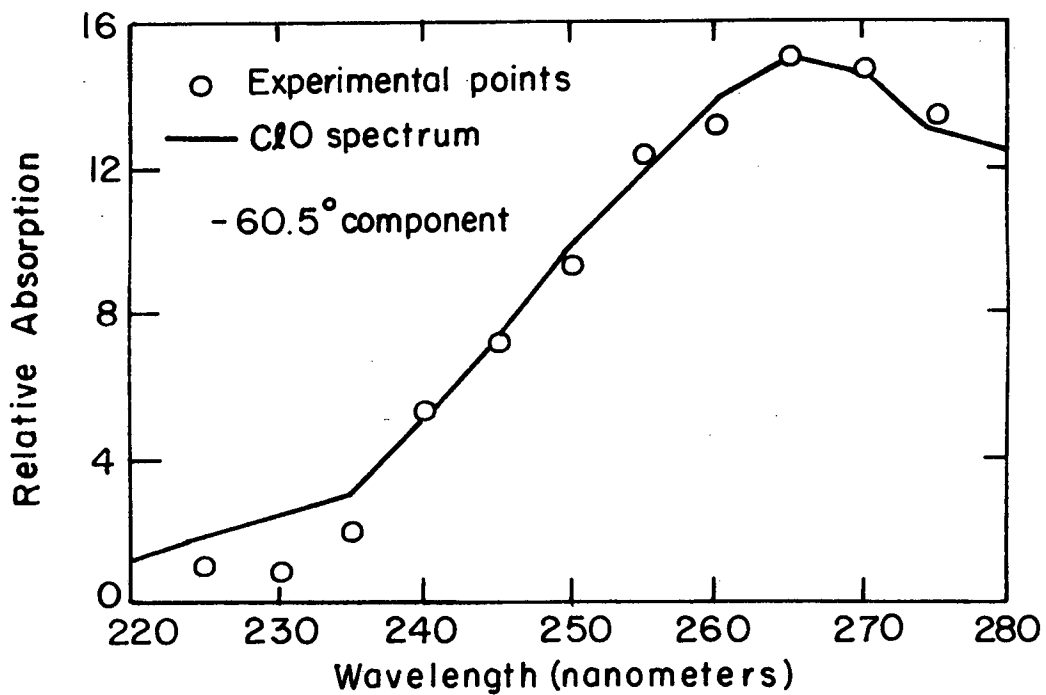
XBL728-6851

Fig. 18a and 18b.  Decomposed ultraviolet spectrum showing
the two absorptions which were overlapped in Fig. 17.
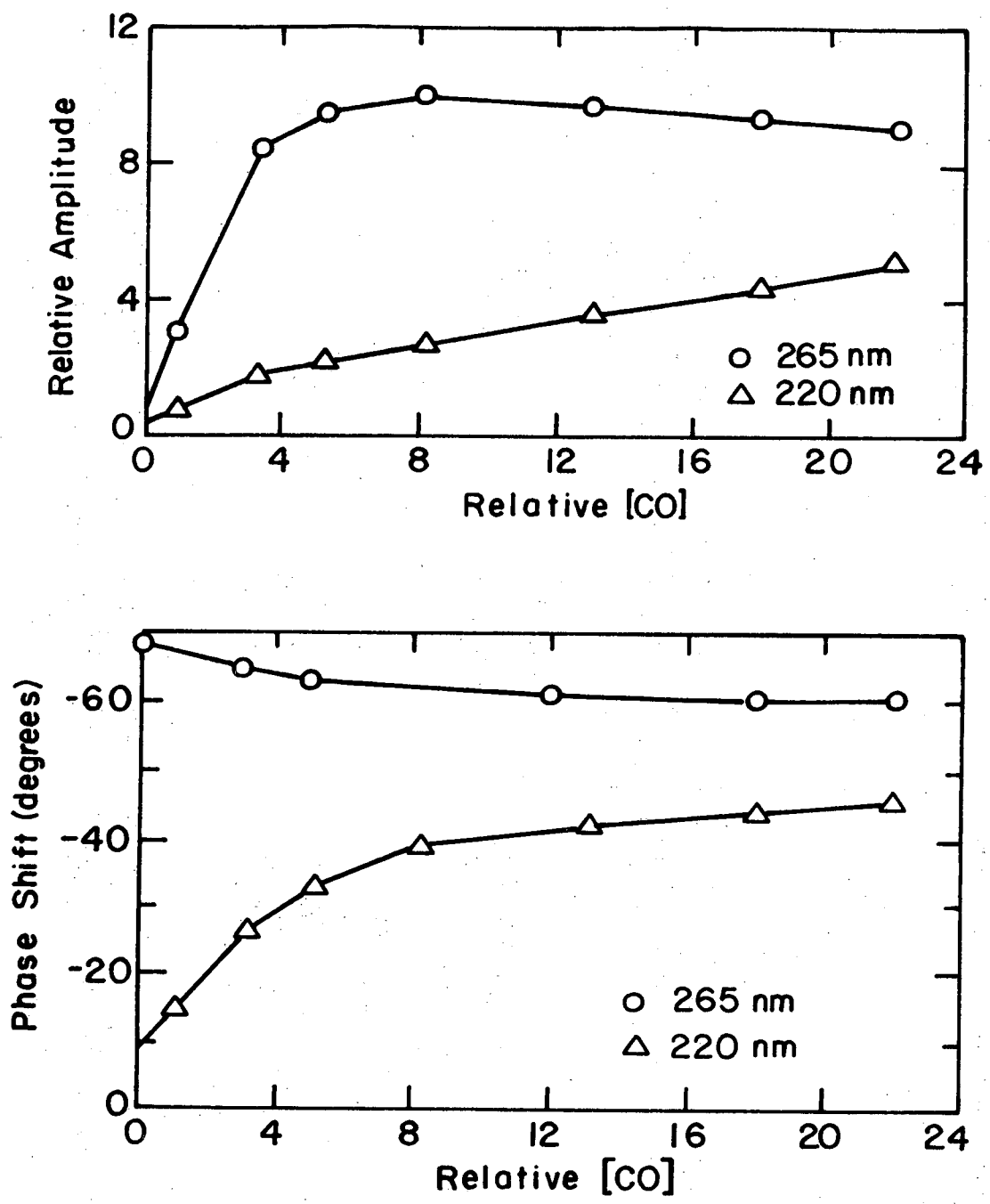
XBL 728-6852

Fig. 19.  Modulation phase shift and amplitude behavior
as a function of carbon monoxide concentration at
2 cps flashing frequency.

of the two free radicals become closer together with increasing carbon

monoxide concentration. The amplitude of the 220 nm. absorption

increases monotonically with carbon monoxide, while the ClO concentration,

after an initial increase, levels off and then begins to fall with

increasing carbon monoxide.

Another way of expressing these changes in the relative amplitudes

of the two absorptions is to plot the ratio of their absorption

amplitudes versus the ratio of [CO] to [$Cl_2$]. Figure (20) shows this

plot. From this figure it can be seen that the relative amount of

ClO continues to drop with respect to the concentration of the 220 nm.

absorber as the ratio of [CO] to [$Cl_2$] increases.

3. Relating the Modulation Behavior to the $CO_2$ Quantum Yield For the Ultraviolet Absorptions

A more quantitative measurement of the kinetic behavior of the ultra-

violet absorptions can be derived by relating the modulation phase

shift and amplitude to the quantum yield for production of $CO_2$ by the

chain reaction. This quantum yield will be defined as:

$\emptyset_{CO_2}$ = ($CO_2$ produced per sec.)/($Cl_2$ dissociated per sec.)

In a long chain reaction, the free radical intermediates soon

reach a steady-state in which they are regenerated, as soon as they

decompose, by the chain propagating steps. The effect this has upon

modulation behavior can be seen from the example shown below.
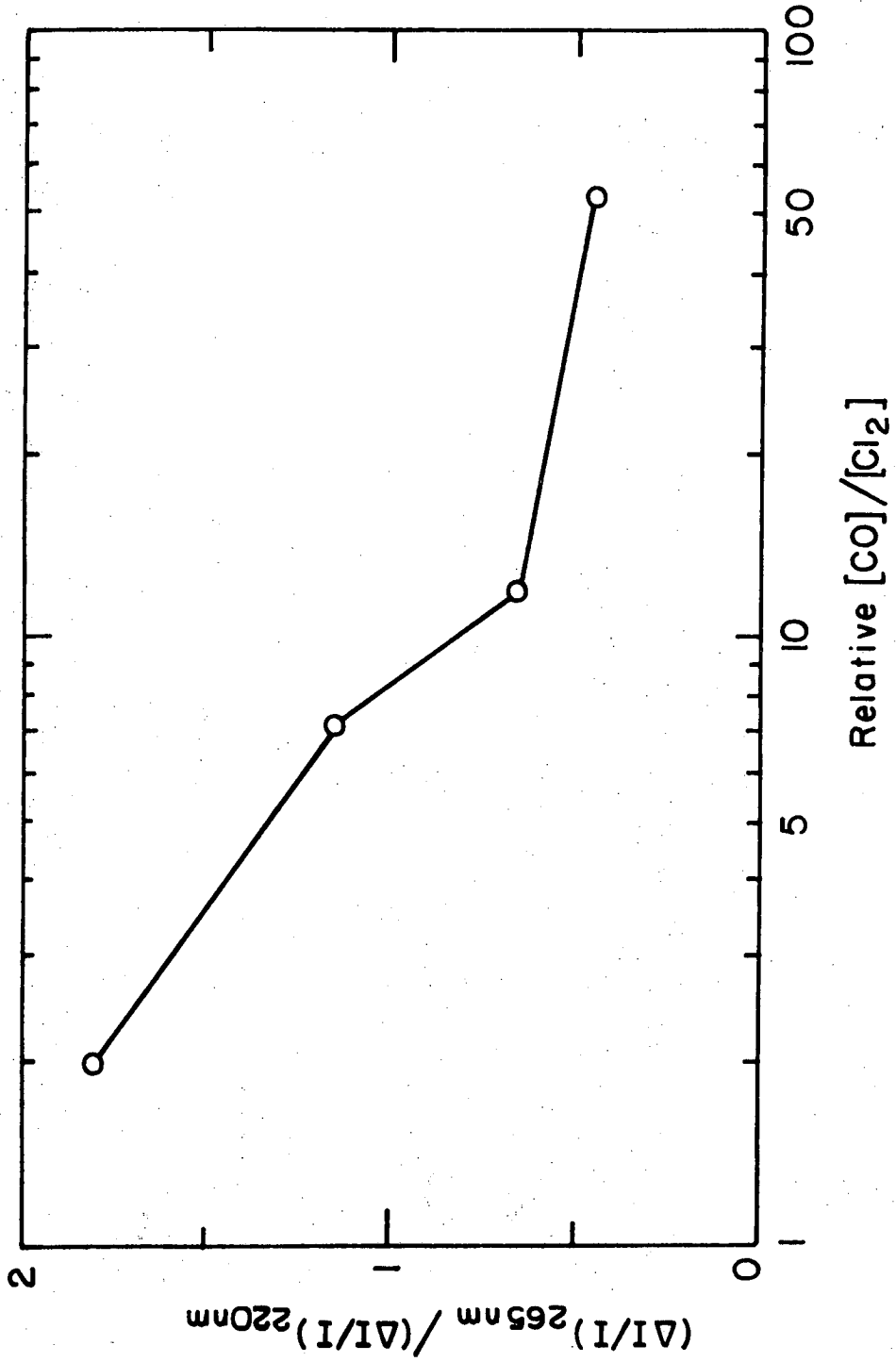
XBL 728-6853

Fig. 20. Plot of the ratio of the modulation amplitude of the 265 to the 220 nm. absorptions, versus the ratio of the relative CO to $Cl_2$ concentrations. The ratio $[CO]/[Cl_2]$ shown on the logarithmic scale is based on flow rates and is strictly a qualitative relationship.

Model 1.

Rate Constant

$$A + h\nu \rightarrow 2X \qquad \alpha I$$

$$X + B \rightarrow Y + P \qquad k_1$$

$$Y + C \rightarrow X + P \qquad k_p \qquad \text{Propagation step}$$

$$X + X \rightarrow A \qquad k_t \qquad \text{termination step}$$

A, B, and C are reactants; X and Y are free radical intermediates; and P is the product. In this example the destruction step for radical Y is first order in its own concentration, and radical X is removed second order in its own concentration. Working up the steady-state, long chain differential equations for this example gives:

$$[X]_{ss} = \frac{2\alpha I [A] + k_p [Y][C]}{k_1 [B] + 2k_t [X]} \tag{74}$$

$$\frac{d[Y]}{dt} = \frac{2\alpha I [A] \, k_1 [B]}{k_1 [B] + 2k_t [X]} - k_p [Y][c] \left\{ 1 - 1/(1 + 2k_t [X]/k_1 [B]) \right\} \tag{75}$$

Depending upon the value of the ratio $2k_t [X]/k_1 [B]$, the radical Y will show more or less "first order" decay behavior. When [B] is large the reaction sequence will be a long chain with a high value of $\emptyset_p$, $k_1 [B]$ will be much greater than $2k_t [X]$, making their ratio less than one. This will cause the free radical Y to have a smaller decay term and it will exhibit a greater phase shift away from the exciting light. This will make the chain terminating step the controlling decay rate, and radical Y will demonstrate "second order" radical decay behavior.

In the opposite case when [B] is very small, the chain reaction will have a low quantum yield and the ratio will be greater than one, ie. $2k_t[X] > k_1[B]$. This will give the free radical Y essentially "first order" decay kinetics, with its modulation phase shift becoming smaller at lower quantum yields. This is the type of behavior exhibited by the free radical absorption at 220 nm.

The $CO_2$ quantum yield in the $Cl_2-CO-O_2$ system can be varied by changing the ratio $\dfrac{d[CO_2]/dt}{\alpha I[Cl_2]}$ . If the term $\alpha I[Cl_2]$ is kept constant, then the $CO_2$ quantum yield can be changed by varying the carbon monoxide concentration. Figure (21a) shows a plot of the modulation phase shift versus $\phi_{CO_2}$ for the 220 nm. absorption at 4 cps. flashing frequency. The phase shift monotonically decreases with the quantum yield with the phase shift approaching a limiting value at a quantum yield of two. The fact that the free radical phase shift approaches a limiting value at $\phi_{CO_2}$ = 2 shows that the chain terminating step is not the same as that given in model 1. This important detail will be taken up later in this work.

This limiting behavior also indicates that the phase shift versus 1/f curve for the 220 nm. absorption should be that for a radical which decays first order in its own concentration, under the conditions of a $CO_2$ quantum yield of 2. In the high quantum yield limit, this model also predicts that the 220 nm. absorption should display a phase shift versus 1/f curve characteristic of a radical which decays second order in radical concentration. Figures (21b) and (21c) show the measured phase shifts for the 220 nm. absorption, as a function of 1/f
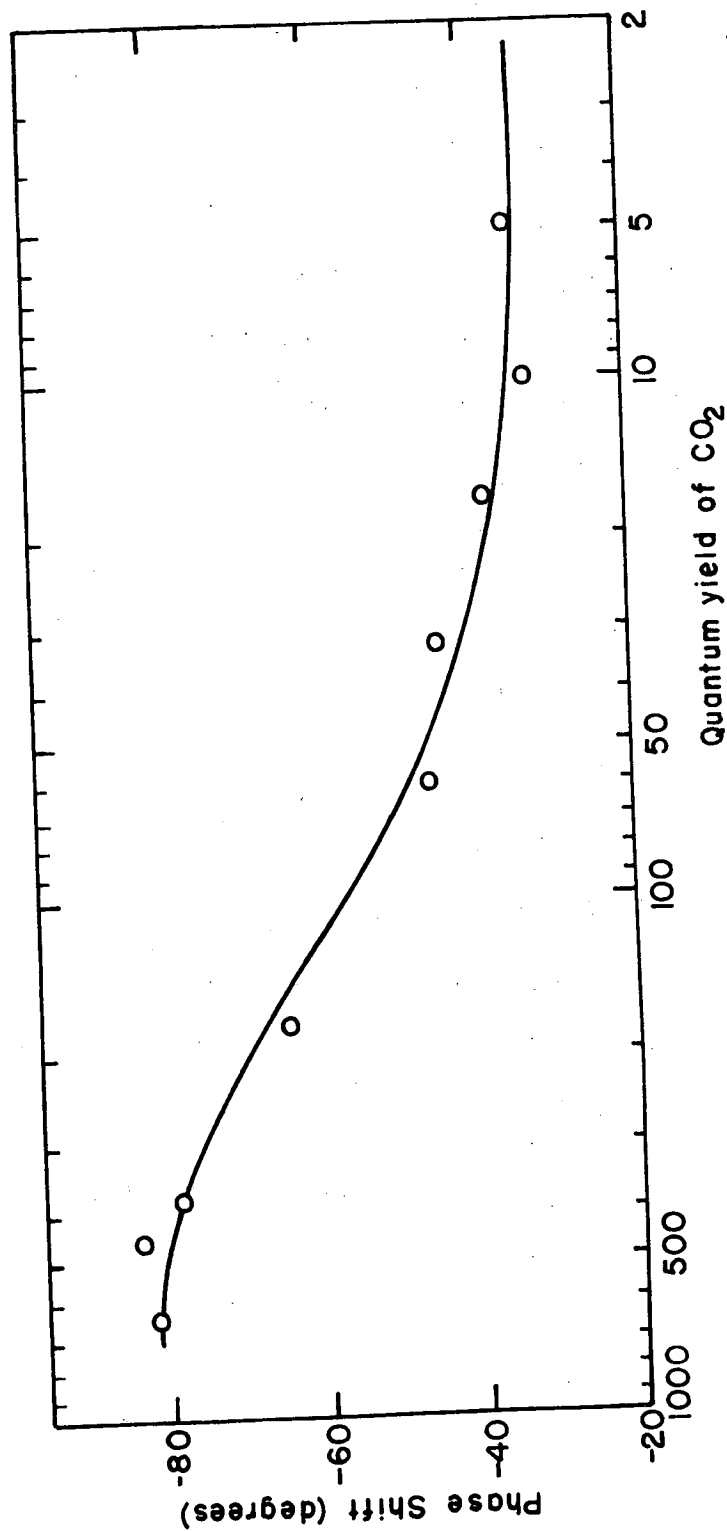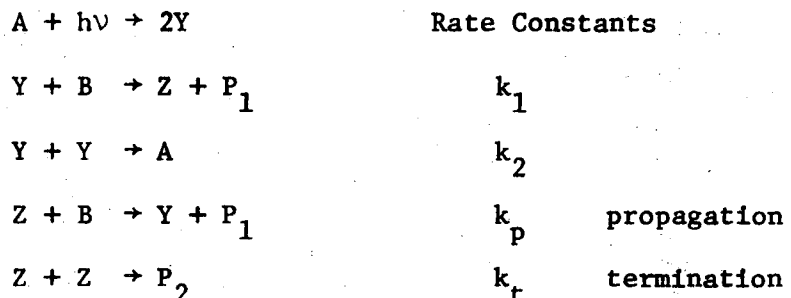
Fig. 21a. Phase shift versus the $CO_2$ quantum yield for 220 nanometer absorption at 4.9 cps, plotted on a logarithmic scale.

XBL 728-6854

for the cases of $\phi_{CO_2}$ = 32, and for $\phi_{CO_2}$ = 648. The theoretical curve

for a first order decaying radical is superimposed on Fig. (21b) and

that for a second order decaying radical on Fig. (21c).

The ClO absorption at 265 nm. exhibits a different phase shift

relationship to the $CO_2$ quantum yield. As shown in Fig. (22), the ClO

phase shift increases as the quantum yield drops. This behavior is

characteristic of another type of chain reaction intermediate, shown

in the example below:

Model 2.

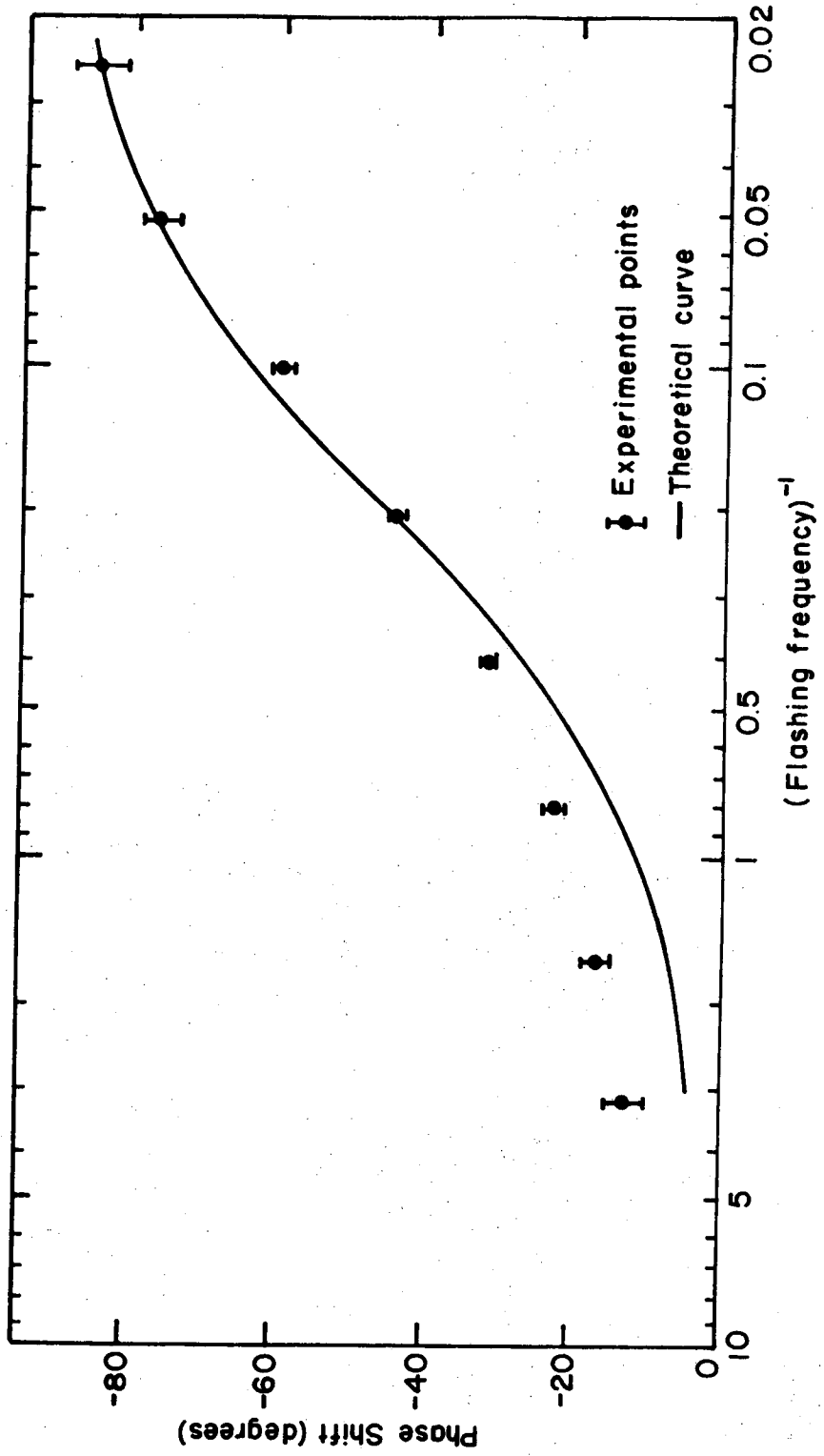| $A + h\nu \rightarrow 2Y$ | Rate Constants | |
|---|---|---|
| $Y + B \rightarrow Z + P_1$ | $k_1$ | |
| $Y + Y \rightarrow A$ | $k_2$ | |
| $Z + B \rightarrow Y + P_1$ | $k_p$ | propagation |
| $Z + Z \rightarrow P_2$ | $k_t$ | termination |

A and B are reactants, Y and Z are free radical intermediates, and

the P's are products. In the case of a long chain reaction, Y can

be considered to be in its steady state. This gives the following

expressions:

$$[Y]_{ss} = \frac{2\alpha I[A] + k_p[Z][B]}{k_1[B] + 2k_2[Y]} \tag{76}$$

and

$$\frac{d[Z]}{dt} = k_1[Y][B] - k_p[Z][B] - 2k_t[Z]^2 \tag{77}$$

Fig. 21b. The 1/f versus phase shift behavior for the 220 nm absorption at a $CO_2$ quantum yield of 32, plotted on a logarithmic scale. The theoretical curve for first order radical decay is matched to the data at $-45°$. For these data: $[Cl_2] = 2.2 \times 10^{16}$ molecules/cm$^3$, $[CO] = 2.5 \times 10^{16}$ molecules/cm$^3$, $[O_2] = 2.44 \times 10^{19}$ molecules/cm$^3$.

XBL728-6855

Fig. 21b.

Phase Shift (degrees)

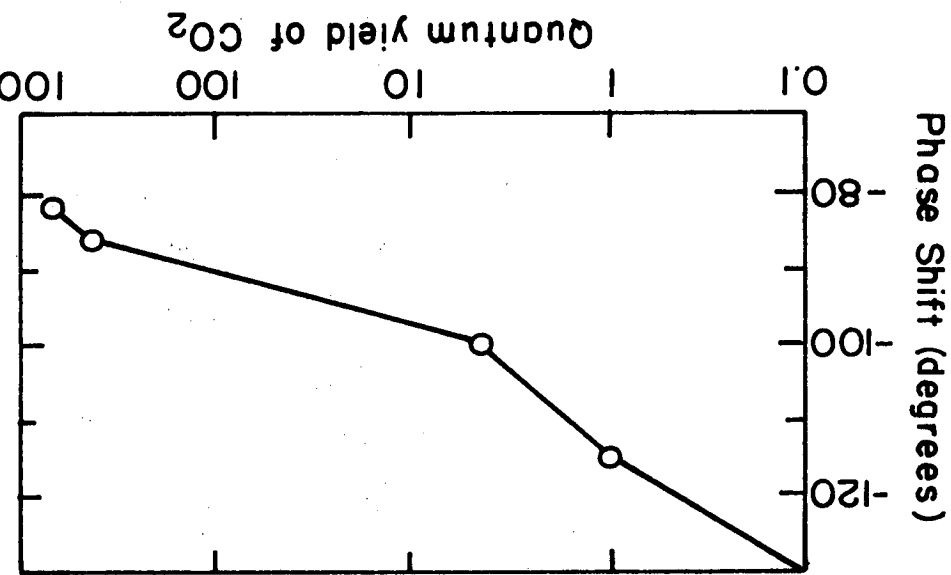(Flashing frequency)$^{-1}$

⏘ Experimental points
— Theoretical curve

Fig. 21c. Phase shift versus 1/f behavior for the 220 nm. absorption at a quantum yield of 648 plotted on a logarithmic scale. The theoretical curve overlay for second order radical decay is matched to the data at $-52°$. For these data: $[Cl_2] = 2.6 \times 10^{15}$ molecules/$cm^3$ $[CO] = 5. \times 10^{17}$ molecules/$cm^3$, $[O_2] = 2.4 \times 10^{19}$ molecules/$cm^3$.

Fig. 22. The change in phase shift of the 265 nm. ClO absorption with quantum yield of $CO_2$ at 8 cps flashing frequency. The quantum yield is shown on a logarithmic scale.
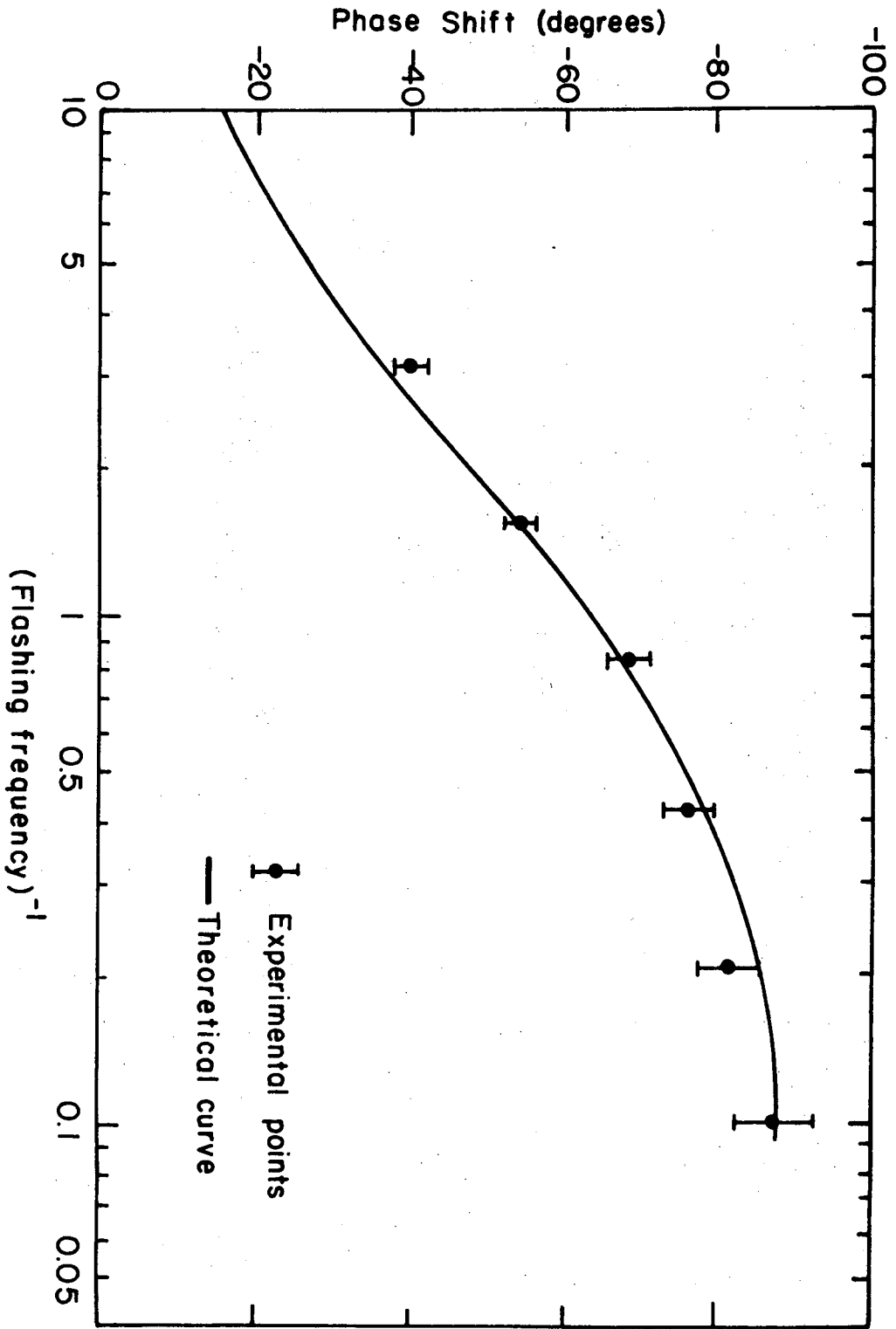
XBL 728-6857

Fig. 21c.

XBL 728-6856

In the long chain case, $2k_2[Y] \ll k_1[B]$ and :

$$\frac{d[Z]}{dt} \approx 2\alpha I[A] - 2k_t[Z]^2 \tag{78}$$

Thus, in a modulation system, the radical [Z] in the long chain limit will display the phase shift versus $1/f$ behavior of a radical decaying second order in its own concentration. Its phase shift will vary from 0 to $-90°$ with flashing frequency, as shown in the example calculated for Fig. (12).

When the reactant B is decreased, so that $k_1[B] \ll 2k_2[Y]$ and $2\alpha I[A] \gg k_p[Z][B]$, the quantum yield will be very small, and the free radical [Y] will no longer be in a steady state. In this case:

$$\frac{d[Y]}{dt} \approx 2\alpha I[A] - 2k_2[Y]^2 \tag{79}$$

and

$$\frac{d[Z]}{dt} \approx k_1[Y][B] - 2k_r[Z]^2 \tag{80}$$

Then Y will have a phase shift varying from 0 to $-90°$ and the free radical Z will always follow Y. So Z will have its phase shift approaching $-180°$ in the high frequency limit. This is labeled "2nd generation radical behavior". The C10 free radical like the radical Z in this example has its phase shift increasing, while the $CO_2$ quantum yield drops.

To demonstrate that C10 has this type of behavior, Fig. (23a) shows the C10 phase shift behavior for a $CO_2$ quantum yield of 32, and

Fig. 23a.   Phase shift versus 1/f behavior for the 265 nm. ClO absorption at a quantum yield of 32, plotted on a logarithmic scale. For these data: $[Cl_2]$ = 2.2 × $10^{16}$ molecules/$cm^3$ [CO] = 2.5 × $10^{16}$ molecules/$cm^3$, $[O_2]$ = 2.44 × $10^{19}$ molecules/$cm^3$.
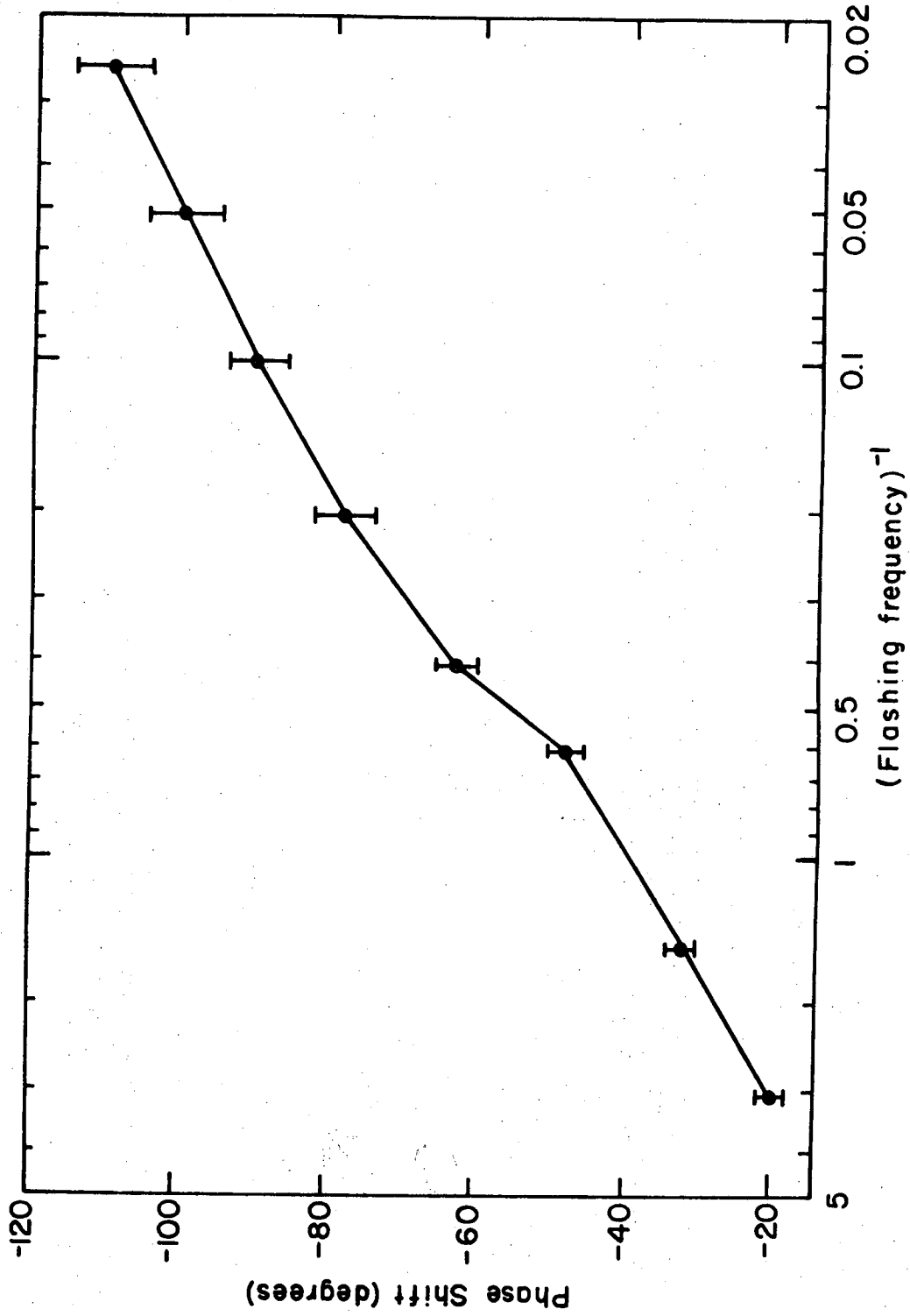
XBL 728 - 6858

Fig. 23a.

Fig. (23b) shows the phase shift curve for $\phi_{CO_2}$ = 648. In the high

quantum yield case, the ClO phase shift behavior is very close to that

predicted by the "second order" radical decay curve. In the low

quantum yield case, however, the ClO phase shift passes -90° and does

not reach a high frequency limit. This indicates that the role of

ClO in the chain reaction is very similar to that of the radical Z in

Model 2.

## B. Infrared Spectroscopic Results

The infrared modulation spectrum shows four new absorption peaks

with free radical behavior when carbon monoxide is added to the $Cl_2$-$O_2$

system. Figure (24) shows modulation phase shift and amplitude versus

wavelength plots for these absorptions taken under one set of reaction

conditions. It can be seen from these graphs that the peaks at 937,

1835, and 1905 $cm^{-1}$ have the same phase shift within experimental

error. The smaller side band at 970 $cm^{-1}$ shows a phase shift of about

-16 degrees greater than the other three absorptions. This indicates

that the three absorptions at 937, 1835, and 1905 $cm^{-1}$ could belong

to the same absorbing species, while the weaker 970 $cm^{-1}$ side band is

caused by a second radical species.

To test this, a series of experiments were carried out under

different reaction conditions. By comparing the phase shifts and the

ratios of the amplitudes of the absorptions, it is possible to identify

which peaks belong to the same absorbing species. Table (14) lists

the results of these experiments.

Table 14. Summary of the results of the qualitative experiments measuring the phase shifts and amplitudes of the infrared absorptions under a variety of reaction conditions.

### Phase Shift Comparison

| f cps. | Case | 937 | 970 | 1835 | 1905 $(cm^{-1})$ |
|--------|------|-----|-----|------|------|
| 2 | 1 | $-50 \pm 1°$ | $-65 \pm 2°$ | $-49.3 \pm 4°$ | $-49.8 \pm 4°$ |
| 2 | 2 | $-42 \pm 1°$ | $-58 \pm 2°$ | $-43 \pm 3°$ | $-42 \pm 3°$ |
| 1/4 | 3 | $-64 \pm 1°$ | $-82 \pm 5°$ | $-68 \pm 4°$ | $-66 \pm 4°$ |
| 1/4 | 4 | $-41 \pm 1°$ | $-52 \pm 1°$ | $-40.8 \pm 2°$ | $-39.8 \pm 2°$ |

### Amplitude Ratios $\frac{\Delta I}{I}$ X $\frac{\Delta I}{I}$ 937

Case

### Ratios $\Delta I/I$

| Case | 937/937 | 970/937 | 1835/937 | 1905/937 |
|------|---------|---------|----------|----------|
| 1 | 1 | 0.30 | 0.30 | 0.28 |
| 2 | 1 | 0.25 | 0.28 | 0.22 |
| 3 | 1 | 0.6 | 0.27 | 0.25 |
| 4 | 1 | 0.19 | 0.285 | 0.24 |

### Conditions

| Case | (molecules/cm$^3$) | f = | | Case | (molecules/cm$^3$) | f = |
|------|--------------------|-----|---|------|--------------------|-----|
| 1 | $[Cl_2] = 2.5 \times 10^{16}$ | 2 cps | | 3 | $[Cl_2] = 7.3 \times 10^{16}$ | 1/4 cps |
| | $[CO] = 1.2 \times 10^{17}$ | | | | $[CO] = 9.3 \times 10^{16}$ | |
| | $[O_2] = 2.45 \times 10^{19}$ | | | | $[O_2] = 1.45 \times 10^{19}$ | |
| | | | | | $[N_2] = 1.0 \times 10^{19}$ | |
| 2 | $[Cl_2] = 6.8 \times 10^{16}$ | 2 cps | | 4 | $[Cl_2] = 3.2 \times 10^{15}$ | 1/4 cps |
| | $[CO] = 8.0 \times 10^{17}$ | | | | $[CO] = 5.0 \times 10^{17}$ | |
| | $[O_2] = 2.44 \times 10^{19}$ | | | | $[O_2] = 2.4 \times 10^{19}$ | |

Fig. 23b. Phase shift versus 1/f behavior for the 265 nm. ClO absorption at a quantum yield of 648, plotted on a logarithmic scale. The overlay is a theoretical curve for a radical decaying second order in radical concentration, matched to the data at data at $-60°$. For these data: $[Cl_2] = 2.6 \times 10^{15}$ molecules/cm$^3$, $[CO] = 5.0 \times 10^{17}$ molecules/cm$^3$, $[O_2] = 2.4 \times 10^{19}$ molecules/cm$^3$.
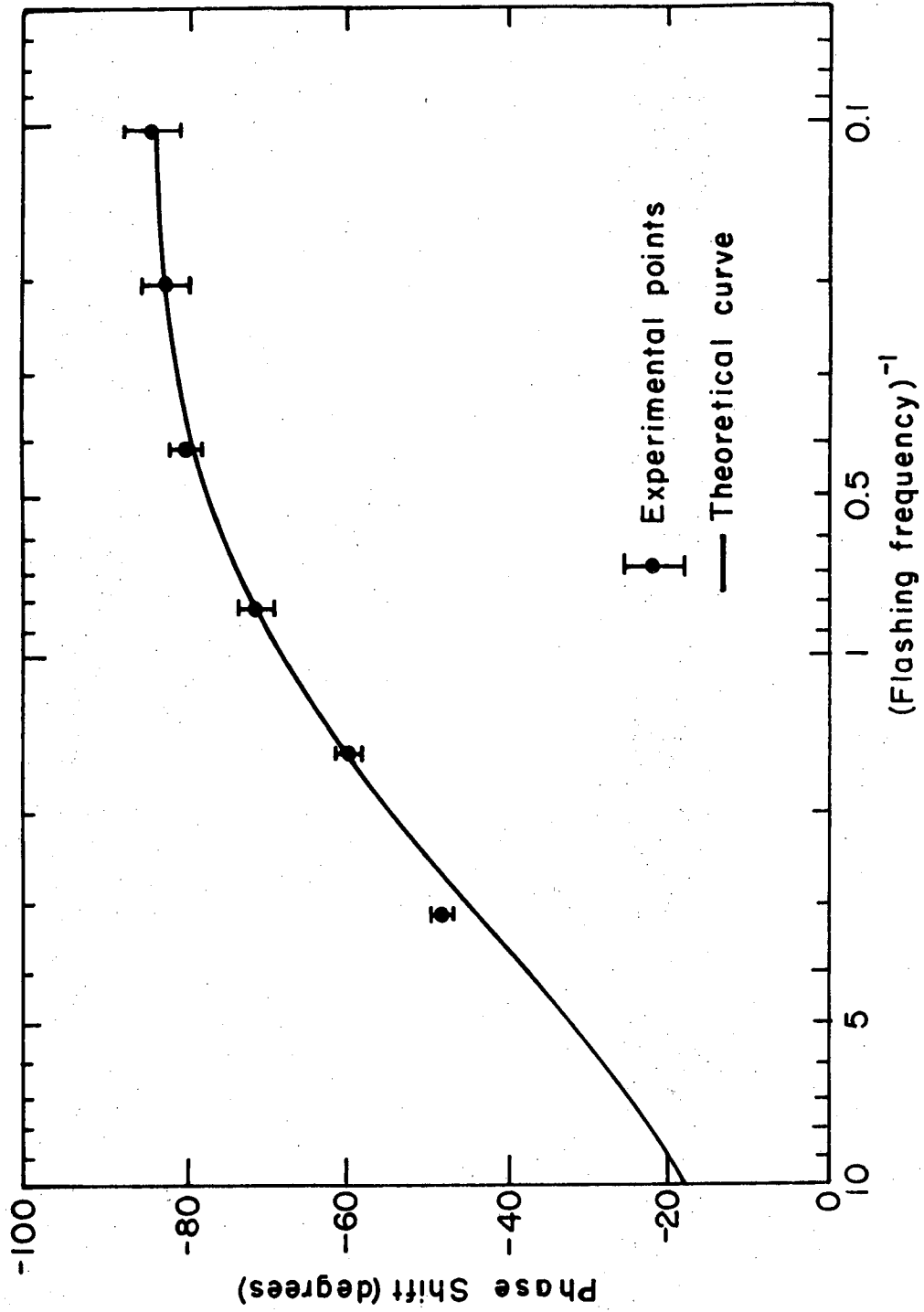
XBL728-6859

Fig. 23b.
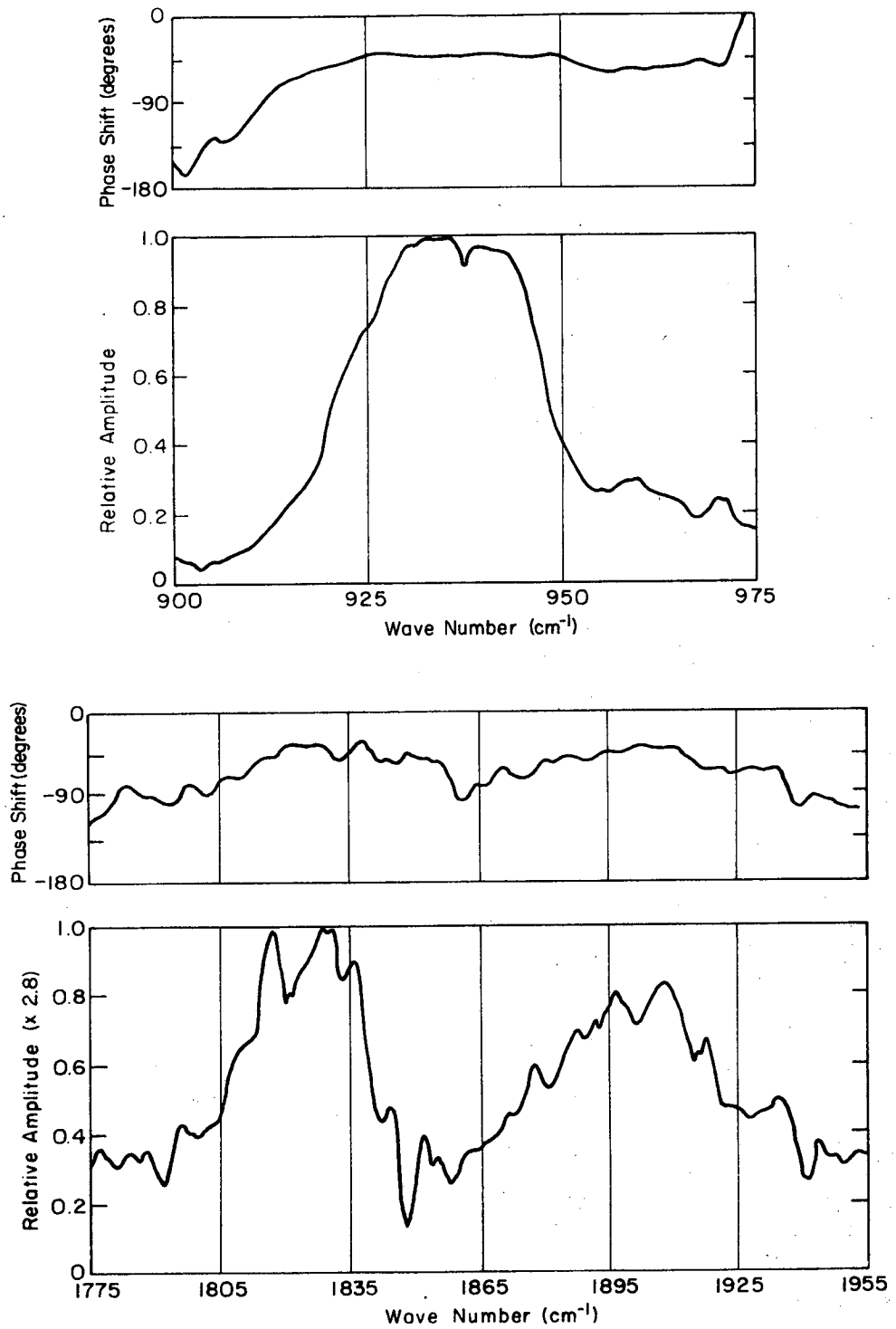
XBL 728-6860

Fig. 24. Modulation phase shift and amplitude spectra of the infrared free radical absorptions. The spectra were taken at 2 cps. flashing frequency, with $[Cl_2]$ = $6.4 \times 10^{16}$, $[CO]$ = $2.7 \times 10^{16}$, and $[O_2]$ = $2.45 \times 10^{19}$ molecules/cm$^3$.
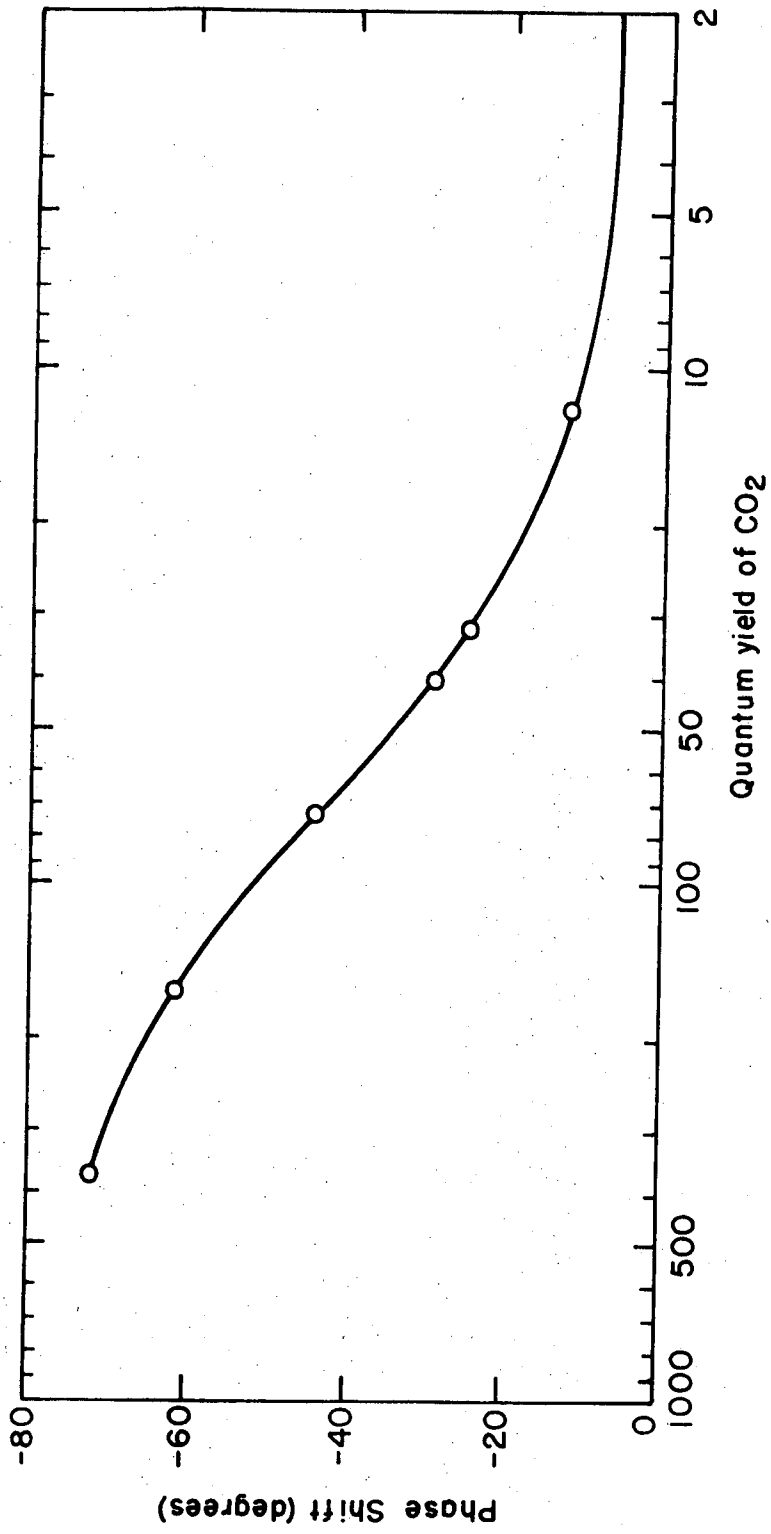
XBL 728-6862

Fig. 26. Phase shift versus $\phi_{CO_2}$ for the 937 $cm^{-1}$ infrared absorption at 1 cps. The quantum yield is shown on a logarithmic scale.

Fig. 27. Phase shift versus 1/f behavior of the 937 cm$^{-1}$ absorption at a $CO_2$ quantum yield of 40. The 1/f values are shown on a logarithmic scale. The overlay is the theoretical curve for a first order decaying radical. For this plot: $[Cl_2]$ = 1.06 × $10^{16}$ molecules/cm$^3$, $[CO]$ = 2.6 × $10^{16}$ molecules/cm$^3$, $[O_2]$ = 2.4 × $10^{19}$ molecules/cm$^3$.
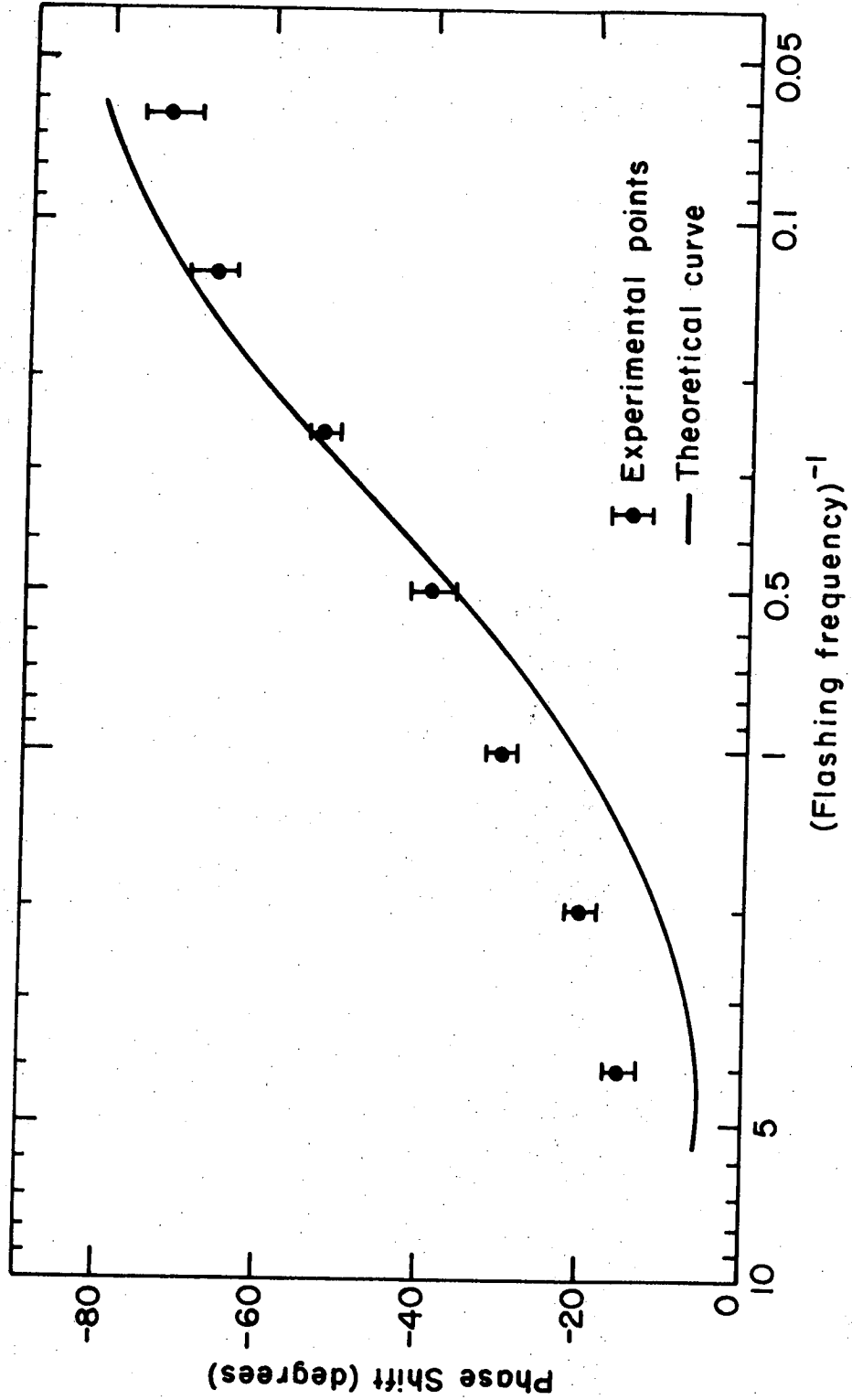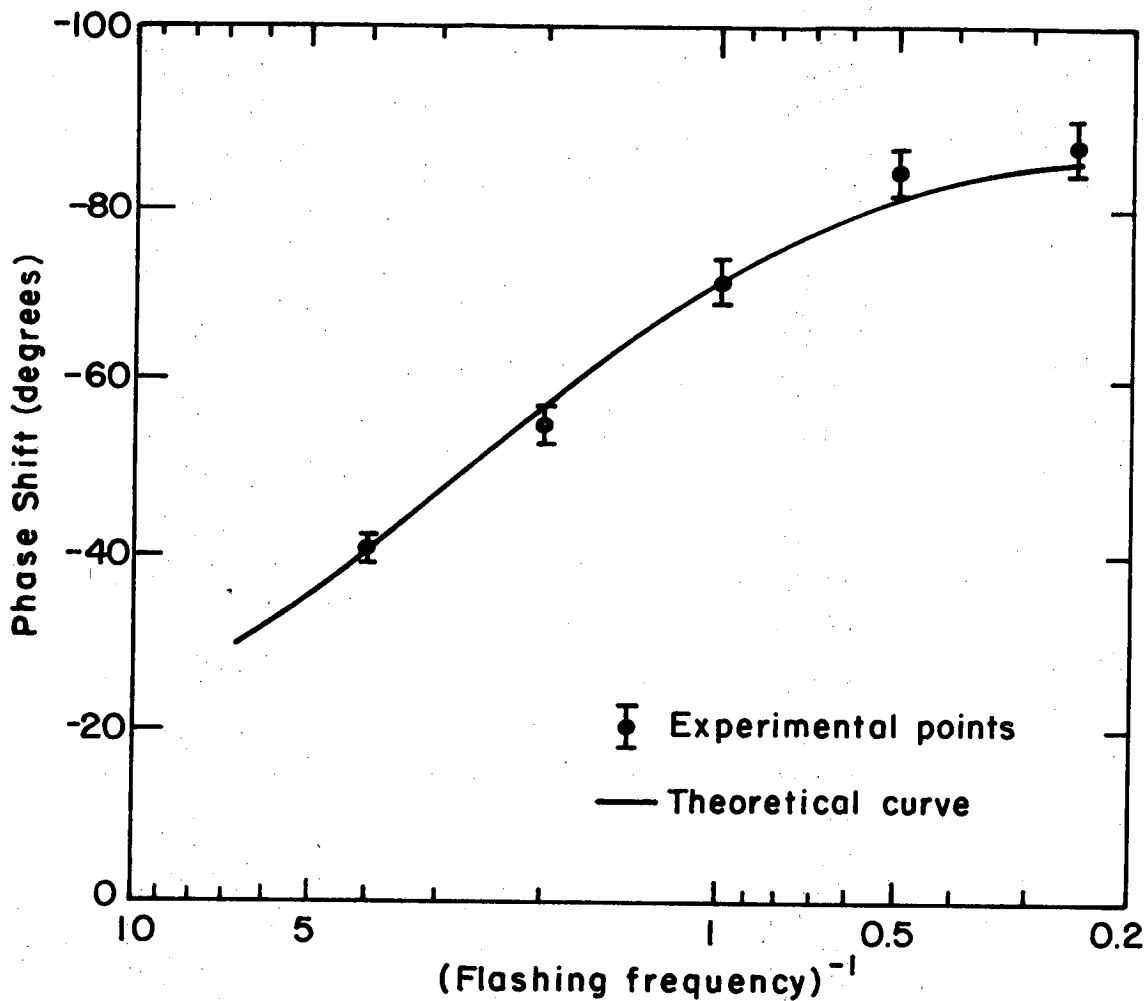
XBL 728-6863

Fig. 27.

A second set of experiments was conducted in the infrared cell to relate the absorptions to the quantum yield of the $CO_2$ production chain. Figure (26) shows the phase shift versus quantum yield behavior of the 937 $cm^{-1}$ absorption. Like the ultraviolet band at 220 nm., the infrared peak shows a decrease in phase shift with decreasing quantum yield. The 937 $cm^{-1}$ phase also approaches a limiting value as the $CO_2$ quantum yield reaches 2, in the same manner as the 220 nm. band.

Since the 937 $cm^{-1}$ peak's phase shift approaches a limiting value as the quantum yield goes to 2, the phase shift versus 1/f plot for this absorption should display the behavior of a first order decaying radical in this limit, as predicted by model 1. Figure (27) shows the phase shift versus 1/f data with a theoretical first order decay curve overlayed upon it for an infrared experiment with a quantum yield of 40. To illustrate how this curve will change with quantum yield, Fig. (28) shows a phase shift versus 1/f plot for the 937 $cm^{-1}$ peak at a quantum yield of 360. This data has a second order decay theoretical curve overlay.

The 970 $cm^{-1}$ band at low quantum yields shows phase versus 1/f behavior characteristic of a radical formed from a radical precursor, such as radical Z in model 2. To illustrate this behavior, Figs. (29) and (30) show comparisons of the 937 and 970 $cm^{-1}$ phase shift versus 1/f curves under the conditions of low and high quantum yield. Figure (29) is for the conditions of $\phi_{CO_2} = 40$, and Fig. (30) represents a $\phi_{CO_2} = 360$. The phase shift separation between these two absorptions increases as the quantum yield drops. This is the "second generation"

XBL728-6864

Fig. 28. Phase shift versus 1/f behavior of the 937 cm$^{-1}$ absorption at a $CO_2$ quantum yield of 360. The 1/f values are shown on a logarithmic scale. The overlay is the theoretical curve for a radical decaying second order in radical concentration. For this experiment:

$$[Cl_2] = 2.6 \times 10^{15} \text{ molecules/cm}^3$$
$$[CO] = 5.8 \times 10^{17} \text{ molecules/cm}^3$$
$$[O_2] = 2.4 \times 10^{19} \text{ molecules/cm}^3$$

Fig. 29.  Comparison of the phase shift versus 1/f behavior of the 937 and 970 cm$^{-1}$ absorptions at a $CO_2$ quantum yield of 40.  The 1/f values are shown on a logarithmic scale.

Fig. 30.  Comparison of the phase shift versus 1/f behavior of the 937 and 970 cm$^{-1}$ absorptions at a $CO_2$ quantum yield of 360.  The 1/f values are shown on a logarithmic scale.

As the data shows the phase shifts of the 937, 1835, and 1905 $cm^{-1}$ absorptions are the same within experimental error in each of the experimental runs. The data also show that the amplitude ratios of these three peaks are constant under all the experimental conditions. This identifies the three absorptions at 937, 1835, and 1905 $cm^{-1}$ as belonging to the same absorber, or perhaps to a pair of kinetically identical absorbers, such as two isomers.

The changes in the amplitude ratio of the 937 peak to the 970 $cm^{-1}$ peak, as well as the differences in their phase shifts at each set of experimental conditions, definitely shows the 970 $cm^{-1}$ absorption to be caused by a second species.

In an attempt to relate the infrared absorptions to those in the ultraviolet, the same series of experiments was carried out in both reaction cells. In most of these experiments in the infrared cell, only the 937 and 970 $cm^{-1}$ peaks were monitored, since the other two absorptions show the same behavior as the 937 $cm^{-1}$ band.

Figure (25) shows a graph of the ratio of the amplitude of the 970 $cm^{-1}$ absorption to that of the 935 $cm^{-1}$ band plotted against the ratio of the relative carbon monoxide concentration to that of the chlorine. This graph can be compared to Fig. (20) which shows the same plot for the ultraviolet absorptions. In this case the 970 $cm^{-1}$ absorption amplitude decreases with respect to that of the 937 $cm^{-1}$ peak, as the carbon monoxide concentration is increased over that of the chlorine. This behavior is very similar to that of the ultraviolet absorptions.
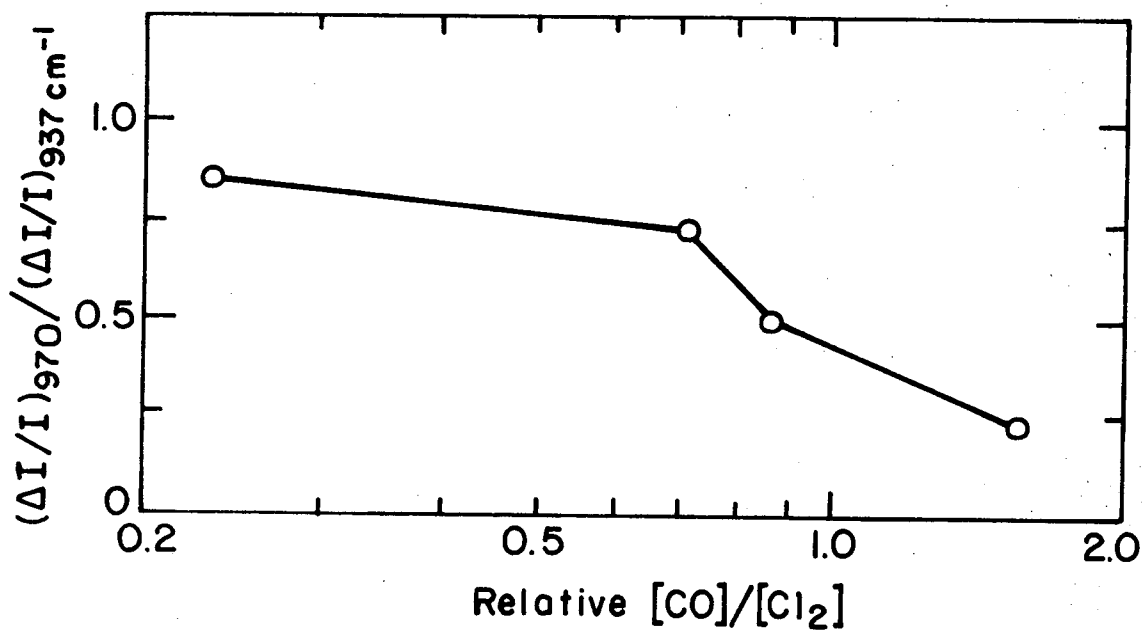
XBL 728-6861

Fig. 25. Plot of the ratio of the modulation amplitude of
the 970 to the 937 $cm^{-1}$ absorptions, versus the ratio
of the relative CO to $Cl_2$ concentrations, which is shown
on a logarithmic scale. The ratio $[CO]/[Cl_2]$ is based
on flow rates and is strictly qualitative.

Fig. 29.
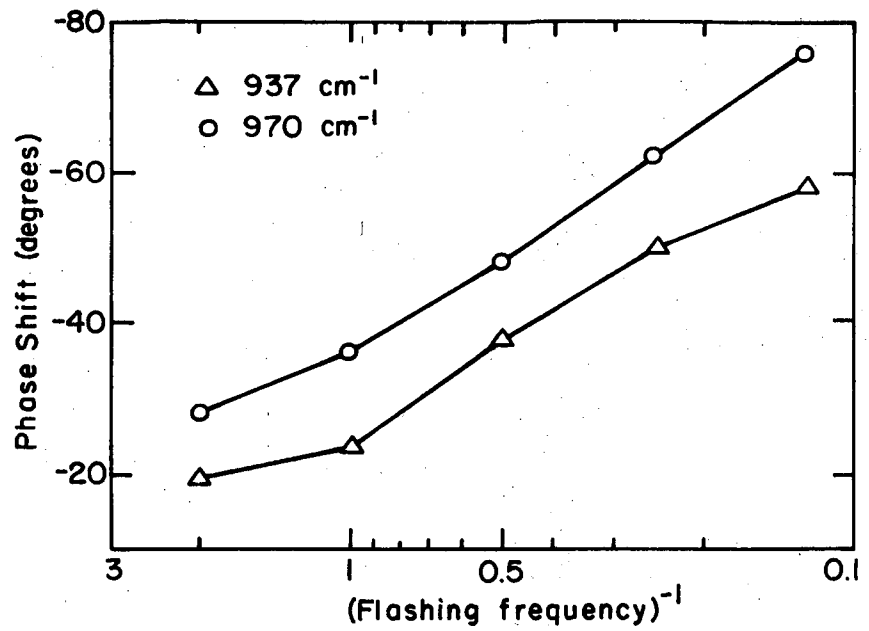
For this data:
$[Cl_2] = 6.4 \times 10^{16}$ molecules/cm$^3$
$[CO] = 2.7 \times 10^{16}$ molecules/cm$^3$
$[O_2] = 2.44 \times 10^{19}$ molecules/cm$^3$



Fig. 30.

For this data:
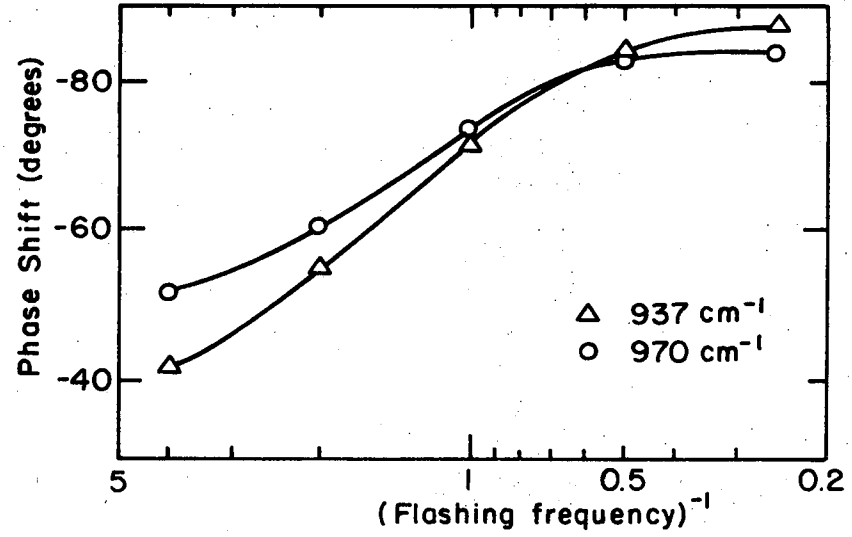$[Cl_2] = 2.6 \times 10^{15}$ molecules/cm$^3$
$[CO] = 5.8 \times 10^{17}$ molecules/cm$^3$
$[O_2] = 2.4 \times 10^{19}$ molecules/cm$^3$

XBL 728-6865

radical behavior predicted by model 2, and demonstrated by both the 970 $cm^{-1}$ peak and the ClO absorption.

## C. Comparison of the Ultraviolet and Infrared Spectra

To relate this information about the spectra taken in the two reaction cells it is necessary to look at all the qualitative data shown in the preceding sections. To facilitate this, the individual observations and conclusions will be listed in tabular form.

### 1. Conclusions from Experimental Data

1) Both the ultraviolet and infrared modulation spectra show two distinct absorbing species displaying free radical kinetic behavior.

2) The 265 nm. absorption has been identified as belonging to the ClO free radical.

3) The 937, 1835, and 1905 $cm^{-1}$ absorptions have been identified as belonging to one absorber.

### 2. Observations Relating the 937 $cm^{-1}$ and 220 nm. Absorptions

1) As the carbon monoxide concentration is varied, both of these absorptions show decreasing phase shift with decreasing $CO_2$ quantum yield, with the phase shift approaching a limit at a value of $\phi_{CO_2}$ = 2.

2) Both of these absorptions show first order radical decay behavior in the low quantum yield limit.

3) Both of the absorptions show second order radical decay kinetics under high $CO_2$ quantum yield conditions.

4) Since both the 937 $cm^{-1}$ and 220 nm. absorptions exhibit first order radical behavior in the limit of low quantum yield, a lifetime can be

calculated for each of these absorptions. For the first order decaying radical species the lifetime was defined as: $\tau = 1/k_r[C] = 1/(-2\pi f/\tan\delta)$. Thus from the single measurement of the limiting phase shift at $\emptyset_{CO_2} = 2$ the lifetime can be determined for each of these absorptions.

As shown in Fig. (26a) the 937 $cm^{-1}$ phase shift appears to approach a limiting angle of $-7.5 \pm 2°$ at a 1 cps flashing frequency. This gives a calculated lifetime for the absorber of $\tau_{937\ cm^{-1}} = 0.021 \pm .005$ seconds. Figure (21a) shows the 220 nm. phase shift approaching a limiting phase shift of $-33.5 \pm 1°$ at a flashing frequency of 4 cps. This angle predicts a lifetime of $\tau_{220\ nm.} = 0.0215 \pm .001$ sec.

The combination of these calculated lifetimes, and the qualitative observations indicate that the species causing the 220 nm. absorption is also responsible for the 937, 1835, and 1905 $cm^{-1}$ infrared absorptions.

3. Observations Relating the 970 $cm^{-1}$ and 265 nm. Absorptions

1) As the $CO_2$ quantum yield decreases, both the ClO 265 nm. absorption and the 970 $cm^{-1}$ peak show an increasing phase shift separation from the phase shift of the absorber associated with the 220 nm. and 937 $cm^{-1}$ absorptions. This type of behavior indicates that in the low quantum yield range the 970 $cm^{-1}$ absorber and the ClO both are begining to show "second generation" radical behavior with respect to the 220 nm., 937 $cm^{-1}$ absorber. This behavior is confirmed for the ClO absorption since its phase shift goes beyond $-90°$ in Fig. (23a) for the case of $\emptyset_{CO_2} = 32$.

2) Another comparison can be made by examining an overlay of the phase shift versus 1/f curves for the two infrared species in the high quantum yield region. Figure (30) shows these curves for the 937 and 970 cm$^{-1}$ for a reaction system with $\phi_{CO_2}$ = 360. The different slopes and crossing behavior of these two curves is characteristic for the phase shifts of these two species in the high quantum yield range.

Figure (31) shows a similar overlay plot of the phase shift versus 1/f behavior of the 220 and 265 nm. absorptions. These measured phase angles were done in a reaction system with a quantum yield of 392. These curves show the same difference in slope and crossing behavior as the infrared absorptions.

The crossing occurs at the same phase angle in both cases, but at different flashing frequencies. This is probably due to the difference in reaction conditions in the two cells. A radical decaying second order in its own concentration has its lifetime given by:

$$\tau = 1/(2k_r[Z]) \text{ with } [Z] = (2\alpha I_o[A]/2k_r)^{1/2} \tag{81}$$

This was derived in the section on experimental method. This shows that the radical decay rate is inversely proportional to the rate of radical formation. Hence, the second order decaying radicals in the ultraviolet cell will have a shorter life time since the product of the light intensity, carbon monoxide, and chlorine is greater in that cell under the conditions of the two graphs. Since the radicals will have a shorter lifetime, they will also have a smaller phase angle at any given flashing frequency than that same radical in the infrared cell.
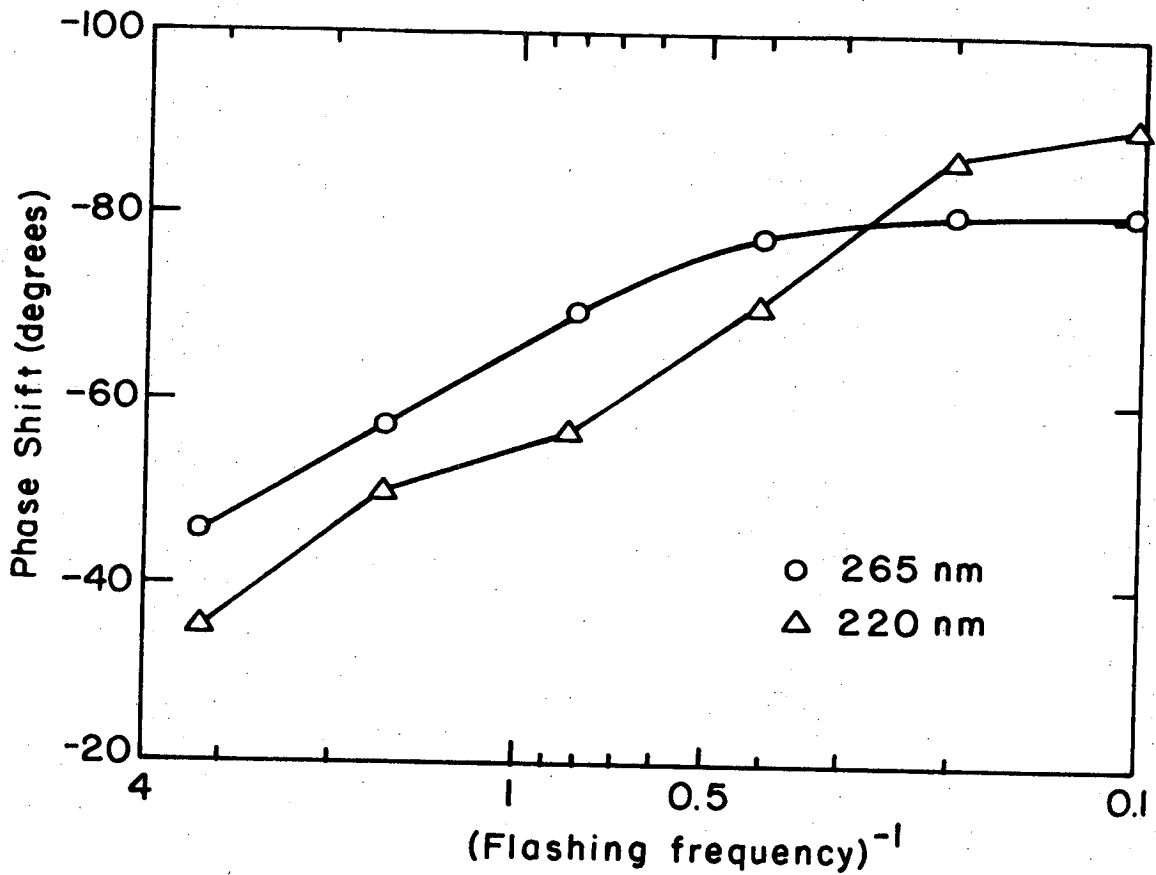
XBL 728-6866

Fig. 31. Comparison of the phase shift versus 1/f behavior of the 265 and 220 nm. absorptions at a $CO_2$ quantum yield of 392. The 1/f values are shown on a logarithmic scale. For this experiment:

$$[Cl_2] = 4.7 \times 10^{15} \text{ molecules/cm}^3$$
$$[CO] = 4.4 \times 10^{17} \text{ molecules/cm}^3$$
$$[O_2] = 2.42 \times 10^{19} \text{ molecules/cm}^3$$

The reason for this crossing over behavior could be due to the 220 nm. and 937 $cm^{-1}$ absorber having partial first order and partial second order decay behavior. The overlay graph of the theoretical curves for first and second order radical decay in Fig. (12) shows this same cross over effect. Since the ClO radical shows pure second order decay under these conditions as seen in Fig. (23b) it is possible that any first order decay behavior on the part of the other free radical would produce the crossing effect.

4) As shown in Figs. (20) and (25) the modulation amplitude versus reaction conditions behavior of the 970 $cm^{-1}$ and 265 nm. absorptions is very similar.

This direct correspondence in kinetic behavior between the 265 nm. and 970 $cm^{-1}$ absorptions leads to the identification of the infrared band as the fundamental vibrational absorption of the ClO free radical.

## D.  ClO Infrared Spectrum

The ClO fundamental absorption frequency has been the subject of some interest since the discovery of the ultraviolet absorption spectrum of the free radical. The most recent analysis of the electronic fine structures done by O'Hare and Wahl in 1971 predicts a frequency of 975 $cm^{-1}$ for this vibration.[48]

Rochkind and Pimentel in 1966 did an _in situ_ photolysis of molecular $Cl_2O$ at 20°K, producing 8 absorption bands near 960 $cm^{-1}$ and a quartet near 375 $cm^{-1}$. They attributed two of these absorptions at 945 and 982 $cm^{-1}$ to a ClO dimer $(ClO)_2$. From this they speculated

that the ClO absorption is probably near 970 ± 20 $cm^{-1}$.[38]

More recently, Andrews and Raymond report having observed the ClO radical in an argon matrix at 995 $cm^{-1}$. They reacted $Cl_2O$ with alkali metal atoms in a matrix to produce the free radical. They based their assignment upon their observation of the appropriate calculated oxygen isotopic shift in the 995 $cm^{-1}$ band, and on the fact that the 995 $cm^{-1}$ band has an appropriate chlorine isotopic counterpart.[49]

The isotopic rotational constants for the ClO radical have been reported by Carrington, Dyer and Levy.[50] Using these constants, the shape of the ClO band envelope can be calculated using the Honl-London formulas for the intensity of the rotational lines in the P, Q, and R branches of a diatomic molecule.[51] Figure (32) shows the calculated ClO band envelope with the Q branch centered at 950 $cm^{-1}$ overlaid on the modulation absorption. This figure shows how it is not possible to accurately predict a Q branch location from the band envelope due to the severe overlap of the two absorptions. Unfortunately, it is not possible to do a separation of these two bands utilizing the phase shifts since the 937 $cm^{-1}$ absorption is so much more intense than the side band.

The side band appears to have its maximum between 955 and 975 $cm^{-1}$ which would place the maximum of the R branch in this area. The separation between the Q branch and the maximum of the R branch predicted by the Honl-London calculation is about 15 $cm^{-1}$. This would place the center of the ClO band at about 950 $cm^{-1}$ ± 15 $cm^{-1}$
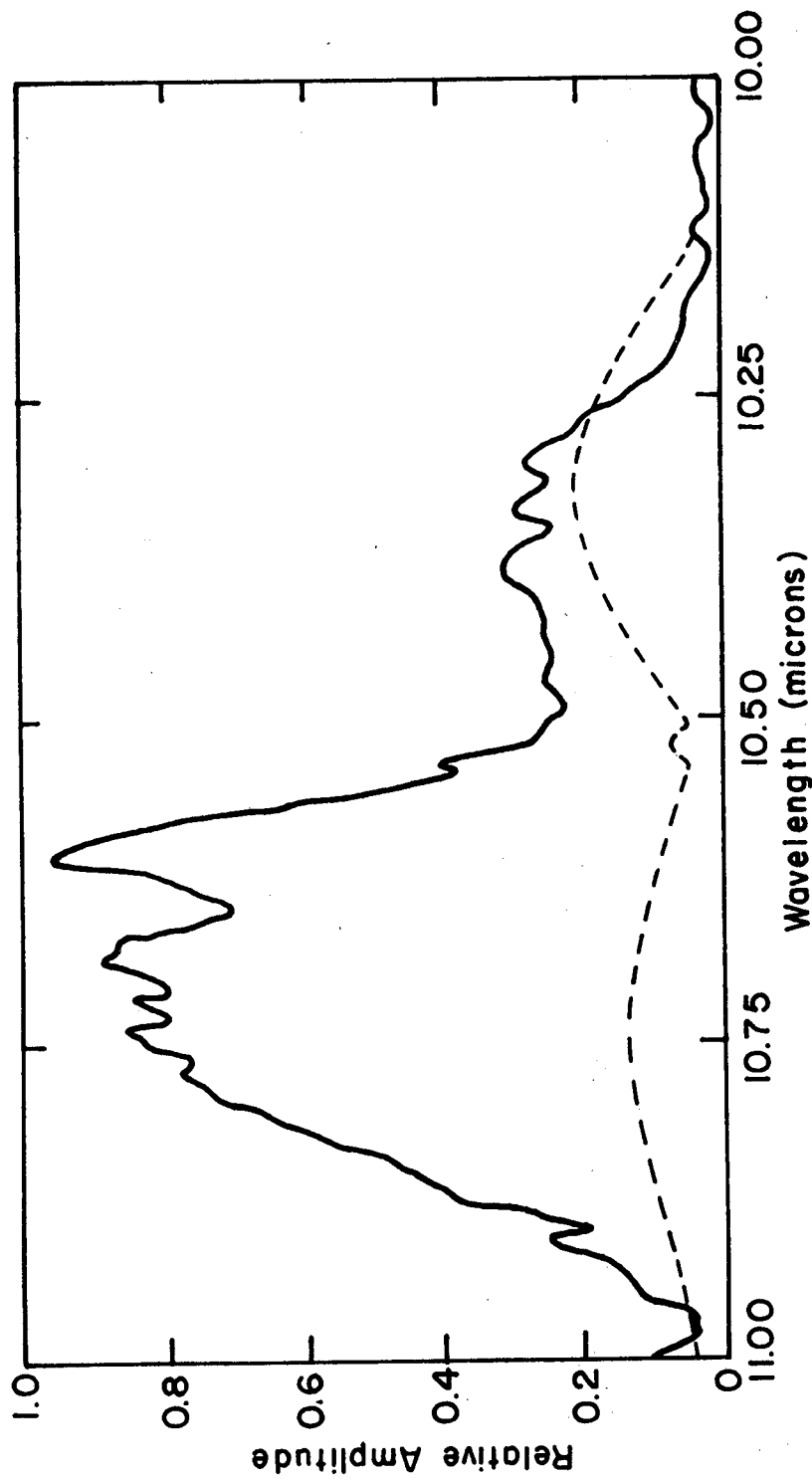
XBL728-6867

Fig. 32. Predicted infrared absorption spectrum of ClO for an assumed band center at 950 cm$^{-1}$ overlayed on the measured spectrum of the two free radical absorption bands.

This assignment of $950 \pm 15$ $cm^{-1}$ to the ClO fundamental is 45 wave

numbers lower than the 995 $cm^{-1}$ value reported by Andrews and Raymond,

but it is in the area of the 945 and 982 $cm^{-1}$ doublet observed by

Pimentel and Rochkind for the $(ClO)_2$ dimer. The normal matrix shift for

a vibrational frequency is about $\pm$ 10 $cm^{-1}$.[52]

The infrared band at 970 $cm^{-1}$ is definitely an intermediate radical

species in the $Cl_2 + O_2 + CO + h\nu$ system, and it shows very similar

kinetic behavior to that displayed by the ClO free radical, as monitored

in the ultraviolet. Aside from this, it would be difficult to postulate

another free radical in this system with only one strong infrared

absorption. Therefore, the 970 $cm^{-1}$ absorption has been identified as

the R branch of the ClO fundamental. This predicts the Q branch to be

centered at $950 \pm 15$ $cm^{-1}$, on the basis of the band envelope calcula-

tions.

### E. Unknown Radical Spectrum

The remaining four modulation absorptions have also been linked

together by their kinetic behavior. The observation that the unknown

radical species has a smaller phase shift at the lower flashing fre-

quencies indicates that it is a faster forming radical than ClO. Since

the appearance of this unknown free radical is accompanied by a marked

increase in the ClO absorption and the production of $CO_2$, it is

possible that this free radical is a precursor of both ClO and $CO_2$.

The absorption bands at 1835 $cm^{-1}$ and 1905 $cm^{-1}$ indicate that the

radical contains at least one, and perhaps two strong carbonyl bonds.

These absorptions are characteristic of a carbonyl group with partial triple bonding, such as in ClCO, where the extra electron is localized around the oxygen atom.

The ClCO radical is one possible explanation for these absorptions. It is present in the $Cl_2$ + CO + $h\nu$ system, and does contain a strong carbonyl bond. The ClCO vibrational fundamentals have been observed in a matrix at 14°K by Jacox and Milligan.[36] The reported fundamental vibrational absorptions are at 281, 570, and 1880 $cm^{-1}$. This radical does not account for all the infrared absorptions observed, and it is not likely to be present in large enough concentrations to have produced these absorptions.

Another more likely possibility for the unknown absorber's identity is the intermediate free radical $ClCO_3$ postulated by Brenschede.[35] Brenschede predicted the existence of such a free radical to explain the temperature dependence of the $CO_2$ production. This intermediate could be formed by either:

$$ClOO + CO + M \rightleftharpoons ClCO_3 + M \qquad (82)$$

or

$$ClCO + O_2 + M \rightleftharpoons ClCO_3 + M \qquad (83)$$
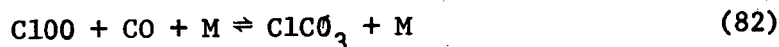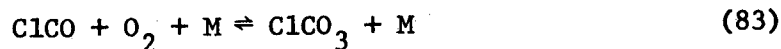
The decay reaction $ClCO_3 + M \rightarrow ClO + CO_2$, would explain the phase shift of the unknown absorber being smaller than that of ClO over most of the flashing frequency range. More definite confirmation of this radical's identity as the major precursor to ClO comes from the low quantum yield limiting behavior of its phase shift.

As noted in the qualitative spectroscopic observations, the unknown radical approaches a limiting phase shift at a $CO_2$ quantum yield of two. This type of behavior is characteristic of one type of chain reaction intermediate, as shown in the example below:

| Model 3 | Rate Constants |
|---------|----------------|
| (a) $A + h\nu \rightarrow 2X$ | $\alpha I$ |
| (b) $X + B + M \xrightarrow{\text{fast}} Y + M$ | $k_b$ |
| (c) $Y + M \rightarrow Z + P$ | $k_c$ |
| (d) $Z + B \rightarrow X + P$ | $k_d$  Propagation step |
| (e) $Z + Z + M \rightarrow P_2 + M$ | $k_e$  Termination step |

In this model, A and B are reactants; X, Y and Z are free radical intermediates; P is the major chain product; and M is the third body molecule.

Consider reaction (b) to be fast, so that the chain carrier X can be considered to be in a steady state. The production rate of product P in a steady state modulation flow system is given by:

$$\frac{d[P]}{dt} = \frac{-d[B]}{dt} = \frac{-(\text{flow rate})([A] \text{ in} -[A]\text{out})}{(\text{volume of cell})} + k_b[X][B][M]$$

$$+ k_d[Z][B] = 0 \tag{84}$$

This reduces to:

$$\frac{F(\Delta[A])}{V} = k_b[X][B][M] + k_d[Z][B] \tag{85}$$

The quantum yield is defined by:

$$\phi_P = \frac{k_c[Y][M] + k_d[Z][B]}{\alpha I[A]} \tag{86}$$

The radical X can be considered to be considered to be in a steady state.

$$[X]^* = \frac{2\alpha I[A] + k_d[Z][B]}{k_b[B][M]} \tag{87}$$

Under the conditions of a flow experiment, all the radicals will be in their steady state concentrations. This gives:

$$[Y]_{ss}^* = \frac{k_b[X][B][M]}{k_c[M]} = \frac{2\alpha I[A] + k_d[Z][B]}{k_c[M]} \tag{88}$$

$$[Z]_{ss}^* = \frac{k_c[Y][M]}{k_d[B] + k_e[Z][M]} \tag{89}$$

Substituting into Eqs. (85) and (86) gives:

$$\frac{f(\Delta[A])}{V} = 2(\alpha I[A] + k_d[Z][B]) \tag{90}$$

and

$$\phi_P = \frac{2(\alpha I[A] + k_d[Z][B])}{\alpha I[A]} \tag{91}$$

---

*Radical flow out terms are small and have been omitted for simplicity.

Under these conditions, the larger the term $k_d[Z][B]$ becomes, the larger the quantum yield of P. The modulation behavior of the free radicals Y and Z will be controlled by the ratio of the chain propagation rate to the chain termination rate:

$$\frac{k_d[Z][B]}{k_e[Z]^2[M]}$$

If the propagation rate is greater than the termination rate, the quantum yield will be high; and both radicals will display very similar phase behavior, since they will both be controlled by the same decay reaction. The phase shift of radical Y will be smaller than that of radical Z, since Y is the precursor; but both radicals will exhibit second order radical decay behavior.

When reactant B is decreased to the extent that the termination rate is much greater than the propagation rate, the form of the mechanism changes. In this low quantum yield limit, the equation describing the reactions will be: In the limit B → 0

$$[X]_{ss} = \frac{2\alpha I[A]}{k_b[B][M]} \qquad [Y]_{ss} = \frac{2\alpha I[A]}{k_c[M]} \qquad (92)$$

$$\frac{d[Y]}{dt} = 2\alpha I[A] - k_c[Y][M] \qquad (93)$$

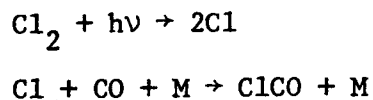$$\frac{d[Z]}{dt} = k_c[Y][M] - k_e[Z]^2[M] \qquad (94)$$

$$\frac{d[P]}{dt} = k_c[Y][M] = 2\alpha I[A] \qquad (95)$$

$$\lim_{B \to 0} \emptyset_p = 2$$

In this limit, the phase shift behavior of radical Y will be characteristic of first order radical decay. Its phase shift at any given flashing frequency will decrease with the quantum yield to a limiting phase shift at the limit $\emptyset_p = 2$. The radical Z will have its phase shift increasing as $\emptyset_p$ drops, since it will start to exhibit the modulation behavior of a second generation radical whose phase shift will vary from 0 to $-180°$ with flashing frequency. This behavior is identical to that displayed by the two radical species observed by molecular modulation in this work. Fitting Model 3 to the $Cl_2 + O_2 + CO$ system gives:

$$A = Cl_2 \qquad\qquad X = ClCO$$
$$B = CO \qquad\qquad Y = ClCO_3$$
$$Z = ClO$$

Of course, provision must be made for the ClCO and ClOO free radicals by slightly modifying Model 3. The exact algebraic manipulation showing how Model 3 fits the $Cl_2 + O_2 + CO$ system will be taken up in the next section on kinetic results, but the major reactions are the following:

$$Cl_2 + h\nu \to 2Cl$$
$$Cl + CO + M \to ClCO + M$$

$$\text{ClCO} + \text{O}_2 + \text{M} \rightarrow \text{ClCO}_3 + \text{M}$$

$$\text{ClCO}_3 + \text{M} \rightarrow \text{ClO} + \text{CO}_2 + \text{M}$$

$$\text{ClO} + \text{CO} \rightarrow \text{Cl} + \text{CO}_2$$

$$\text{ClO} + \text{ClO} + \text{M} \rightarrow 2\text{Cl}_2 + \text{O}_2$$
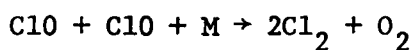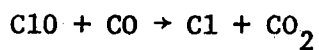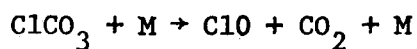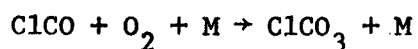
Since the ClCO radical is quickly destroyed by reaction with oxygen, it is always in a steady state. This series will reduce quite nicely to the form of Model 3.

This kinetic evidence confirms that the unknown radical absorption is the precursor to ClO, and indicates that its chemical composition is $\text{ClCO}_3$.

It is possible to speculate about the structure of this free radical from its absorption spectra. The 1835 and 1905 $\text{cm}^{-1}$ peaks indicate a species with two strong carbonyl bonds, or perhaps two isomeric forms of a species with one strong carbonyl bond. The 937 $\text{cm}^{-1}$ absorption would indicate a bond like that in the ClO radical. Several structures are possible:
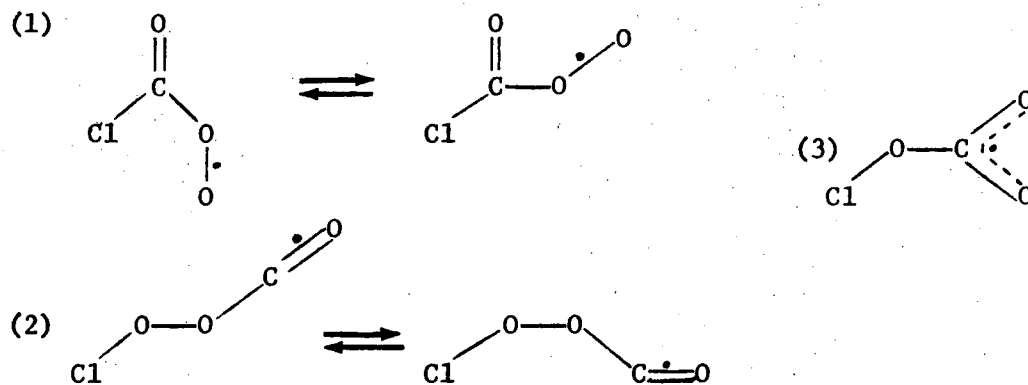
Structure (1) is a possible structure forming from the direct combination of ClCO + $O_2$. The nonbonded electron would probably be localized around the peroxide bond. An analog to this structure would be phosgene:

$$\begin{array}{c} O \\ \| \\ C \\ \diagup \quad \diagdown \\ Cl \qquad Cl \end{array}$$
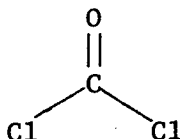
The carbonyl bond vibration in phosgene occurs at 1827 $cm^{-1}$, and has a strong force constant for the carbonyl stretching vibration. It is likely that the force constant for the carbonyl stretch in structure (1) would be similar to that for phosgene. Two carbonyl stretches for this form would require two isomeric forms, perhaps caused by a hindered rotation of the peroxy group about the C——O bond.

Structure (2) is another peroxy form presumably formed from the reaction ClOO + CO + M → ClOOCO + M, or from a structural rearrangement during collision of ClCO and $O_2$. It would also have to exist in two isomeric forms to produce the two carbonyl peaks.

Structure (3) could arise from internal rearrangement of either structure (1) or (2). By having two carbonyl groups in a resonance structure, it is possible that this form could produce two strong carbonyl absorptions.

Any of these three forms could conceivably produce the infrared absorptions observed, as well as decompose to form $CO_2$ and ClO.

Trying to judge between any of the structures is guess work at best, but (3) appears to have a more realistic chance of having two distinct carbonyl stretches with a high force constant. One other

possibility for the source of the two peaks in the carbonyl region

could be Fermi resonance between one carbonyl absorption and the first

overtone of the strong 937 cm$^{-1}$ band. This would produce two bands of

approximately equal intensity similar to those observed. This argu-

ment of course cannot be carried further without complete knowledge

of the symmetry of the vibrational modes of the free radical.

## IV. KINETIC RESULTS

### A. $Cl_2$ Dissociation Rate

The first quantitative experiments carried out were calibration runs to determine the first order photolytic decay rate constant for the chlorine. The value for this rate constant was determined in both reaction cells by measuring the initial decay rate of nitrogen dioxide. This was then related to the chlorine decay rate through the published absorption spectra and quantum yields for these two species. The photolysis of $NO_2$ was treated in detail in Part I of this paper; and as was shown, the initial slope of the photolytic decay is given by:

$$\underset{t \to 0}{\text{Limit}} \quad \frac{d[NO_2]}{dt} = 2k_2 \alpha_{NO_2} I[NO_2]/(k_2 + k_3[M])$$

or

$$\ln([NO_2]/[NO_2]_i) = 2k_2 \alpha_{NO_2} It/(k_2 + k_3[M])$$

(96)

By measuring this first order initial decay rate, a value can be obtained for $2k_2 \alpha_{NO_2} I/(k_2 + k_3[M])$. In Part I an experimental value was measured for $k_3[M]/k_2$, which allows a determination of $\alpha_{NO_2} I$ from the $NO_2$ decay.

If the concentrations of the light absorbing reactants are maintained at a low enough level such that there is a uniform distribution of light throughout the cell, there will be very little change in the light intensity as the absorbers decay. In this case the light intensity in the Beer's Law expression will be a constant over the

whole decay curve. Therefore, $\alpha_{NO_2}$ can be expressed as a wavelength averaged product of the photolysis light output spectrum, the $NO_2$ absorption coefficient, and the $NO_2$ quantum yield for dissociation. This is expressed below:

$$\alpha_{NO_2} = \int (\sigma_{NO_2})_\lambda P_\lambda (Q_{NO_2})_\lambda d\lambda \qquad (97)$$

with $(\sigma_{NO_2})_\lambda$ = The $NO_2$ absorption coefficient at wavelength $\lambda$.

$P_\lambda$ = The fraction of the total photon flux at wavelength $\lambda$.

$(Q_{NO_2})_\lambda$ = The quantum yield for $NO_2$ dissociation at wavelength $\lambda$.

This same wavelength averaged product can be expressed for $\alpha_{Cl_2}$.

$$\alpha_{Cl_2} = \int (\sigma_{Cl_2})_\lambda P_\lambda d\lambda \qquad (98)$$

$Q_{Cl_2}$ is equal to 1 at all wavelengths where $Cl_2$ absorbs in this region of the spectrum, since it is a simple molecule with a straight forward decay mechanism.

Once $(\alpha_{NO_2} I)$ has been measured, $(\alpha_{Cl_2} I)$ can be calculated from these two equations by taking a ratio.

$$\alpha_{Cl_2} I = \int (\sigma_{Cl_2})_\lambda P_\lambda d\lambda \; \frac{\alpha_{NO_2} I}{\int (\sigma_{NO_2})_\lambda P_\lambda (Q_{NO_2})_\lambda d\lambda} \qquad (99)$$

These integrals can be approximated by using summations of the products over 10 nm intervals. The values for $P_\lambda$ can be taken from the manufacturer's output spectrum for the black lamps shown in Fig. (3b). The values of $Q_{NO_2}$ are taken from the literature and are shown in Fig. (2). The absorption coefficients for $Cl_2$ and $NO_2$ are also from the literature and are shown in Figs. (16) and (2) respectively.

The calculation of $\alpha_{NO_2}$ was done in Part I of this paper with the result of $\alpha_{NO_2} = 5.41 \times 10^{-19}$ cm$^2$. The data for this calculation was given in Table (10). The data for the calculation of $\alpha_{Cl_2}$ is given in Table (15),[53] and the calculated value is $\alpha_{Cl_2} = 0.935 \times 10^{-19}$ cm$^2$. Therefore the experimental value for the first order decay rate constant for chlorine is given by:

$$\alpha_{Cl_2} = \alpha_{NO_2} \times 0.173$$

The experimentally determined values for the $NO_2$ decay slopes in the two reaction cells are given below.

Ultraviolet Cell:

measured $\alpha_{NO_2} I = 1.02 \times 10^{-2}$ sec$^{-1}$

calculated $\alpha_{Cl_2} I = 1.77 \times 10^{-3}$ sec$^{-1}$

Infrared Cell:

For 2 flashing lamps: $(\alpha_{NO_2})_2 I = 0.46 \times 10^{-2}$ sec$^{-1}$

$(\alpha_{Cl_2})_2 I = 0.796 \times 10^{-3}$ sec$^{-1}$

For 4 flashing lamps: $(\alpha_{NO_2})_4 I = 0.83 \times 10^{-2}$ sec$^{-1}$

$(\alpha_{Cl_2})_4 I = 1.43 \times 10^{-3}$ sec$^{-1}$

Table 15.  Calculation of average $Cl_2$ photolytic rate constant.

| Spectral Range | $\dfrac{\text{Photons}}{\text{sec-100A}} \times 10^{-18}$ | Mean $p_\lambda$ | Mean $\sigma_\lambda$ (1./mole-cm) | $p_\lambda \sigma_\lambda$ |
|---|---|---|---|---|
| 2700-2800Å | 0.015 | .00065 | 4.6 | .0040 |
| 2800-2900 | 0.045 | .00190 | 11.8 | .0224 |
| 2900-3000 | 0.095 | .00405 | 24.0 | .0972 |
| 3000-3100 | 0.185 | .00785 | 38.8 | .3045 |
| 3100-3200 | 0.460 | .0196 | 55.3 | 1.083 |
| 3200-3300 | 0.750 | .0319 | 65.2 | 2.080 |
| 3300-3400 | 1.360 | .0578 | 65.2 | 3.770 |
| 3400-3500 | 1.930 | .0820 | 56.0 | 4.590 |
| 3500-3600 | 2.395 | .1018 | 42.2 | 4.300 |
| 3600-3700 | 2.940 | .1250 | 27.8 | 3.475 |
| 3700-3800 | 2.700 | .1149 | 17.3 | 1.990 |
| 3800-3900 | 2.405 | .1023 | 10.5 | 1.075 |
| 3900-4000 | 1.990 | .0846 | 6.7 | 0.567 |
| 4000-4100 | 2.000 | .0850 | 4.3 | 0.3655 |
| 4100-4200 | 1.075 | .0457 | 3.0 | 0.1371 |
| 4200-4300 | 0.720 | .0306 | 2.2 | 0.0673 |
| 4300-4400 | 1.793 | .0763 | 1.6 | 0.1220 |
| 4400-4500 | 0.280 | <u>.0119</u> | 1.1 | <u>0.0131</u> |
| 4500-4600 | 0.175 | $\Sigma$=.9836 | | $\Sigma$=24.063 |
| 4600-4700 | 0.105 | | | 1./mole-cm (base 10) |
| 4700-4800 | 0.060 | | | |
| 4800-4900 | 0.035 | | | |
| 4900-5000 | <u>0.010</u> | | | |

$\Sigma$=23.523×10$^{18}$ photons/sec

Therefore,

$$(\alpha_\varepsilon)_{Cl_2} = \frac{\Sigma\, p_\lambda\, \sigma_\lambda}{\Sigma\, p_\lambda} = \frac{(24.063)(2.303)}{(0.9836)(6.023 \times 10^{20})}$$

$$= 0.935 \times 10^{-19}\ cm^2$$

## B. Proposed Mechanism

On the basis of the work by Brenschede, Johnston et al., and the observations stated in the preceding sections, the following mechanism is proposed for the chlorine sensitized formation of $CO_2$:

(1') $Cl_2 + h\nu \rightarrow 2Cl$

(2') $Cl + O_2 + M \rightleftharpoons ClOO + M$

(3') $Cl + CO + M \rightleftharpoons ClCO + M$

(4') $ClOO + Cl \rightleftharpoons 2ClO$

(5') $ClOO + Cl \rightarrow Cl_2 + O_2$

(6') $ClCO + Cl_2 \rightarrow Cl_2CO + Cl$

(7') $ClCO + Cl \rightarrow CO + CO + Cl_2$

(8') $ClO + ClO + M \rightleftharpoons Cl_2O_2 + M \rightarrow Cl_2 + O_2 + M$

(9') (a) $ClCO + O_2 + M \rightleftharpoons ClCO_3 + M$

or

(b) $ClOO + CO + M \rightleftharpoons ClCO_3 + M$

(10') $ClCO_3 + M \rightarrow ClO + CO_2 + M$

(11') $ClO + CO \rightarrow Cl + CO_2$

(12') $Cl + Cl + M \rightarrow Cl_2 + M$
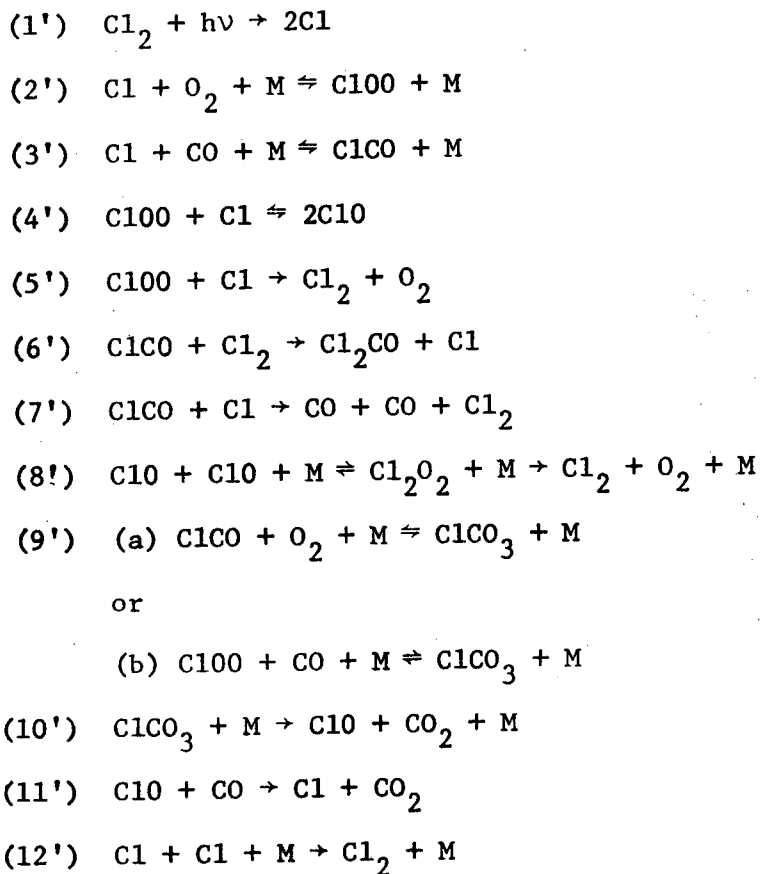
Most of this reaction scheme is a combination of the mechanism for the formation of phosgene derived by Bodenstein,[32] and the mechanism used by Johnston, Morris and Van den Bogaerde[39] to explain their studies of the $Cl_2 + O_2$ photolytic system. Reactions (9'), (10') and (11') are proposed from the observations in this work indicating the role of the new free radical species discovered by molecular modulation spectroscopy.

### 1. $Cl_2$ + CO + h$\nu$ System

The reactions dealing with the formation of phosgene from the ClCO free radical have been thoroughly studied, and it is generally agreed that they explain all the qualitative aspects of the phosgene forming chain reaction. The major rate constants for this system were reported in 1952 by Burns and Dainton.[54] Another measurement of some of these same rate constants was performed by Clark, Clyne and Stedman in 1966.[55] The results of these two investigations are shown in Table 16. As the table shows, there is considerable disagreement over the value of the equilibrium constant for the ClCO radical formation. The value of $K_{ClCO}$ reported by Burns and Dainton comes from kinetic measurements on the $Cl_2$ + CO + h$\nu$ system, using the rotating sector method. The $K_{ClCO}$ reported by Clark, Clyne and Stedman is based upon the thermodynamic properties of ClCO deduced by several investigations. They used Jacox and Milligan's[36] calculated value of the absolute entropy of ClCO, $S^{\circ}_{298}$ = 63.49 cal/deg mole, which leads to a value of $\Delta S^{\circ}_{298}$ = -23.2 cal/deg mole for reaction (3'). The consensus of a number of investigations[54,55,56] is that $\Delta H^{\circ}_{298}$ for reaction (3') is approximately -6.5 kcal/mole. From this, Clark et al. calculated their value of:

$$K_{eq_{ClCO}} = \frac{k_{3'}}{k_{-3'}} = \exp\frac{-\Delta S^{\circ}}{k} \exp\frac{\Delta H^{\circ}}{RT}$$

$$= 2.1 \times 10^{-20} cm^3/molecule \text{ at } 298°$$

Table 16. Literature values for the rate constants in the $Cl_2 + CO + h\nu$ reaction system.

| Rate Constant | Value $(cc^x/molecules^x\text{-sec})$ | T °K | Reference |
|---|---|---|---|
| $k_{3'}$ | $9.1 \times 10^{-34}$ | 300 | Clark et al. (55) |
| $k_{6'}$ | $2.74 \times 10^{-14}$ | 298 | Burns & Dainton (54) |
| $k_{7'}$ | $1.62 \times 10^{-10}$ | 298 | Burns & Dainton (54) |
| $K_{ClCO}$ | $1.1 \times 10^{-19}$ | 298 | Burns & Dainton (54) |
| $K_{ClCO}$ | $2.1 \times 10^{-20}$ | 300 | Calculated from thermodynamic values by Clark et al. (55) |
| $\dfrac{k_{-3'}}{k_{3'}k_{7'}}$ | $6.5 \times 10^{30}$ | 300 | Clark et al. (55) |

Though there is this quantitative disagreement over the rates of reaction (3'), (6') and (7'), all the investigations agree that the reactions do describe the kinetic behavior of the phosgene production system.

## 2. $Cl_2 + O_2 + h\nu$ System

The reactions concerning the $Cl_2 + O_2 + h\nu$ system have been the subject of several investigations in the last few years.[57,39,58] Table (17) shows a summary of the rate constants reported for these reactions. The major controversy between the investigators is over the mechanism and rate constant of the ClO decay. Johnston et al. investigated the $Cl_2 + O_2 + h\nu$ system through molecular modulation techniques, and observed a M gas dependence in the ClO decay. They attributed this to reaction (8').

(8')  $ClO + ClO + M \rightleftharpoons Cl_2O_2 + M \rightarrow Cl_2 + O_2 + M$
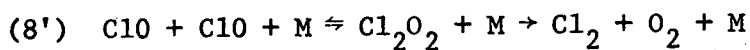
A recent flash photolysis study by Basco and Dogra[57] reports observing no M gas dependence in the ClO second order recombination reaction, and they report a lower value for the recombination rate constant than Johnston et al. The only major experimental difference between these investigations was the order of magnitude of the photolytic light intensity. Johnston et al. had a photolytic light intensity of approximately $10^{16}$ photons/$cm^2$-sec, while that used in most of the flash photolysis experiments was on the order of $10^{20}$ to $10^{21}$ photons/$cm^2$-sec. In order to account for the disagreement between these reports of the mechanism for the ClO decay, it would be necessary to postulate a light dependency in the ClO decay.

Table 17. Summary of the literature rate constants for the $Cl_2 + O_2 + h\nu$ system.

| Rate Constant | Value ($cc^x$/molecules$^x$-sec) | T °K | Reference |
|---|---|---|---|
| $k_{C100}$ | $3.62 \times 10^{-21}$ | 298 | Calculated by Johnston et al. from thermodynamic arguments (39) |
| $k_{2'}$ | $1.7 \times 10^{-33}$ | | Nichols & Norrish (59) |
| $k_{-4'}$ | $2.2 \times 10^{-14}$ | | Clyne & Coxon (58) |
| $k_{8'}$ | $2.2 \times 10^{-14}$ | | Basco & Dogra (57) |
| $K_{C100}(k_{5'}+k_{4'})$ | $5.4 \times 10^{-31}$ | | Porter & Wright (40) |
| $k_{4'}$ | $1.44 \times 10^{-12}$ | | Johnston et al. (39) |
| $k_{5'}$ | $1.56 \times 10^{-10}$ | | (39) |
| $k_{8'}$ | $5. \times 10^{-32}$ (in $O_2$) | | (39) |
| $k_{12'}$ | $1.17 \times 10^{-32}$ (in Ar) | | (39) |

The experiments in this work were carried out under the same conditions as those used by Johnston et al., and several of their experiments were repeated during this investigation. The results of the experiments done on the $Cl_2 + O_2$ system in this work agree with those of Johnston et al.: that the empirical rate constant for ClO decay at one atmosphere and 298°K is k = 1.23 × 10$^{-12}$cm/particle-sec. The issue of whether the rate constant is M gas dependent cannot be determined from this work.

C. Determination of Experimental Rate Law for the $Cl_2 + O_2 + CO$ System

A series of experiments was carried out to determine the rate law for production of $CO_2$ under the conditions of approximately one atmosphere of oxygen, 15 mm/Hg of carbon monoxide, and .5 mm/Hg of $Cl_2$. These conditions were selected to optimize the ability to monitor the free radical intermediates by modulation spectroscopy.

In these experiments, the initial slope of the carbon monoxide decay was monitored during static cell D.C. photolysis runs for a wide variety of initial conditions. Figure (33) shows a graph of the initial CO decay slope as a function of the square root of the initial chlorine concentration. The good linear plot indicates a half power dependence on chlorine dissociation for the $CO_2$ production.

Another set of photolysis experiments was carried out holding the initial $Cl_2$ and CO concentrations constant, and varying the amount of $O_2$ in the cell. In these experiments, the balance of the pressure was made up to one atmosphere with $N_2$. The results of these experiments are shown in Table (18). The initial slope showed no significant
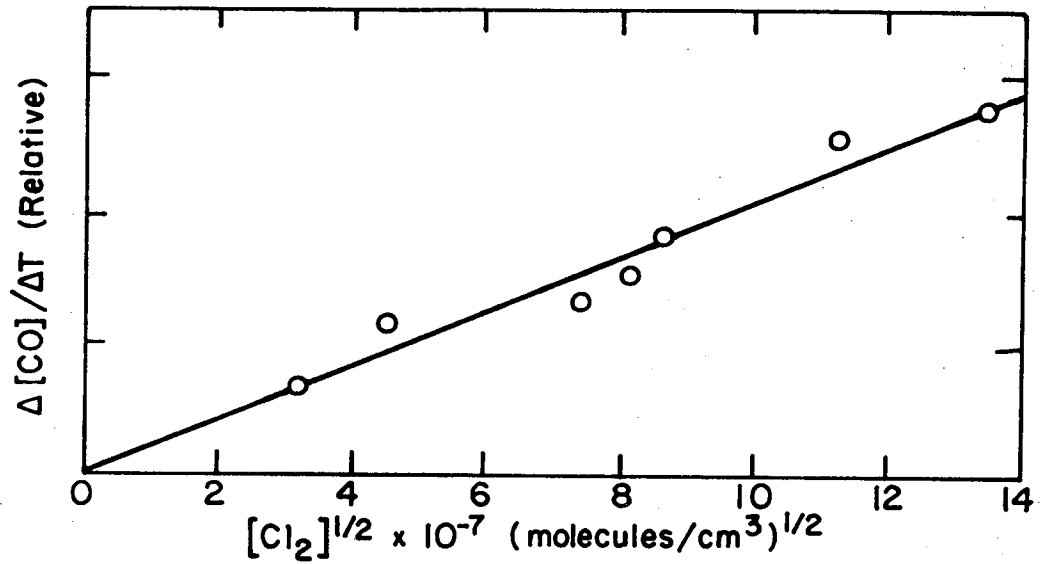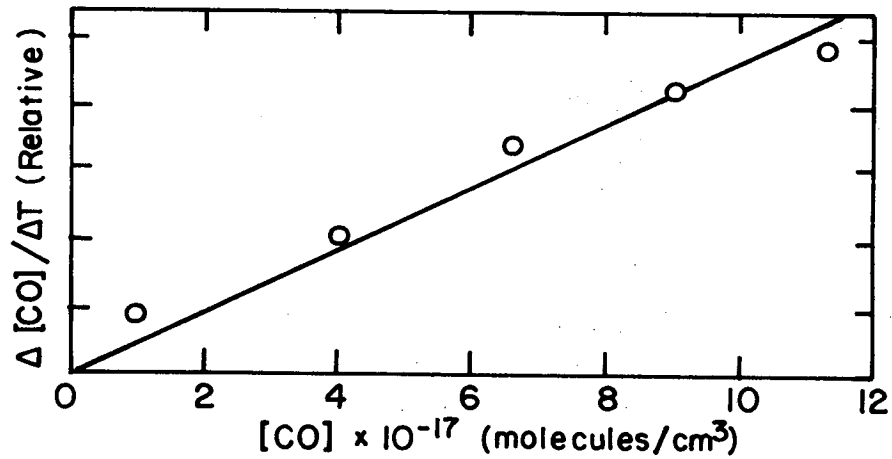
Fig. 33. Graph of the relative initial decay rate of carbon monoxide as a function of the square root of the chlorine concentration. The initial $[CO] = 5.9 \times 10^{17}$ molecules/cm$^3$ $[O_2] \approx 1$ atm.



XBL 728-6868

Fig. 34. Graph of the relative initial decay rate of CO as a function of the initial carbon monoxide concentration. $[Cl_2] = 2.6 \times 10^{16}$ molecules/cm$^3$ $[O_2] \approx 1$ atm.

Table 18.  Results of the experiments measuring the dependence of the

$CO_2$ production rate on initial oxygen concentration.

Initial Conditions:  $[Cl_2] = 6.0 \times 10^{15}$ molecules/cm$^3$

$[CO] = 5.5 \times 10^{16}$ molecules/cm$^3$

Case 1   $[O_2] = 2.45 \times 10^{19}$ molecules/cm$^3$

Relative   $\Delta[CO]/\Delta T = 0.26 \pm .04$

Case 2   $[O_2] = 1.2 \times 10^{19}$ molecules/cm$^3$

$[N_2] = 1.2 \times 10^{19}$ molecules/cm$^3$

Relative   $\Delta[CO]/\Delta T = 0.23 \pm .04$

Case 3   $[O_2] = 0.75 \times 10^{19}$ molecules/cm$^3$

$[N_2] = 1.7 \times 10^{19}$ molecules/cm$^3$

Relative   $\Delta[CO]/\Delta T = 0.21 \pm .03$

change down to 250 mm of Hg pressure of oxygen. This shows that the production of $CO_2$ is independent of oxygen concentration over the full range of experimental conditions used in this study.

A third series of initial slope experiments was performed to monitor the effect of changing the carbon monoxide concentration. Figure (34) shows the results of these experiments. Over the range [CO] = 0 to [CO] = 38 mm of Hg, the production of $CO_2$ is approximately first order in carbon monoxide for the conditions: $O_2$ = 1 atm. and $Cl_2$ = 2. × $10^{15}$ molecules/$cm^3$. This gives an experimental rate law of:

$$\frac{d[CO_2]}{dt} = K(I[Cl_2])^{1/2}[CO] \tag{100}$$

for the conditions used in these experiments. This contrasts with the half power dependency for CO found by the investigators in the 1920's and 1930's for their experiments at one atmosphere; but in their work they normally used carbon monoxide pressure of up to 1/2 atmosphere. This point will be examined later.

This rate law can be related to the mechanism proposed at the start of this section. In the derivation of the rate law, reaction (9') will be taken as proceeding by $ClCO + O_2 + M \rightarrow ClCO_3 + M$. Rollefson's work in 1933 showed that the ratio of phosgene production to $CO_2$ production depends only on the ratio $[Cl_2]/[O_2]$.[34] This independence from the CO concentration indicates that the same precursor leads to $CO_2$ and $Cl_2CO$. This supports ClCO as the precursor to $ClCO_3$ and favors reaction (9'a). To confirm this would require the ability to detect ClCO or CLOO spectroscopically, but under the conditions of

these experiments the $ClOO$ and $ClCO$ absorptions were too weak to detect.

Using the proposed mechanism, the formation rate of $CO_2$ is given by:

$$\frac{d[CO_2]}{dt} = k_{10'}[ClCO_3][M] + k_{11'}[ClO][CO] \tag{101}$$

If reaction $(-9')$ can be taken as negligible at room temperature as suggested by Brenschede[35] then the steady state radical concentrations are given by:

$$[ClCO_3]_{ss} = \frac{k_{9'}}{k_{10'}}[ClCO][O_2] \tag{102}$$

$$[ClO]_{ss} = \frac{k_{10'}[ClCO_3][M] + 2k_{4'}[ClOO][Cl]}{k_{11'}[CO] + 2(k_{-4'} + k_{8'}[M])[ClO]}$$

When carbon monoxide is added to the system, the $ClO$ concentration is enhanced by approximately a factor of ten, under the conditions used in this work. This indicates that $k_{10'}[ClCO_3][M] \geqslant 10(2k_{4'}[ClOO][Cl])$. In the case of a large quantum yield, the propagation step will dominate over termination so $k_{11'}[CO]$ will be considerably greater than $(2(k_{4'} + k_{8'}[M])[ClO])$. This leads to the approximation:

$$[ClO]_{ss} = \frac{k_{10'}[ClCO_3][M]}{k_{11'}[CO]} = \frac{k_{9'}[ClCO][O_2][M]}{k_{11'}[CO]} \tag{103}$$

Then, substituting these steady state assumptions into the equation for $CO_2$ production gives:

$$\frac{d[CO_2]}{dt} \text{ (steady state)} = 2k_9,[ClCO][O_2][M] \tag{104}$$

Further reduction of this equation requires a knowledge of which termination step predominates at one atmosphere pressure. The major termination reaction can be found by comparing the magnitude of the termination reactions using literature rate constants and approximate radical concentrations for a given set of conditions. When $[O_2]$ = $2.4 \times 10^{19}$, $[CO] = 5.0 \times 10^{17}$, and $[Cl_2] = 5.0 \times 10^{15}$ (molecules/$cm^3$), the approximate $ClO$ steady state concentration is $2.4 \times 10^{12}$ molecules/$cm^3$, as determined from its ultraviolet absorption spectrum. Under these same conditions the quantum yield is 452. The $ClOO$ concentration can be approximated from its infrared absorption band. The $1443 cm^{-1}$ absorption of $ClOO$ was monitored for a long period of time, and no signal was observed under these reaction conditions. Since the maximum sensitivity of the infrared instrument in this region of the spectrum is $\Delta I/I = 1.6 \times 10^{-5}$, a maximum $ClOO$ concentration can be calculated using the absorption coefficient reported by Van den Bogaerde.[27]

> If: $\Delta I/I = \alpha l[ClOO] \leq 1.6 \times 10^{-5}$
>
> with $l = 40$ meters
>
> $\alpha = 1.4 \times 10^{-19}$ $cm^2$/molecule
>
> Then: $[ClOO] \leq 2.8 \times 10^{10}$ molecules/$cm^3$

Assuming that the $ClOO$ will be in equilibrium, one can calculate the chlorine atom concentration using the value for $K_{ClOO}$ reported by Johnston et al.

$$[Cl] \leqslant \frac{[ClOO]}{K_{ClOO}[O_2]} = 3.0 \times 10^{11}$$

The [ClCO] concentration can be approximated by its equilibrium constant for formation, as reported by Burns and Dainton in Table (16).

$$[ClCO] = K_{eq}[Cl][CO] = 1.6 \times 10^{10}$$

Using these numbers and the rate constants in Table (16), the relative values of the four termination reactions can be evaluated at one atmosphere total pressure:

$$k_{8'}[ClO]^2[M] = 7.1 \times 10^{12} \quad \text{(particles/cm}^3\text{-sec)}$$

$$k_{5'}[ClOO][Cl] \leqslant 1.3 \times 10^{12}$$

$$k_{7'}[ClCO][Cl] \leqslant 0.8 \times 10^{12}$$

$$k_{12'}[Cl]^2[M] \leqslant 2.6 \times 10^{10}$$

These calculated rates show that for the reaction conditions used in this investigation, reaction (8') is the major termination step. Applying the long chain approximation, that the chain terminating rate equals the chain initiating rate at steady state, gives the following equation:

$$\alpha I[Cl_2] = k_{8'}[ClO]_{ss}^2[M], \quad \text{or} \quad [ClO]_{ss} = \left\{ \frac{\alpha I[Cl_2]}{k_{8'}[M]} \right\}^{1/2} \tag{105}$$

Substituting this relationship into Eq. (103) gives:

$$k_{9'}[ClCO][O_2][M] = k_{11'}[CO] \left\{ \frac{\alpha I[Cl_2]}{k_{8'}[M]} \right\}^{1/2} \tag{106}$$

Using this in Eq. (104), for the $CO_2$ production rate gives:

$$\frac{d[CO_2]}{dt} = 2k_{11'}[CO] \left\{ \frac{\alpha I[Cl_2]}{k_{8'}[M]} \right\}^{1/2} \qquad (107)$$

This is the form found for the experimental rate law in this investigation.

### D. Calculation of Rate Constant $k_{10'}$

The proposed mechanism meets the requirements set by the experimental rate law for these experiments, and it fully describes the kinetic behavior observed for the $ClO$ and $ClCO_3$ free radicals. Fulfilling these conditions then, the mechanism can be used to calculate the rate constants of reactions 10' and 11'.

In the limit of low quantum yield the mechanism shows that:

$$\frac{d[ClCO_3]}{dt} = k_{9'}[ClCO][O_2][M] - k_{10'}[M][ClCO_3] \qquad (108)$$

As shown previously, the $ClCO_3$ phase shift reaches a limiting value at $\phi_{CO_2} = 2$. If it is assumed that all chlorine atoms formed enter into the $CO_2$ producing chain, then a quantum yield of two says that each chlorine atom produces one $CO_2$ molecule. The factor of two is obtained from the fact that each chlorine molecule dissociating produces two chlorine atoms.

In order to have a quantum yield of two using the proposed mechanism, it is necessary that each $ClO$ radical formed from $ClCO_3$ be removed by

the termination step before it can react with CO to produce another carbon dioxide molecule. For this to occur the chain termination rate must be much greater than the chain propagation rate.

$$k_{11'}[ClO][CO] \ll k_{8'}[ClO]^2[M] \qquad (109)$$

In this limit the $ClCO_3$ decay behavior will be strictly first order in radical concentration, with its limiting phase shift defining its lifetime. The lifetime calculations and curves, showing the approach to a limiting phase shift with decreasing quantum yield, were shown in the spectroscopic results section. (Fig. 21a and Fig. 26) The results for the $ClCO_3$ lifetime were:

$$\tau_{220 \text{ nm.}} = 0.022 \pm .001 \text{ sec.}$$

$$(110)$$

$$\tau_{937 \text{ cm.}^{-1}} = 0.021 \pm .005 \text{ sec.}$$

For a radical decaying first order in radical concentration $\tau = 1/k_r[C]$. In this case $k_{10'} = k_r$, and $[C] = [M]$. Then using the 220 nm. value for the lifetime gives:

$$k_{10'} = 1.9 \pm .2 \times 10^{-18} \text{ cm}^3/\text{molecules-sec} \qquad (111)$$

E. Calculation of $k_{11'}$

The rate constant $k_{11'}$ can be calculated from the quantum yield of the $CO_2$ production. Since no phosgene formation is observed, this quantum yield for a steady state flow system with flashing photolysis lamps, can be defined as:

Fig. 35. Modulation amplitude versus 1/f behavior of the 265 nm. absorption at a quantum yield of 392. The 1/f values are shown on a logarithmic scale. The overlay is the theoretical curve for a second order decaying radical. These data are from experiment 2 in Table (19).
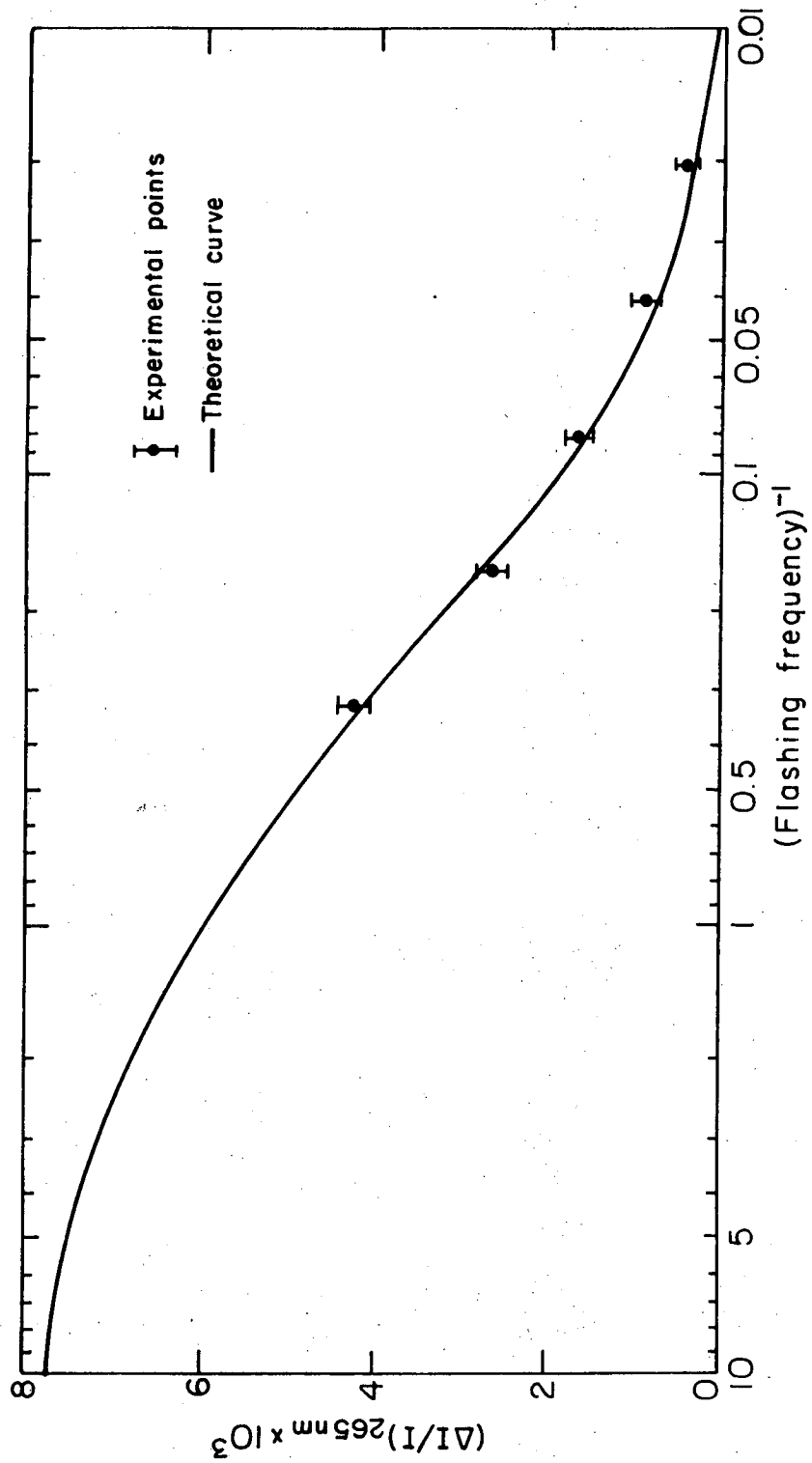
Fig. 35.

XBL 728-6869

$$\phi_{CO_2} = \frac{(\text{Flow Rate})([CO] \text{ in} - [CO] \text{ out})}{(\text{Cell Volume})(\alpha_{Cl_2} I_o [CL_2]/2)} \qquad (112)$$

The light intensity term is divided by two to account for the flashing

of the lamps, since this leaves the lamps on only half of the time. If

it is assumed that all the chlorine atoms formed from the initial

photolysis enter the $CO_2$ production chain reaction, then the quantum

yield is a ratio of the rate of chain propagation to the rate of chain

termination. This will be a quantative relationship if the quantum

yield is divided by 4, since every dissociating $Cl_2$ molecule produces

two chlorine atoms, and every chlorine atom that passes completely through

the chain produces two $CO_2$ molecules. This gives:

$$\phi_{CO_2}/4 = k_{11} \cdot [CO]_{ss}/(2k_8 \cdot [ClO]_{ss}[M]) \qquad (113)$$

The value of $[ClO]_{ss}$ can be approximated to about ± ten percent

from the modulation amplitude measurements and the literature value

for the ClO absorption coefficient. Clyne and Coxon report a value of

$\sigma(257.7 \text{ nm.}) = 4.83 \times 10^{-18} \text{ cm}^2/\text{particle},$[58] and the value used for

265 nm. will be based upon their number, with a correction for relative

absorption at the two wavelengths.

At high $CO_2$ quantum yields the ClO modulation behavior closely

resembles that of a second order decaying radical. This allows the

steady state ClO concentration to be approximated from the modulation

amplitude versus log 1/f curve. Figure (35) illustrates this for the

case of $\emptyset_{CO_2}$ = 648. The graph shows the modulation data superimposed on a theoretical curve for a second order decaying radical's modulation amplitude behavior.

The ClO concentration derived from this graph is a value for $[ClO]_{ss}$ at a light intensity of $I_o$. Since the flow steady state has a light intensity of $I_o/2$, due to the flashing lights, the modulation ClO concentration must be reduced. The correction factor is $1/(2)^{1/2}$ due to the radical's having a half power dependence upon the term $\alpha_{Cl_2} I[Cl_2]$. All the radicals in the system show this dependence under these conditions, due to the termination reaction being bi-radical.

The data used for the calculation of $k_{11'}$ is shown in Table (19). The only other value required for this calculation is $k_{8'}$. The value reported by Johnston et al. is used for this rate constant, since it was measured under the same experimental conditions as those used in this investigation.

The average value for $k_{11'}$ from these measurements is:

$$k_{11'} = 1.4 \pm .14 \times 10^{-15} \text{ cm}^3/\text{molecules-sec} \qquad (114)$$

### F. Absorption Coefficient for $ClCO_3$ in the Ultraviolet

Once $k_{10'}$ and $k_{11'}$ have been determined it is possible to calculate absorption coefficients for the $ClCO_3$ absorptions. As shown in Eq. (101), in the high quantum yield range, the $ClCO_3$ steady state concentration is given by: $[ClCO_3]_{ss} = \dfrac{k_{9'}}{k_{10'}} [ClCO][O_2]$

Table 19. Calculation of $k_{11}'$ from ultraviolet experiments

all concentrations (molecules/cm³)

| Exp. | [Cl₂] | [CO]$_{in}$ | [CO]$_{out}$ | F(Δ[CO])/vol. (molecules/cm³-sec) | φ$_{CO_2}$ | [ClO]$_{ss}$/√2 ±10% | $k_{11}'$ (cm³/molecules-sec) |
|---|---|---|---|---|---|---|---|
| 1 | $2.6 \times 10^{15}$ | $1.16 \times 10^{18}$ | $5.0 \times 10^{17}$ | $1.49 \times 10^{15}$ | 648 | $1.8 \times 10^{12}$ | $1.45 \times 10^{-15}$ |
| 2 | $4.7 \times 10^{15}$ | $1.16 \times 10^{18}$ | $4.4 \times 10^{17}$ | $1.63 \times 10^{15}$ | 392 | $2.5 \times 10^{12}$ | $1.38 \times 10^{-15}$ |
| 3 | $5 \times 10^{15}$ | $1.2 \times 10^{18}$ | $5 \times 10^{17}$ | $1.94 \times 10^{15}$ | 452 | $2.4 \times 10^{12}$ | $1.33 \times 10^{-15}$ |

ave. $= 1.4 \pm 0.14 \times 10^{-15}$

$$\phi_{CO_2} = \frac{F(\Delta[CO])/(volume)}{\alpha_{Cl_2} \frac{I_o}{2} [Cl_2]}$$

$$k_{11}' = \phi_{CO_2} (2k_8'[ClO][M]/(4[CO]))$$

Utilizing the relationship in Eq. (106), equating

$$k_9, [ClCO][O_2] \text{ to } k_{11}, [CO][M]^{-1}(\alpha_{Cl_2} I[Cl_2]/k_8, [M])^{1/2},$$

the $ClCO_3$ concentration can be approximated as:

$$[ClCO_3]_{ss} = \frac{k_{11}, [CO]}{k_{10}, [M]} \left( \frac{\alpha_{Cl_2} I[Cl_2]}{k_8, [M]} \right)^{1/2} \tag{115}$$

Using Eq. (115) and the data in Table (19) a value can be cal-
culated for the $ClCO_3$ steady state concentration in a modulation flow
experiment. The corresponding absorption intensity can be calculated
in the same manner as the ClO concentration in the previous section.
Since the $ClCO_3$ shows second order decay modulation behavior in the
high quantum yield range, its steady state absorption intensity can
also be approximated by overlaying a theoretical curve on the measured
modulation amplitude versus log 1/f graph. The extrapolated $[ClCO_3]_{ss}$
absorption intensities and the calculated concentrations are listed
in Table (20) along with the calculated absorption coefficients.

The value of $1. \pm .25 \times 10^{-18} cm^2$/particle for this absorption
coefficient has a large uncertainty due to the approximation used to
calculate $[ClCO_3]_{ss}$. This can be seen by comparing the values of
$[ClO]_{ss}$ calculated from Eq. (105) with those extrapolated from the
observed modulation amplitude. The concentrations calculated from
Eq. (105) average about 25 percent lower than the experimental values
as shown in Table (21). This could be due to error in extrapolating

Table 20. Calculation of the $ClCO_3$ 220 nm. absorption coefficient.

(base e)

| Exp. No. | $[ClCO_3]_{ss}$ (molecules/cm$^3$) | $(\Delta I/I)_{ss}$ | $\sigma = \dfrac{\Delta I/[C]L}{I} \dfrac{cm^2}{particle}$ |
|----------|-----------------------------------|---------------------|------------------------------------------------------------|
| 1 | $2.06 \times 10^{13}$ | $1.0 \times 10^{-2}$ | $1.2 \times 10^{-18}$ |
| 2 | $2.44 \times 10^{13}$ | $0.86 \times 10^{-2}$ | $0.89 \times 10^{-18}$ |
| 3 | $2.84 \times 10^{13}$ | $1.13 \times 10^{-2}$ | $1.0 \times 10^{-18}$ |

$$\text{average } \sigma_{ClCO_3} (220 \text{ nm.}) = 1. \pm .25 \times 10^{-18} \frac{cm^2}{part.}$$

Table 21. Comparison of the experimental values for $[ClO]_{ss}$ with those calculated from Eq. (105).

| Exp. | $[ClO]_{ss}$ Experimental (molecules/cm$^3$) | $[ClO]_{ss}$ calculated | Difference |
|---|---|---|---|
| 1 | $1.8 \times 10^{12}$ | $1.37 \times 10^{12}$ | 24% |
| 2 | $2.5 \times 10^{12}$ | $1.85 \times 10^{12}$ | 26% |
| 3 | $2.4 \times 10^{12}$ | $1.9 \times 10^{12}$ | 21% |

The calculated values are about 25% lower than the observed.

the experimental values, or it could be that the other termination reactions cause the approximations in (105) to be low. In either case this produces an uncertainty in the numerical results greater than the precision would indicate.

### G. Absorption Coefficients for ClO and $ClCO_3$ in the Infrared

The infrared absorption coefficients can be approximated in the same manner as the ultraviolet absorption coefficient for $ClCO_3$. The absorption intensities for the steady state concentrations can be extrapolated from the curves of modulation amplitude behavior versus log $1/f$, and the steady state concentrations of ClO and $ClCO_3$ can be calculated from Eqs. (106)and (115).

Table (22) shows the data for and results of these calculations. Only two high quantum yield experiments were run in the infrared, and in both of these the ClO absorption was very small. In these runs the observed absorption intensities at 970 cm.$^{-1}$ were caused by both ClO and $ClCO_3$ due to the band overlap problem. Because of this, the predicted intensities for the ClO absorptions in these two runs were divided by a factor of two. As the results show, the calculated absorption coefficient for ClO is approximately $3 \times 10^{-19}$ cm$^2$/particle. The approximated error in this prediction is about the same order of magnitude, indicating that the absorption coefficient is probably bewteen 0.5 and 5. $\times 10^{-19}$ cm$^2$/particle.

The results for the $ClCO_3$ absorption coefficient are more reliable, with the predicted value being $3.8 \pm 1. \times 10^{-19}$ cm.$^2$/particle.

Table 22.  Calculation of the Infrared  <u>Absorption Coefficients of ClO</u>

<u>and ClCO$_3$</u>:

(a)  Data  (all concentrations are in molecules/cm$^3$)

| Exp. | $[Cl_2]$ | $\alpha_{Cl_2}I(sec^{-1})$ | $[CO]_{ss}$ | $\Phi_{CO_2}$ |
|---|---|---|---|---|
| 1 | $2.6 \times 10^{15}$ | $1.44 \times 10^{-3}$ | $5.8 \times 10^{17}$ | 360 |
| 2 | $5. \times 10^{15}$ | $1.44 \times 10^{-3}$ | $2. \times 10^{17}$ | 170 |

(b)  Results  $(ClCO_3)$

| Exp. | $\dfrac{(\Delta I/I)}{\sqrt{2}}$ .937 cm$^{-1}$ | $[ClCO]_{ss}$ | $\sigma_{ClCO_3}$(937 cm$^{-1}$) (cm$^2$/particle) | L = 32 meters |
|---|---|---|---|---|
| 1 | $2.8 \times 10^{-2}$ | $2.14 \times 10^{13}$ | $4.1 \times 10^{-19}$ | |
| 2 | $1.1 \times 10^{-2}$ | $1. \times 10^{13}$ | $3.6 \times 10^{-19}$ | |

average  $\sigma_{ClCO_3}$(937 cm$^{-1}$) = 3.8 ± 1. $\times 10^{-19}$ cm$^2$/particle

(c)  Results (ClO)

| Exp. | $\approx \dfrac{(\Delta I/I)}{\sqrt{2}}$ 970 cm$^{-1}$ (reduced for ClCO$_3$ absorption overlap) | $[ClO]_{ss}$ | $\sigma_{970 \text{ cm}^{-1}}$ |
|---|---|---|---|
| 1 | $1.7 \times 10^{-3}$ | $1.23 \times 10^{12}$ | $0.43 \times 10^{-18}$ |
| 2 | $1.2 \times 10^{-3}$ | $1.67 \times 10^{12}$ | $0.24 \times 10^{-18}$ |

average  $\sigma_{ClO}$(970 cm$^{-1}$) = 3. ± 2.5 $\times 10^{-19}$ cm$^2$/particle

This approximate absorption coefficient for ClO can be compared to those measured in this laboratory for other diatomic molecules.

$$\sigma_{CO} \approx 1. \times 10^{-20} \text{ cm}^2/\text{particle}$$

$$\sigma_{NO} \approx 3.7 \times 10^{-20} \text{ cm}^2/\text{particle}$$

$$\sigma_{ClO} \approx 3 \times 10^{-19} \text{ cm}^2/\text{particle}$$

These results are quite reasonable when the dipole moments for these molecules are examined. The ClO dipole is a factor of ten greater than either of the others which could explain a larger absorption coefficient.

$$\mu_{CO} = 0.112 \text{ D.} \quad [60]$$

$$\mu_{NO} = 0.158 \text{ D.} \quad [61]$$

$$\mu_{ClO} = 1.26 \text{ D.} \quad [50]$$

Absolute proof of this side band's identity as ClO would be to observe the free radical in another system. Since ClO is produced in the $Cl_2-O_2$ photolysis system, experiments were attempted at 4 mm of Hg. of $Cl_2$ and 754 mm of Hg. $O_2$. These experiments failed to produce any meaningful results because the large amount of $Cl_2$ degraded the mirrors during the reaction. This caused low frequency transients which blotted out any modulation signals.

I believe that another series of experiments along these same lines using magnesium fluoride coated aluminum reflecting surfaces on the mirrors would prove more fruitful. From experiments in the ultra-violet apparatus we have observed this mirror surface to be more resistant to Cl atom reaction.

## V. DISCUSSION

### A. Comparison of the Proposed Mechanism with the Literature

#### 1. $Cl_2$-$O_2$ System

The reported literature rate constants for the second order

recombination reaction of ClO disagree by a factor of 60. Basco and

Dogra reported a M gas independent recombination rate constant of

$2.25 \times 10^{-14}$ $cm^3$/molecule-sec from their measurements at 200 mm of Hg.

total pressure in a flash photolysis system. The present investigation

and that done by Johnston et al.[39] agree that the observed one atmosphere

recombination rate constant for ClO is $k_8$,[M] $= 1.23 \times 10^{-12}$ $cm^3$/

molecules-sec. in oxygen.

Using the larger recombination rate constant predicts that this

reaction will be the major termination step in the $Cl_2$-$O_2$-CO system

at one atmosphere total pressure and low CO concentration. With this

chain termination step the experimentally observed rate law is easily

derived from the proposed mechanism, whereas using any other termination

step would not produce the proper results. From this supporting

evidence it appears that Johnston et al.'s value for the one atmosphere

rate constant is correct. This also indicates that there exists a

light dependent step in the $Cl_2$-$O_2$ system, which has not as yet been

explained, to correlate the work of Johnston's group with that of

researchers doing high energy flash photolysis.

#### 2. $Cl_2$-$O_2$-CO System

The literature on this system indicates a half power dependence

on carbon monoxide in the rate law for formation of $CO_2$ over the whole

pressure range from 10 → 760 mm of Hg. These literature studies were all done with large initial concentrations of carbon monoxide, typically a factor of ten higher than those used in this study. Under these conditions the ratio of [ClCO]/[ClO] would increase, since the ClO radical is removed by carbon monoxide while ClCO is generated from it. This would enhance the rate of reaction (7') while decreasing the significance of reaction (8'). This would make $ClCO + Cl \rightarrow Cl_2 + CO$ the major termination step, causing a change in the rate law for $CO_2$ formation.

In this case the rate law can be derived as follows:

$$[ClCO]_{ss} \approx k_{3'}[Cl][CO]/(k_{9'}[O_2] + k_{-3'})$$

$$\frac{d[CO_2]}{dt} \approx 2k_{9'}[ClCO][O_2][M]$$

and from the long chain approximation:

$$\alpha_{Cl_2} I[Cl_2] = k_{7'}[ClCO]_{ss}[Cl]$$

Then:

$$[Cl] = \left\{ \frac{\alpha_{Cl_2} I[Cl_2](k_{9'}[O_2] + k_{-3'})}{k_{7'}k_{3'}[CO]} \right\}^{1/2}$$

Substituting into the rate law:

$$\frac{d[CO_2]}{dt} = \frac{2k_{3'}k_{9'}[O_2][M][CO]^{1/2}}{(k_{9'}[O_2] + k_{-3'})^{1/2}} (\alpha_{Cl_2} I[Cl_2]/k_{7'}k_{3'})^{1/2} \qquad (116)$$

This gives the half power dependence upon carbon monoxide that the earlier investigators reported, but it also predicts an oxygen dependence that was not observed.

A much more realistic approach is to consider all termination reactions as going on simultaneously rather than trying to predict the rate law for a special case. This approach uses the relation:

$$\alpha_{Cl_2}I[Cl_2] = k_{5'}[ClOO][Cl] + k_{7'}[ClCO][Cl] + k_{8'}[ClO]^2[M]$$

This equation can be rearranged, using the steady state expressions for the free radicals, to give:

$$[Cl] = (\alpha_{Cl_2}I[Cl_2])^{1/2}\left\{ k_{5'}K_{ClOO}[O_2] + \frac{k_{7'}k_{3'}[CO]}{k_{9'}[O_2]+k_{-3'}} + \frac{k_{8'}k_{3'}^2[M]^3}{k_{11'}^2} \right\}^{-1/2}$$

(117)

Following through to derive the rate law:

$$\frac{d[CO_2]}{dt} = \frac{2k_{9'}[CO][O_2][M]}{k_{9'}[O_2]+k_{-3'}} (\alpha_{Cl_2}I[Cl_2])^{1/2} \left\{ \quad \right\}^{-1/2}$$

(118)

where the brackets indicate the expression which is bracketed in Eq. (117).

This rate law will show dependence on carbon monoxide which will vary between 1/2 and 1 as the ratio $[CO]/[O_2]$ decreases. The oxygen dependence will also be variable. In the high $[O_2]$ case the rate law will be independent of oxygen, and in the low $[O_2]$ case the rate law

will show half a half power dependence on oxygen.

This form of the rate law will explain all of the observations in the literature except the lack of dependence on oxygen reported by the early investigators in the region of conditions where the rate law was half power in CO.

One more interesting relationship can be derived from this mechanism. At low pressures, where the M gas dependent reactions become less important, a new pathway for $CO_2$ formation emerges through the ClOO free radical.

$$(4') \quad ClOO + Cl \rightarrow 2 \, ClO$$

$$(11') \quad ClO + CO \rightarrow CO_2 + Cl$$
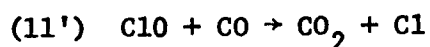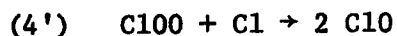
The rate law for this reaction can be approximated as:

$$[ClOO]_{ss} = K_{ClOO}[Cl][O_2^-]$$

$$[ClO]_{ss} \approx \frac{2k_4 \cdot [ClOO][Cl]}{k_{11} \cdot [CO]} = \frac{2k_4 \cdot K_{ClOO}[Cl]^2[O_2]}{k_{11} \cdot [CO]} \tag{119}$$

Then:

$$\frac{d[CO_2]}{dt} = 2k_4 \cdot k_{ClOO}[Cl]^2[O_2] + k_9 \cdot [ClCO][O_2][M] \tag{120}$$

This expression will still have a term containing the same complex dependence upon carbon monoxide, but the new term does not have any half power dependence upon chlorine molecule or light. The

appearence of this side reaction at low pressures could explain the observed low pressure change in the chlorine molecule dependence in the rate law. It was observed to change from a power of 1/2 to 1 as the pressure was lowered, while the carbon monoxide dependence remained the same.[31]

## VI. CONCLUSIONS

In this investigation kinetic arguments have been made to show that the six free radical modulation absorptions in the $Cl_2-O_2-CO$ system can be identified with two distinct species. One of these species has been identified as the ClO free radical on the basis of its ultraviolet absorption spectrum around 265 nm.

The second free radical species with absorptions at 220 nm., 937, 1835, and 1905 $cm^{-1}$ has been shown to be a precursor of ClO and $CO_2$ through molecular modulation kinetic experiments. On the basis of these experiments and the free radical's showing two strong carbonyl absorptions in the infrared, it has been identified as the $ClCO_3$ free radical. Support for this identification comes from the work of Brenschede.[35] His experiments showed a change in the $CO_2$ production mechanism at 150°C, which could be explained in terms of a free radical intermediate such as $ClCO_3$. The radical's ability to decompose to $CO_2$ + ClO at low temperatures and to ClCO + Cl at high temperatures could cause the mechanism change.

The 970 $cm^{-1}$ infrared absorption has been identified as the R branch of the ClO fundamental vibrational frequency. This identification was made on the basis of the similarities in kinetic behavior between the 265 nm. ClO absorption and the 970 $cm^{-1}$ peak. A Honl-London band envelope calculation matched to the infrared spectrum indicates that the Q branch of the ClO vibrational absorption would come at $950 \pm 15$ $cm^{-1}$.

An experimental rate law was determined for the $CO_2$ formation, and it was explained in terms of a mechanism combining the new free radical with the reactions of the $Cl_2-O_2$ and $Cl_2-CO$ photolysis systems. From the experimental measurements, a rate constant was calculated for the decomposition of the $ClCO_3$ radical to $CO_2$ and $ClO$. A rate constant was also determined for the reaction of $ClO$ with $CO$. These rate constants were respectively:

$$k_{10'} = 1.9 \pm .2 \times 10^{-18} \text{ cm}^3/\text{molecules-sec}$$

$$k_{11'} = 1.4 \pm .14 \times 10^{-15} \text{ cm}^3/\text{molecules-sec}$$

From these calculated rate constants and the assumed mechanism, it was possible to calculate absorption coefficients for the modulation absorption peaks. These values to the base e are:

$$\sigma_{ClCO_3}(220 \text{ nm.}) = 1. \pm .25 \times 10^{-18} \text{cm}^2/\text{particle}$$

$$\sigma_{ClCO_3}(937 \text{ cm}^{-1}) = 3.8 \pm 1. \times 10^{-19} \text{cm}^2/\text{particle}$$

$$\sigma_{ClO}(970 \text{ cm}^{-1}) = 3. \pm 2.5 \times 10^{-19} \text{cm}^2/\text{particle}$$

The proposed mechanism has explained the observed kinetic behavior of all observable species in the reaction system, and can be extended to explain some of the observations in the literature. It has failed to explain the lack of oxygen dependence in the $CO_2$ formation rate reported by several investigators in the 1930's for the reaction conditions which produce a half power dependency upon carbon monoxide.

In general it is felt that the complexity of this system, containing five highly reactive free radicals, requires that it be studied

in the different reactant concentration extremes. It appears very difficult to derive any simple expression for the reaction behavior at intermediate concentrations, as was attempted by the earlier researchers. This study has fully described the behavior of the system in the extreme of one atmosphere of oxygen and small concentrations of chlorine and carbon monoxide.

## REFERENCES

1. A. J. Haagen-Smit, Ind. Eng. Chem. 44, 1342 (1952).

2. S. E. Schwartz and H. S. Johnston, J. Chem. Phys. 57, 1286 (1969).

3. R. G. W. Norrish, J. Chem. Soc., pp 1158 and 1611 (1929).

4. T. C. Hall, Jr., "Photochemical Studies of Nitrogen Dioxide and Sulfur Dioxide," Doctoral Thesis, University of California, L. A.

5. T. C. Hall, Jr. and F. E. Blacet, J. Chem. Phys. 20, pp 1745-1749 (1952).

6. J. N. Pitts, Jr., J. H. Sharp and S. I. Chan, J. Chem. Phys. 39, 238 (1963); 40, 3655 (1964).

7. S. Sato and R. J. Cvetanović, Can. J. Chem. 36, 279, 970, 1668 (1958).

8. I. W. M. Smith, Trans. Faraday Soc. 64, 378 (1968).

9. R. E. Huie, J. T. Herron, D. D. Davis, Preprint of J. Chem. Phys. (1972).

10. A. A. Westenberg and N. de Haas, J. Chem. Phys. 50, 707 (1969).

11. J. Troe, Ber Bunsenges, Physik. Chem. 73, 906 (1969).

12. F. Stuhl and H. Nikki, J. Chem. Phys. 55, 3943-3957 (1971).

13. F. S. Klein and J. T. Herron, J. Chem. Phys. 41, 1285 (1964).

14. F. Kaufman, Proc. Roy. Soc. A247, 123 (1958).

15. P. Hartek, R. R. Reeves, and G. G. Mannella, Air Force Cambridge Research Center, Technical Report, AFCRC-TR60-264 (1960).

16. M. A. A. Clyne and B. A. Thrush, Proc. Roy. Soc. A269, 404 (1962).

17. E. A. Ogryzlo and H. I. Schiff, Can. J. Chem. 37, 1690 (1959).

18. S. Takahashi and S. Miyazaki, Mem. Def. Acad., Jap., $\underline{8}$, 611 & 777, (1968).

19. R. L. Mills and H. S. Johnston, J. Am. Chem. Soc. $\underline{73}$, 938 (1951).

20. G. Schott and N. Davidson, J. Am. Chem. Soc. $\underline{80}$, 1841 (1958).

21. I. C. Hisatsune, B. Crawford, Jr., and R. A. Ogg, Jr., J. Am. Chem. Soc. $\underline{79}$, 4648 (1957).

22. H. W. Ford and N. Endow, J. Chem. Phys. $\underline{27}$, 1156 (1957).

23. H. S. Johnston, "Gas Phase Reaction Kinetics of Neutral Oxygen Species," N.S.R.D.S.-National Bureau of Standards-20.

24. H. S. Johnston and H. J. Crosby, J. Chem. Phys. $\underline{22}$, 689 (1954).

25. E. A. Schuck, E. R. Stephens, and R. R. Schrock, J. Air Pollution Control Ass. $\underline{16}$, 695 (1966).

26. H. S. Johnston, Gas Phase Reaction Rate Theory, (Ronald Press Co., N.Y., 1966) p 32.

27. J. M. Van den Bogaerde, "Infrared Spectra and Reaction Kinetics of Free Radicals in the $Cl_2-O_2$ System," Doctoral Thesis, University of Calfiornia, Berkeley, UCRL-18682.

28. Bütefisch, Thesis, Hannover, 1920.

29. H. J. Schumacher, Z. Physikal Chem., $\underline{129}$, 241 (1927).

30. M. Bodenstein and T. Onoda, Z. Physikal Chem., $\underline{131}$, 153 (1927).

31. H. J. Schumacher and G. Stieger, Z. Physikal Chem., $\underline{13B}$, 169 (1931).

32. M. Bodenstein, S. Lenher, and C. Wagner, Z. Physikal Chem., $\underline{3B}$, 394 (1929).

33. W. Franke and H. J. Schumacher, Z. Physikal Chem., $\underline{B40}$, 115 (1938).

34. G. K. Rollefson, J. Am. Chem. Soc., $\underline{55}$, 148, (1933).

35. W. Brenschede, Z. Physikal Chem., 41B, 254 (1938).

36. D. E. Milligan and M. E. Jacox, J. Chem. Phys. 43, 866 (1965).

37. G. Porter, Discussions Faraday Soc. 9, 60 (1950).

38. M. M. Rochkind and G. C. Pimentel, J. Chem. Phys. 46, 4481 (1967).

39. H. S. Johnston, E. D. Morris, Jr., and J. Van den Bogaerde, J. Am. Chem. Soc., 91, 7712 (1969).

40. G. Porter and F. J. Wright, Disc. Faraday Soc. 14, 23 (1953).

41. H. S. Johnston and F. Cramarossa, in Advances in Photochemistry, Ed. W. A. Noyes, Jr., G. S. Hammond, and J. N. Pitts, Jr. (New York: Interscience, 1965) vol. 4, p. 1.

42. T. T. Paukert, Doctoral Thesis, University of California at Berkeley, November 1969, UCRL-19109.

43. E. D. Morris, Jr. and H. S. Johnston, Review of Scientific Instruments, 39, No. 4, 620 (1968).

44. Gibson and Bayliss, Physical Review 44, 188 (1933).

45. J. Van den Bogaerde, op. cit. p. 120.

46. E. D. Morris, Doctoral thesis, University of California at Berkeley, 1969.

47. R. A. Durie and D. A. Ramsay, Can. J. Phys. 36, 35 (1958).

48. P. A. O'Hare and A. C. Wahl, J. Chem. Phys. 54, 3770 (1971).

49. L. Andrews and J. I. Raymond, J. Chem. Phys. 55, 3087 (1971).

50. A. Carrington, P. N. Dyer and D. H. Levy, J. Chem. Phys. 47, 1756 (1967).

51. G. Herzberg, Spectra of Diatomic Molecules (Princeton: D. Van Nostrand Co., Inc. 1950) Second Edition, p. 208.

52. G. C. Pimentel and S. W. Charles, Pure and Applied Chem. $\underline{7}$, 111 (1963).

53. Van den Bogaerde, op.cit. p 140.

54. W. G. Burns and F. S. Dainton, Trans. Faraday Soc. $\underline{48}$, 39 (1952).

55. T. C. Clark, M. A. A. Clyne and D. H. Stedman, Trans. Faraday Soc. $\underline{62}$, 3352, (1966).

56. L. C. Walker and H. Prophet, Transactions of the Faraday Society $\underline{63}$, 879 (1967).

57. N. Basco and S. K. Dogra, Proc. Roy. Soc. Lond. $\underline{A323}$, 29-68 (1971).

58. M. A. A. Clyne and J. A. Coxon, Proc. Roy. Soc. Ser. A, $\underline{303}$, 207 (1968).

59. J. E. Nicholas and R. G. W. Norrish, Proc. Roy. Soc. $\underline{A307}$, 39 (1968).

60. C. A. Burrus, J. Chem. Phys. $\underline{28}$, 427 (1958).

61. C. A. Burrus and J. D. Graybeal, Phys. Rev. $\underline{109}$, 1553 (1958).

-195-

## ACKNOWLEDGEMENTS